SURFACE PARAMETERS AND PORE-SIZE DISTRIBUTIONS

OF STANNIC OXIDE GEL FROM NITROGEN AND

HYDROGEN ADSORPTION ISOTHERMS

By

THEODOROS GALACTION VERNARDAKIS

Bachelor of Science
College of Emporia
Emporia, Kansas
1965

Master of Science
Oklahoma State University
Stillwater, Oklahoma
1968

Submitted to the Faculty of the Graduate College
of the Oklahoma State University
in partial fulfillment of the requirements
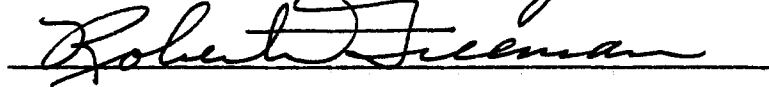for the Degree of
DOCTOR OF PHILOSOPHY
May, 1972

SURFACE PARAMETERS AND PORE-SIZE DISTRIBUTIONS

OF STANNIC OXIDE GEL FROM NITROGEN AND

HYDROGEN ADSORPTION ISOTHERMS

Thesis Approved:

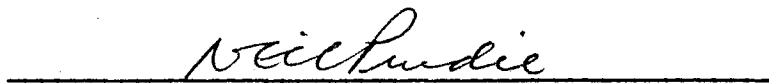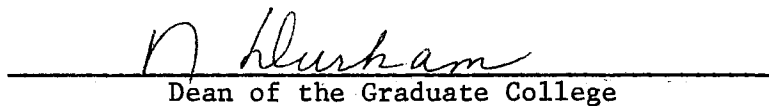Thesis Adviser

Dean of the Graduate College

ACKNOWLEDGMENT

TABLE OF CONTENTS

TABLE OF CONTENTS (Continued)

LIST OF TABLES

LIST OF FIGURES

vii

CHAPTER I

INTRODUCTION

The study of the adsorption of gases on finely divided and porous solids has received considerable attention in the last 40 or so years because of its extreme importance in many chemical processes where gas reactions occur either on the surface or under the influence of the surface of solids. Gas adsorption data can be used very effectively to calculate the total surface area and to investigate the geometrical structure of the surface of porous solids.

The phenomenon of adsorption is almost two centuries old, going as far back as 1773 when Scheele first described the uptake of gases by charcoal. A few years later, in 1785, it was discovered that when colored solutions were filtered through charcoal their coloring was removed. It was not, however, until the early part of the twentieth century that quantitative work was done on this phenomenon. During the years prior to 1938 a number of theoretical isotherm equations, notably the monomolecular adsorption equation of Langmuir[1,2,3] and the Polanyi potential theory[4,5,6,7,8] with the polarization theory of De Boer and Zwikker[9] for multilayer adsorption, have been applied quite successfully in the treatment of adsorption data.

The year 1938 marks the introduction of one of the most important multimolecular adsorption theories, namely that of Brunauer, Emmett, and Teller[10]. The BET theory, as it is usually referred to, has occupied a

central position in adsorption studies since its development because it yields an equation with only two constants which can be used very effectively to calculate surface areas and approximate heats of adsorption. The derivation of the BET adsorption theory will be reviewed in Chapter II.

In seeking information about the structure of porous solids one would always have to consider capillary condensation phenomena. Such effects are not included in the theories of adsorption just mentioned. The theory of capillary condensation which takes place in the fine pores of solid adsorbents in combination with the BET multimolecular adsorption theory would produce a more realistic physical picture of the mechanism of adsorption. For this reason Wheeler[11,12] has combined both viewpoints into a unified modern theory of adsorption.

The primary source of information regarding the size of pores in highly porous solids comes exclusively from considerations of capillary condensation phenomena which take place at low relative pressures. Multilayer adsorption proceeds simultaneously with condensation in the capillaries. In the evaluation of pore-size distributions this type of adsorption is to be disregarded as not arising from the filling of pores; therefore, corrections for it are necessary. In general, if a definite pore geometry is assumed and if the Kelvin equation is considered applicable to capillaries such as those in porous solids then distributions of pore size can be readily evaluated. Several methods have been developed in recent years to deal with computations of this type. The most important of them will be reviewed in Chapter III.

It is the purpose of the present investigation to carry out physical adsorption studies which are used to characterize the surface of a

porous solid. The material selected for this study is stannic oxide in the gel form because of its expected large surface area and high poros-ity, as well as its probable application as a catalyst. The method used consists of the measurement of the physical adsorption of nitrogen and hydrogen gases on the surface of the gel. The corresponding adsorption isotherms are obtained at the temperature of liquid nitrogen and liquid hydrogen, respectively. Application of the BET theory to the experimen-tal isotherms yields the specific surface area and the approximate heat of adsorption for each adsorbate on the same SnO_2 gel surface.

In addition, the investigation includes a study of the pore struc-ture of the gel with pore-size distributions obtained from considera-tions of capillary condensation. The nitrogen and hydrogen adsorption isotherms together with their corresponding specific surface areas from the BET method are used to furnish the data necessary for the calcula-tions. The evaluation of pore-size distributions is carried out on the basis of the "parallel-plate" model which assumes that the pores are "slit-shaped" and the derivation of which is presented in Chapter III.

The shape of the adsorption isotherms is expected to be the same for the two adsorbates since the same adsorbent is used. The hydrogen isotherm, however, should lie above the nitrogen isotherm because of in-creased adsorption in the former case. This would be possible because the size of the hydrogen molecule is less than that of the nitrogen mol-ecule. This difference in the area of the adsorbate molecules should produce a considerable change in the specific surface area of the adsor-bent in going from nitrogen to hydrogen. Differences are also expected in the pore-size distributions since the smaller hydrogen molecules can penetrate into pores of size smaller than that of the nitrogen molecules.

The cumulative surface areas which are obtained by the method of pore-
size distribution should compare well with the corresponding ones from
the BET method.

As there is a concerted effort to analyze and characterize the na-
ture of the surface of stannic oxide gel further investigations are being
carried out by spectroscopic techniques. Infrared spectroscopy is the
method most widely used in the study of solid surfaces, the molecular
structure of the species adsorbed, the vibrational frequencies of the
adsorbate molecules, and the nature of the interaction between the sur-
face and the adsorbed substance. Its application to many systems often
gives specific information on various types of surface structure; it can
be used to define the nature of the interaction process as well as the
nature of the adsorption site, and it can yield valuable information con-
cerning the molecular perturbations due to the surface forces in physical
adsorption.

The first attempt to use infrared spectroscopy in the study of sur-
faces and adsorption was made in 1937 by Buswell, Krebs, and Rodebush[13],
and followed by a number of Russian investigators, most notably Tere-
nin[14], Yaroslavskii[15,16,17] and others[18,19,20,21,22]. In the United
States the infrared spectroscopic study of adsorption owes much of its
development to the pioneering work of Eischens and Pliskin[23] and Mc-
Donald[24,25] and to Sheppard and Yates[26] in Great Britain. In addition,
two excellent monographs by Little[27] and Hair[28] devoted entirely to in-
frared investigations of adsorbed species, were published in recent
years.

The investigation of the nature of the stannic oxide surface by in-
frared and Raman spectroscopies is already under way. The gel can be

prepared in a very pure state, it has a relatively high surface area, it is transparent when dried, and in the form of thin plates transmits infrared radiation. These properties facilitate spectroscopic studies, especially the high surface area, since a large amount of gas must be present in the path of the radiation for meaningful spectra to be obtained. The infrared and Laser-Raman spectra of the gel, with the interest focused on the hydroxyl groups and adsorbed water on the surface, are presented in Chapter IX.

The future work to be carried out is primarily concerned with infrared and Raman investigations of hydrogen gas adsorbed on the SnO_2 gel surface at the temperature of liquid hydrogen. Of great interest is the presence, as well as the nature, of hydroxyl groups on the surface, and the character of adsorption interaction between the molecules of the hydrogen adsorbate and these surface hydroxyls. The temperature of liquid hydrogen can be achieved with the use of a miniature cryostat apparatus especially designed and modified for studies of this nature.

Both IR and Laser Raman spectra should be taken since these two techniques can be used to complement each other to the extent that vibrations which might remain undetected with IR alone can appear in the Raman due to the differences in the selection rules.

The first facet of the investigation regarding the modifications of the liquid hydrogen cryostat and the construction of all necessary auxiliary equipment to be applied to studies of this nature is nearing completion. A discussion and detailed analysis of the apparatus will be presented in Chapter X.

CHAPTER II

THEORY OF PHYSICAL ADSORPTION

It is well known that molecular forces at the surface of a liquid
are in a state of unbalance. The same is true of the surface of a solid,
where the molecules or ions in the surface are subject to unbalanced
forces of attraction normal to the surface plane. These atoms do not
have all their forces satisfied by union with other particles. As a re-
sult of this unsaturation liquids and solids tend to attract and retain
on their surfaces dissolved substances or gases in order to satisfy their
residual surface forces. When a gas or vapor is allowed to equilibrate
with a solid or liquid surface the concentration of the latter is always
found to be greater on the surface. This phenomenon of surface concen-
tration is called "adsorption". Thus, gas adsorption partially restores
the balance of forces on the surface[29]. The substance attracted to the
surface is termed the adsorbed phase, or adsorbate, while the solid or
liquid to which it is attracted is known as the adsorbent.

Adsorption should be distinguished from "absorption". In the lat-
ter process the gas penetrates into the structure and becomes distrib-
uted throughout the body of the solid or liquid by way of diffusion.
Trapnell[30] indicates that absorption is governed by the laws of diffu-
sion. Therefore, it can be differentiated from adsorption. When doubt-
ful as to whether a process is true adsorption or absorption the general
term "sorption" is usually employed.

6

Adsorption processes may be physical or chemical in nature depending on the kind of surface forces involved. In a great number of cases clear distinction can be made between the two. Physical or van der Waals adsorption is due to molecular interaction forces. The formation of a physically adsorbed layer may be pictured as the condensation of a vapor to form a liquid. In chemical adsorption or chemisorption the adsorbate-adsorbent binding energies are of the order of chemical bonds. Electron transfer between the solid and the gas is involved in chemisorption, by which a chemical compound is formed between the outermost atoms of the adsorbent surface and the first layer of adsorbate molecules.

The heat of adsorption is one of the primary criteria in distinguishing physical adsorption from chemisorption. The heat of physical adsorption is of the same order of magnitude as the heat of liquefaction of the adsorbate and is less than 10 Kcal per mole, while the heat of chemical adsorption is of the same order of magnitude as that of the corresponding chemical reaction and ranges between 10 to 150 Kcal per mole. Molecules that are physically absorbed can be removed from the surface by evacuation at the same temperature of adsorption. Chemisorbed substances, on the other hand, cannot be easily removed, at least at moderate temperatures. Under more extreme conditions the adsorbent as a whole may be damaged permanently. Physical adsorption is often characterized by a multimolecular layer built up under suitable temperature and pressure conditions, whereas chemisorption is usually complete at the thickness of a monomolecular layer.

Physical adsorption, being related to liquefaction, takes place, to a large extent, at temperatures and pressures close to those required for liquefaction. Usually below a relative pressure, P/P_o, of 0.01 ad-

sorption is insignificant unless if the adsorbent has a very fine porous structure. In contrast, chemisorption takes place at much lower pressures and quite high temperatures. Physisorption, like condensation, is a general phenomenon and occurs with any gas-solid system under suitable temperature and pressure conditions. Chemisorption, on the other hand, occurs only if the adsorbate gas can form a chemical bond with the surface atoms.

Physical adsorption is well characterized from a theoretical viewpoint, which must account for the dependence of the amount of gas adsorbed upon pressure and temperature. The relation between the amount of gas adsorbed by an adsorbent and the equilibrium pressure at a constant temperature is called an adsorption isotherm. Isotherms are plots of volume adsorbed, $V_{ads.}$, as a function of relative pressure, P/P_o, where P is the equilibrium pressure of the adsorbed film and P_o is the vapor pressure of the bulk liquid at the constant temperature of the experiment.

The shape of the isotherms can be used to obtain information about the adsorption process, the structure of the surface, and to determine the fraction of the surface covered by adsorbate molecules and hence the specific surface area of the adsorbent. Due to the amount of information and the ease of experimental measurement, isotherms are the most common P-V-T plots used in adsorption studies.

Adsorption isosteres can be useful, especially in obtaining isosteric heats of adsorption. They are impractical, however, because of the difficulty to hold V constant and measure values of P and T. The usual procedure is to obtain a large number of adsorption isotherms for a specific adsorbate-adsorbent system and to interpolate values of P and T corresponding to fixed values of V. Isobars, which are plots of volume

adsorbed as a function of temperature at constant pressure, are of little significance in physical adsorption studies. These too are most often interpolated from isotherms.

A large number of adsorption isotherms have been reported, depending on the nature of the adsorption process. Brunauer et al.[31] have classified commonly observed isotherms into five categories, shown in Figure 1. Type I isotherms are encountered in cases of chemisorption, where adsorption proceeds up to but not beyond a monomolecular layer, and in cases of adsorption on highly porous adsorbents. It is also known as the Langmuir isotherm. Types II and III are the isotherms expected for nonporous materials. Types IV and V are characteristic of highly porous adsorbents with multilayer adsorption. The flattening of the Type I, IV, and V isotherms at the highest pressures is attributed to capillary condensation by Brunauer[32].

The simplest adsorption isotherm utilizes Henry's Law for the solution of gases in liquids[29]. According to Henry's Law the amount of gas adsorbed at constant temperature varies directly with the equilibrium gas pressure. The theoretical derivation assumes that both the gas and the adsorbed phases are dilute enough to be taken as ideal[33,34]. This law appears to hold true at ordinary temperatures and low pressures.

A decidedly superior adsorption equation for Type I isotherms was deduced by Langmuir[1,2] from purely theoretical considerations. Necessary and sufficient conditions to the Langmuir theoretical derivation are: molecules are adsorbed as complete entities or discrete units on definite sites on the surface, each site can accommodate one and only one adsorbed molecule (monomolecular layer) and there is not intermolecular (lateral) interaction between the adsorbed molecules. Further, the

10
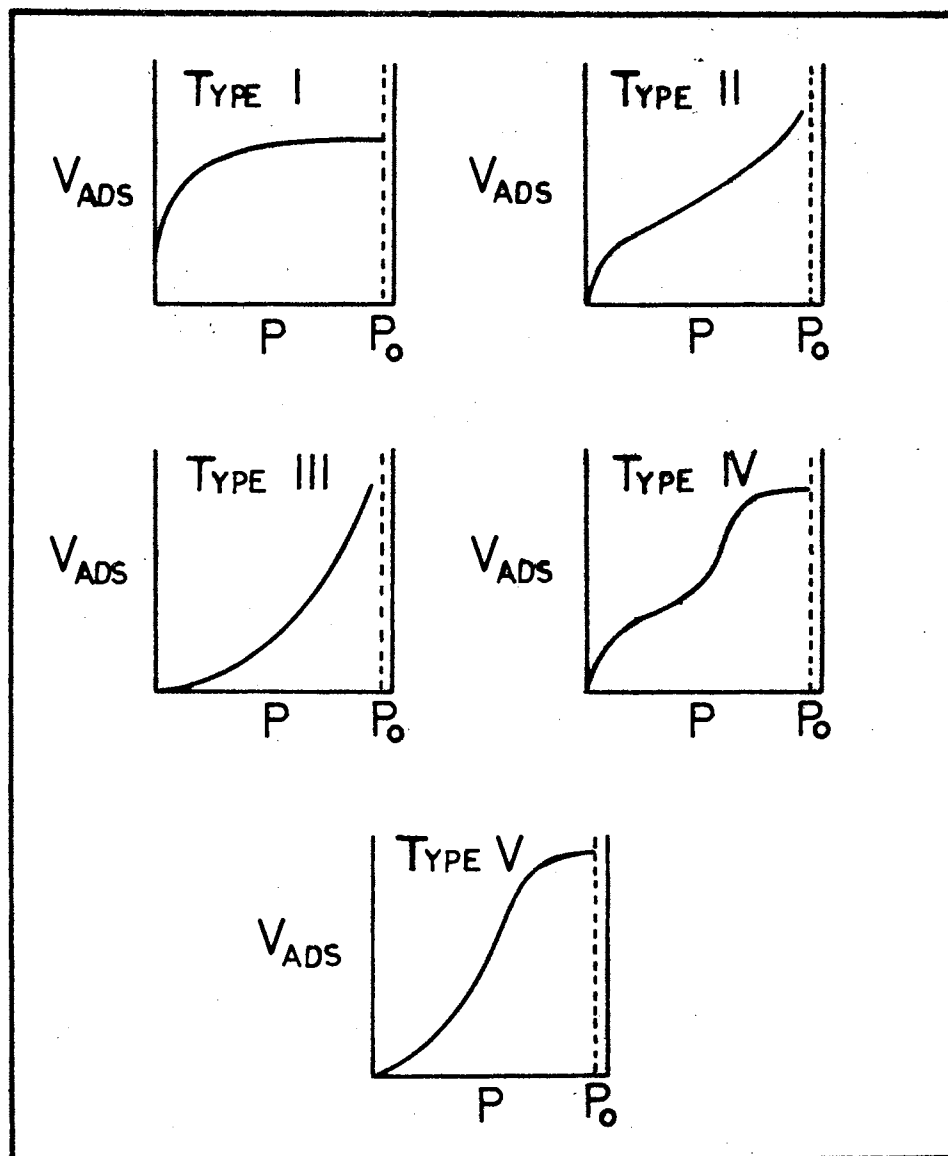
Figure 1. Brunauer's Five Types of Adsorption Isotherms

adsorption process is visualized as consisting of two opposing actions, a condensation of molecules from the gas phase onto the surface and an evaporation of molecules from the surface back into the bulk of the gas. The final form of Langmuir's adsorption isotherm is:

$$\theta = bP/(1 + bP) \tag{1}$$

where θ is the fraction of sites filled or the fraction of the total surface covered, P is the pressure, and b is a constant at each temperature. At low gas pressures this isotherm reduces to Henry's Law.

The most important of all adsorption theories is the multimolecular adsorption theory which was developed in 1938 by Brunauer, Emmett, and Teller[10]. The BET adsorption equation, as it is abbreviated, is of great practical utility since it involves only two parameters and it is applicable to the majority of measured isotherms. It is currently accepted as the best two constant equations for determining surface area of porous solids and calculating approximate heats of adsorption. It will be used in this study to evaluate the surface area of stannic oxide gel (SnO_2) both from the nitrogen and hydrogen adsorption isotherms.

The BET adsorption equation can be theoretically derived equally well either by the kinetic method or from statistical considerations. The kinetic derivation[29,32] is the simplest and most easily understood without the background required for the more complex statistical method.

The BET theory is a generalization of the ideal monolayer treatment of Langmuir extended to include the formation of multimolecular adsorbed layers. In the kinetic derivation it is assumed that each adsorbed molecule of the first layer serves as a site for the adsorption of a molecule in the second or higher layers. In other words, each gas molecule

in a higher layer is adsorbed directly upon a molecule of the layer below it. The concept of layer localization is present throughout all the layers. On a microscopic scale the adsorbed gas exists in vertical piles, with the molecules of a successive layer vertically adsorbed upon molecules of the preceeding layer. In addition, all forces of interaction between adjacent molecules of the same layer (between adjacent piles) are neglected.

In order to characterize adsorption based on this model it is necessary to define s_o, s_1, s_2, s_3, ...s_i .... as the areas covered by 0, 1, 2, 3, ...i .... adsorbed molecular layers. The total area of the adsorbent, S, would then be $\sum_i s_i$. At equilibrium the rate of adsorption (condensation) on s_o is equal to the rate of evaporation from s_1, i.e.,

$$a_1 P s_o = b_1 s_1 e^{-E_1/RT} . \qquad (2)$$

In other words, the rate of adsorption is proportional to the number of molecules striking the lower layer per second and, therefore, proportional to its area, s_o, and the pressure, P, in the gas phase. On the other hand, the rate of evaporation is proportional to the area of the layer, s_1, and depends exponentially on the binding energy (heat of adsorption of the first layer, E_1) and the temperature. In Equation (2) a_1 and b_1 are the constants of proportionality.

In general, for the equilibrium between the (i-1)th and ith layers the equation is:

$$a_i P s_{i-1} = b_i s_i e^{-E_i/RT} . \qquad (3)$$

The total volume of gas adsorbed is given by:

$$V = v_o \sum_{i=0}^{\infty} i s_i \qquad (4)$$

where v_o is the volume of gas required to cover a unit area of surface when the monolayer is completely filled.

The relative volume of gas adsorbed is given by dividing Equation (4) by the total surface area, $S = \sum_i s_i$, which gives:

$$\frac{V}{S v_o} = \frac{V}{V_m} = \sum_{i=0}^{\infty} i s_i / \sum_{i=0}^{\infty} s_i \qquad (5)$$

where V_m is the volume of gas required to cover the surface S with a monolayer.

In order to proceed further and reduce the BET equation it is necessary to assume that the evaporation-condensation properties of the second and higher layers are the same as those of the surface of the bulk liquid. That is:

$$E_1 = \text{constant for the total surface} \qquad (6)$$

$$E_2 = E_3 = \ldots E_i = E_L = \text{Heat of Liquefaction}$$
$$\text{of the bulk liquid adsorbate} \qquad (7)$$

$$\text{and } b_2/a_2 = b_3/a_3 \ldots = b_i/a_i = \text{constant} . \qquad (8)$$

Notation can be simplified by defining

$$y = (a_1/b_1)Pe^{E_1/RT} \qquad (9)$$

and from Equation (2) one obtains

$$s_1 = ys_o . \tag{10}$$

Similarly, defining

$$x = (a_i/b_i)Pe^{E_L/RT} \tag{11}$$

Equation (3) becomes, by considering Equations (7) and (8):

$$s_2 = xs_1 . \tag{12}$$

In general

$$s_i = xs_{i-1} = x^{i-1} s_1 = yx^{i-1} s_o = cx^i s_o \tag{13}$$

where

$$c = \frac{y}{x} = \frac{a_1 b_2}{a_2 b_1} e^{(E_1 - E_L)/RT} . \tag{14}$$

Substitution of Equation (13) in Equation (5) yields:

$$\frac{V}{V_m} = cs_o \sum_{i=1}^{\infty} ix^i / s_o \left(1 + c \sum_{i=1}^{\infty} x^i\right) . \tag{15}$$

Using the sum of an infinite geometric series, for the summation in the denominator, given by

$$\sum_{i=1}^{\infty} x^i = \frac{x}{1-x} \tag{16}$$

and for the summation in the numerator

$$\sum_{i=1}^{\infty} ix^i = x \frac{d}{dx} \sum_{i=1}^{\infty} x^i = x \frac{d}{dx} \left(\frac{x}{1-x}\right) = \frac{x}{(1-x)^2} . \qquad (17)$$

Equations (16) and (17) allow simplification of Equation (15) to give:

$$\frac{V}{V_m} = \frac{\dfrac{cx}{(1-x)^2}}{1 + \dfrac{cx}{1-x}} = \frac{cx}{(1-x)(1-x+cx)} . \qquad (18)$$

In order to make it possible to evaluate x more precisely, consider the case when the surface is thickly covered, in other words, when $P=P_o$. At this point the adsorbate gas will be liquefying while evaporation will be taking place from the liquid phase. In such a gas-liquid equilibrium the rate of condensation will be equal to the rate of evaporation. Therefore, Equation (3) will become:

$$a_i P_o S = b_i S e^{-E_L/RT} \qquad (19)$$

where P_o is the vapor pressure of the adsorbate at temperature T and S is now the total surface area of the adsorbent.

Solution of Equation (19) for (a_i/b_i) and substitution in Equation (11) gives:

$$x = \frac{(Se^{-E_L/RT})(Pe^{+E_L/RT})}{P_o S} . \qquad (20)$$

Therefore,

$$x = \frac{P}{P_o} \qquad (21)$$

Substitution for x in Equation (18) yields what is known as the "simple" or "infinite" form of the BET equation, i.e.,

$$V = \frac{V_m c(P/P_o)}{(1 - P/P_o)[1 + (c - 1) P/P_o]}$$ (22)

Equation (22) is transformed to:

$$\frac{P/P_o}{V(1-P/P_o)} = \frac{1}{V_m c} + \frac{c-1}{V_m c} (P/P_o)$$ (23)

which shows that a plot of $(P/P_o)/V(1-P/P_o)$ versus (P/P_o) gives a straight line the slope of which is $(c-1)/V_m c$ and the intercept is $(1/V_m c)$. Letting s be the slope and I the intercept, V_m can be readily calculated from

$$V_m = \frac{1}{I + s}$$ (24)

The specific surface area, S, of the adsorbent can be conveniently calculated from V_m by use of the equation

$$S = 0.269 \, \sigma_m \, V_m$$ (25)

where σ_m is the area in square angstroms which one adsorbed molecule occupies in the complete monolayer. The value of V_m is given in cm^3 of gas at S.T.P. and S in meters squared per one gram of adsorbent. The derivation of Equation (25) is presented in Appendix A.

Values of σ_m can be derived from the densities of the liquid adsorbates at the temperature of the adsorption isotherm. It is necessary to assume that the molecules adsorbed on the surface have the same packing as the molecules of the condensed phase. For hexagonal close pack-

ing the value of σ_m is given by:

$$\sigma_{mL} = 3.464 \times 10^{16} \left(\frac{M}{4\sqrt{2}\ N\ \rho_L}\right)^{2/3} \tag{26}$$

where σ_{mL} is the area of the adsorbed molecule in the liquid phase, M is the molecular weight of the adsorbate, N is Avogadro's number, and ρ_L is the density of the adsorbate in the liquid phase. Values of σ_{mL} for a number of simple molecules were calculated by Emmett and Brunauer[35,36].

In the particular case of this study where the nitrogen and hydrogen isotherms of stannic oxide gel are obtained at the temperature of liquid nitrogen and liquid hydrogen, correspondingly, values of σ_m and ρ refer to the adsorbate in the liquid phase. For a nitrogen molecule the accepted area calculated from Equation (26) with M = 28 g/mole and ρ_L = 0.808 g/cm^3 is given as 16.26 A^2. The specific surface area of the adsorbent from nitrogen adsorption isotherms would then be from Equation (25):

$$S = 4.37\ V_m \quad (m^2/g) \tag{27}$$

The area of a hydrogen molecule calculated from Equation (26) with M = 2 g/mole and ρ_L = 0.071 g/cm^3 is 14.05 A^2. The specific surface area of the adsorbent from hydrogen adsorption isotherms would then be:

$$S = 3.78\ V_m \quad (m^2/g) \tag{28}$$

The BET constant c of Equation (23) can be evaluated from the experimental data either from the intercept $I = (1/V_m c)$ or the slope $s = (c-1)/V_m c$. Of course, it should be the same in both cases for a

particular adsorbate-adsorbent system.

A measure of the net heat of adsorption may be obtained if the assumption is made that:

$$a_1 b_2 / a_2 b_1 = 1 \qquad (29)$$

The value of c from Equation (14) will be:

$$c = e^{(E_1 - E_L)/RT} \quad . \qquad (30)$$

The term $E_1 - E_L$, which is the energy difference between the heat of adsorption in the first layer and the heat of liquefaction, was called by Lamb and Coolidge[37] the "net" heat of adsorption. From the known heats of liquefaction of the adsorbates one can obtain E_1, the average heat of adsorption in the first layer.

The relative magnitude of the heat of adsorption E_1 and the heat of liquefaction E_L plays an important role in determining the shape of the adsorption isotherm in the low pressure region[31]. If $E_1 > E_L$ in Equation (30), that is, if the attractive forces between the adsorbent and the adsorbed gas are greater than the attractive forces between the molecules of the adsorbate in the liquid state then the isotherm is concave to the relative pressure axis at low pressures. This is true for the Type I, II, or IV isotherms of Figure 1. If, on the other hand, $E_1 < E_L$, that is, if the cohesive forces between the adsorbate molecules are larger than the forces between adsorbent and adsorbate then the isotherm at low pressures is convex to the relative pressure axis. Isotherms of Type III or V belong to systems of this latter category.

The BET multimolecular adsorption theory has several limitations

because of the assumptions made in the derivation. All of these assumptions have been questioned by many authors on the subject[38,39,40,41,42]. Their criticisms are primarily concerned with the reasonableness of the physical picture conveyed by the BET theory. The energy contributions predicted by the theory, on the other hand, are only in semi-quantitative agreement with experiment. The BET heats of adsorption were shown to be too low in papers presented by Davis and DeWitt[43] and also by Kington and co-workers[44,45]. However, despite its theoretical shortcomings most workers in the field agree that the BET theory is of great practical utility in determining the surface area of finely divided and porous solids.

CHAPTER III

ADSORPTION IN PORES AND CAPILLARIES. DETERMINA-

TION OF PORE-SIZE DISTRIBUTION CURVES

The BET, as well as, the Harkins and Jura[46] theories assume that

the surface of the adsorbent is uniform. In addition, they do not take

into consideration the fact that part of the surface is made up of fine

pores or capillaries which fill at a certain pressure and no longer con-

tribute to the adsorption process at higher pressures. According to

these theories the isotherms are valid up to a relative pressure of about

0.3. At higher pressures the deviation is attributed mainly to capillary

condensation effects.

Capillary condensation in adsorption has been recognized as early

as 1911 by Zsigmondy[47] and later by McGavack and Patrick[48]. Liquids

that wet the wall of a capillary have a lower vapor pressure in the cap-

illary than in the normal bulk phase. This effect was applied to capil-

laries of molecular dimensions by Zsigmondy[47], who assumed that conden-

sation can occur in them at pressures lower than the normal vapor pres-

sure.

The theory of capillary condensation has been extented further by

Cohan[49], Brunauer[32], and Wheeler[11,12]. The modern theory of adsorption,

mainly due to Wheeler[11,12], regards physical adsorption as arising from

contributions of both multilayer adsorption and capillary condensation

phenomena. Multilayer films are formed on the "flat" surface of the ad-

sorbent and their number increases as the relative pressure approaches unity, while on the inner walls of the capillaries the thickness of these layers would increase until such capillaries are filled[50]. Capillary condensation, on the other hand, is due to the action of surface tension at a curved meniscus. This surface tension lowers the equilibrium vapor pressure, P, at the meniscus below that of the bulk concentration, P_o, according to the Kelvin equation:

$$\ln(P/P_o) = - (2\gamma\, V_M \cos \alpha/RTr_k) \tag{31}$$

where P/P_o is the relative pressure, γ is the surface tension of the liquid adsorbate, V_M is the molar volume of the liquid adsorbate, α is the contact angle between the surface of the adsorbed liquid and the wall of the capillary (usually taken as zero), R is the ideal gas constant, T is the temperature of the liquid, and r_k is the Kelvin radius.

Pierce and Smith[51] have grouped capillaries into two categories depending on the value of the relative pressure at which they fill. The first type includes capillaries which fill at a low relative pressure (below 0.5), while the second type includes those which fill at a relative pressure between 0.5 and 1.0. These two types exhibit different adsorption isotherms. On desorption the former show no hysteresis, while the latter do. The isotherm for the first class of capillaries is the one designated by Brunauer as Type I (Langmuir isotherm) and it is shown in Figure 1. For the second class of pores the isotherm is given by the Brunauer Type II with hysteresis. The Type II isotherm without hysteresis is that exhibited by adsorption on nonporous solids.

The filling of capillaries occurs in two ways. The first takes place through condensation of the vapor at the meniscus which bridges

the walls of the capillary. The second takes place through the building up of a multilayer film until all the space of the capillary is filled. A third way is the one that combines both. A pore can start filling with a layer on its inner wall and after the layers on opposite walls meet and merge together it will end up with a meniscus. Determination as to the effectiveness of these processes during adsorption comes from considerations of both the size and the shape of the capillaries.

For very narrow pores condensation starts at the very beginning of adsorption, because each one of these pores can be bridged either by a single molecule or by a monomolecular film on each wall. These type of pores are filled at a very low relative pressure and such substances exhibit a Brunauer Type I isotherm without hysteresis. The absence of hysteresis is due to the fact that adsorption and desorption occur in the same manner, from a meniscus. For these highly porous solids the isotherm rises but insignificantly after all pores have been filled, which indicates that contributions from any "flat" surface in the solid are of minor importance.

For relatively wide pores a monomolecular film on each wall will not be able to bridge the particular pore. In this case adsorption takes place as a monomolecular layer on the inner walls of the pore, an effect which is the same as that for a flat surface. The isotherms of substances with this type of pores are exactly like those of nonporous solids at very low pressures. When a value of the relative pressure is reached at which the wall films start merging together, condensation begins in the capillaries and the surface diminishes because of the filling of pores. This process continues as the relative pressure increases towards unity. As the molecular layers in a single pore meet and merge

together, the forces acting on the molecules of the new combined layer become stronger. The explanation of this effect comes from the fact that these molecules are now held on and between two walls, instead of only one as in the case before merging took place. They are, therefore, more strongly bound than previously because forces twice as strong are acting upon them. Consequently, removal of these molecules from the meniscus during desorption takes place at a lower relative pressure than the original adsorption which was builting up in the form of a single wall film. A result of the above is the hysteresis which is observed during desorption. This effect is represented by a Brunauer Type II isotherm with hysteresis.

The absence of pores, as in nonporous solids, gives rise to an S-shaped adsorption isotherm which corresponds to Brunauer's Type II isotherm without hysteresis. The term "nonporous" is not entirely correct because in such solids some capillaries may be present along with a large "flat" or "free" surface. In this case the presence of capillaries causes condensation at a very low relative pressure and at the beginning of adsorption the isotherm is not very much different, although flatter, than the Type I isotherm for highly porous materials. For such solids, as the size of the pores increases the isotherm becomes steeper at the higher values of the relative pressure. When adsorption on the flat surface takes over the isotherm starts getting steeper and becomes very steep at high pressure. On desorption no hysteresis is observed because molecules are removed from the flat surface in the same manner and at the same pressure of the original adsorption.

Several methods dealing with the mathematical evaluation of the size of pores in finely divided and porous materials have been advanced

in recent years. These methods are based on the theories of physical adsorption which have already been mentioned. It is the theory of Wheeler[11,12], however, which when applied to the experimental isotherms, with the necessary corrections for multilayer adsorption, constitutes the basis upon which pore-size distributions are evaluated. The experimental isotherms are usually taken to be the ones determined by the BET method from the corresponding adsorption data. The starting point for all calculations of this type is the Kelvin equation which has already been presented as Equation (31).

Two models have been proposed and methods of calculation corresponding to each model have been developed by a number of investigators. One model assumes that the capillaries are cylindrical while the other assumes that they are "slit-shaped" (parallel-plate model).

Methods based on the cylindrical model are of passing interest and will be reviewed only briefly.

Barrett, Joyner, and Halenda[52] using the model proposed by Wheeler developed a method for circular pores which is rather complicated and time consuming. In addition to the assumption that the pores are cylindrical, another is made, that the amount of adsorbate in equilibrium with the gas phase is retained by the adsorbent either by physical adsorption on the pore walls or by capillary condensation in the inner capillary volume.

Shull[53] and co-workers[54] have applied the Wheeler theory to experimental isotherm data which they compared with standard isotherms represented either by Maxwellian or by Gaussian distribution functions. The reason for this is that the layer thicknesses of the BET theory become much larger than the experimental thicknesses for flat surfaces in the

region of high pressure.

Oulton[55] suggested a method for calculating the pore-size distribution from a desorption isotherm which considers the thickness of the adsorbed film that is attracted to the solid surface by forces greater than the interaction forces of the liquid itself. He assumes that the thickness of the film is constant and equal to the number of molecular layers at the relative pressure at which capillary condensation starts. He further assumes that the radius of the smallest pore present is determined at the closing of the hysteresis loop, i.e., at the pressure at which condensation sets in the capillaries. Clearly, one serious criticism of this method is that pores whose radii are less than those at the closing of the hysteresis loop are neglected entirely.

Anderson[56] has developed a method of numerical differentiation in obtaining differential pore distributions. He assumes that the volume of pores emptied is a function of the volume adsorbed and the thickness of the monolayer.

Methods of calculation of pore-size distributions for "slit-shaped" pores (parallel-plate model) were proposed by Innes[57], De Boer[58], and De Boer and co-workers in a series of articles[59,60,61].

Innes[57] regards the capillary system as being equivalent to a system of parallel plates with varying distances of wall separation. The Kelvin equation is still assumed to be applicable in this case, except that now the pore radius is replaced by the pore wall separation.

It is the method of De Boer et al.[59,60,61], however, which will be applied to the experimental isotherms of the stannic oxide gel in the present investigation. For this reason its derivation will be fully carried out in the subsequent presentation.

Lippens, Linsen, and De Boer[59,60,61] in their calculations of distribution curves make use of the same wall separation term, d, proposed by Innes, assuming that the pores are slit-shaped. The assumption that the pores are filled at a relative pressure of unity is still valid, and starting at that pressure the adsorption isotherm is divided into parts corresponding to equal steps of $2\Delta x$, with x used to denote the relative pressure P/P_o ($x = P/P_o$).

At the beginning of the $\underline{i}$th step the relative pressure is $x_i + \Delta x$, the volume adsorbed in cm^3 of liquid adsorbate is $X_{(x_i + \Delta x)}$, the surface area of that part of pores which are not filled with liquid adsorbate is $S_{(x_i + \Delta x_i)}$, and the layer thickness is $t_{(x_i + \Delta x_i)}$. If the relative pressure is lowered to $x_i - \Delta x$, then the pores with Kelvin radius between $r_{k(x_i + \Delta x)}$ and $r_{k(x_i - \Delta x)}$ are emptied. The average Kelvin radius for this group of pores at x_i may be taken as $(r_k)_{x_i}$ if the single increment x is very small. The average wall separation or pore width at x_i is:

$$d_{x_i} = (r_k)_{x_i} + 2t_{x_i} \tag{32}$$

where t_{x_i} is the thickness of the adsorbed layer at x_i. The surface area of these pores is ΔS_{x_i} and their volume is given by:

$$\Delta V_{x_i} = \frac{1}{2} d_{x_i} \cdot \Delta S_{x_i} \tag{33}$$

At a relative pressure of $x_i - \Delta x$, which corresponds to the end of the $\underline{i}$th step, $X_{(x_i - \Delta x)}$ is the volume of liquid adsorbed, $S_{(x_i - \Delta x)}$ is

the surface area of the pores not completely filled with liquid adsorbate, and $t_{(x_i - \Delta x)}$ is the layer thickness.

Therefore,

$$\Delta X_{x_i} = X_{(x_i + \Delta x)} - X_{(x_i - \Delta x)} \qquad (34)$$

where ΔX_{x_i} is the volume of liquid adsorbate desorbed during the $\underline{i}$th

step.

There are two contributions to the volume ΔX_{x_i}. The first is the

volume due to capillary evaporation from the group of pores at x_i and

from the decrease of the adsorbed layer thickness of the group of pores

when the relative pressure is lowered from x_i to $x_i - \Delta x$. This volume

is given by:

$$\frac{1}{2} \left[d_{x_i} - 2t_{(x_i - \Delta x)} \right] \cdot \Delta S_{x_i} \qquad (35)$$

The second contribution is the volume that comes from the decrease

of the adsorbed layer thickness in the pores which are emptied when the

pressure $x_i + \Delta x$ is lowered to $x_i - \Delta x$. This volume is equal to:

$$\left[t_{(x_i + \Delta x)} - t_{(x_i - \Delta x)} \right] \cdot S_{(x_i + \Delta x)} \qquad (36)$$

where $S_{(x_i + \Delta x)}$ is obtained from the summation of all contributions ΔS_x

of the groups of pores that have a width greater than $d_{(x_i + \Delta x)}$ or

greater than $d_{(x_{i+1} - \Delta x)}$ since:

$$d_{(x_i + \Delta x)} = d_{(x_{i+1} - \Delta x)} \tag{37}$$

Therefore,

$$S_{(x_i + \Delta x)} = \sum_i \Delta S_{(x_{i-1})} \tag{38}$$

and the equation for ΔX_{x_i} will become, after combination of equations (35) and (36) and substitution of Equation (38) in Equation (36):

$$\Delta X_{x_i} = \frac{1}{2}[d_{x_i} - 2t_{(x_i - \Delta x)}] \cdot \Delta S_{x_i}$$

$$+ [t_{(x_i + \Delta x)} - t_{(x_i - \Delta x)}] \cdot \sum_i \Delta S_{x_{i-1}} \tag{39}$$

Solving the above equation for ΔS_{x_i} and substituting in Equation (33) for ΔV_{x_i} one obtains:

$$\Delta V_{x_i} = \frac{1}{2} d_{x_i} \left[\frac{\Delta X_{x_i} - [t_{(x_i + \Delta x)} - t_{(x_i - \Delta x)}] \sum_i \Delta S_{x_{i-1}}}{\frac{1}{2}[d_{x_i} - 2t_{(x_i - \Delta x)}]} \right] \tag{40}$$

Equation (40) upon simplification becomes:

$$\Delta V_{x_i} = \cdot \left[\frac{d_{x_i} \cdot \Delta X_{x_i}}{d_{x_i} - 2t_{(x_i - \Delta x)}} \right] - \left[\frac{d_{x_i}[t_{(x_i + \Delta x)} - t_{(x_i - \Delta x)}] \sum_i \Delta S_{x_{i-1}}}{d_{x_i} - 2t_{(x_i - \Delta x)}} \right] \tag{41}$$

Now letting

$$R_{x_i} = d_{x_i} / [d_{x_i} - 2t_{(x_i - \Delta x)}] \tag{42}$$

and

$$R'_{x_i} = R_{x_i} \cdot [t_{(x_i + \Delta x)} - t_{(x_i - \Delta x)}] \tag{43}$$

the simplified equation for ΔV_{x_i} is obtained in the form:

$$\Delta V_{x_i} = [R_{x_i} \cdot \Delta X_{x_i}] - [R'_{x_i} \cdot \sum_i \Delta S_{x_{i-1}}] \tag{44}$$

When all the contributions ΔV_{x_i} and ΔS_{x_i} are summed up, the cumulative pore-volume $\Sigma \Delta V_{x_i}$ and the cumulative surface area $\Sigma \Delta S_{x_i}$ are respectively obtained. The quantity $\Sigma \Delta V_{x_i}$ represents the total volume while $\Sigma \Delta S_{x_i}$ represents the total surface area of the pores which have a width greater than d_x.

In order to obtain the differential pore-volume and differential pore-area distribution curves all the ΔV_{x_i}'s and ΔS_{x_i}'s are divided by the Δd's over which they were determined. The value of Δd at a particular d_{x_i} is obtained from:

$$\Delta d_{(x_i)} = d_{(x_i + \Delta x)} - d_{(x_i - \Delta x)} \tag{45}$$

The resulting values of $\Delta V/\Delta d$ and $\Delta S/\Delta d$ are then plotted against the corresponding d_{x_i}'s to give the differential pore-volume and pore-area distribution curves.

It is necessary to consider the methods of calculation of the basic parameters r_p [see Equation (46) below], d, r_k, and t.

For pores which are assumed to by cylindrical in shape, the value of r_p, the radius of the largest pore filled with liquid adsorbate at any pressure (Figure 2), is given by:

$$r_p = r_k + t \qquad (46)$$

with r_k and t being, as before, the Kelvin radius and the thickness of the multilayer, respectively.

In the case of "slit-shaped" pores, for which the parallel-plate model has been assumed, the value of d, the maximum distance of wall separation at which capillary condensation can occur at any given relative pressure P/P_o, is represented by the following equation:

$$d = r_k + 2t \qquad (47)$$

with Figure 3 showing the cross section of the parallel-plate model.

The r_k's are evaluated from the Kelvin equation:

$$\ln \frac{P}{P_o} = - \frac{2\gamma V_M}{RTr_k} \qquad (48)$$

where the assumption has been made that the contact angle α in Equation (31) is zero degrees and, therefore, $\cos \alpha$ equals unity.

This equation can be simplified further for the nitrogen and hydrogen adsorption isotherms at the respective liquid temperatures. In the case of nitrogen adsorption the values of γ (8.72 dynes/cm), V_M (34.68 cm^3/mole of the liquid), T (78°K), and R (8.316 x 10^7 ergs/$^\circ$K·mole) when substituted into the Kelvin equation give, in terms of common logarithms,

$$\log (P/P_o) = - (4.05/r_k) \qquad (49)$$
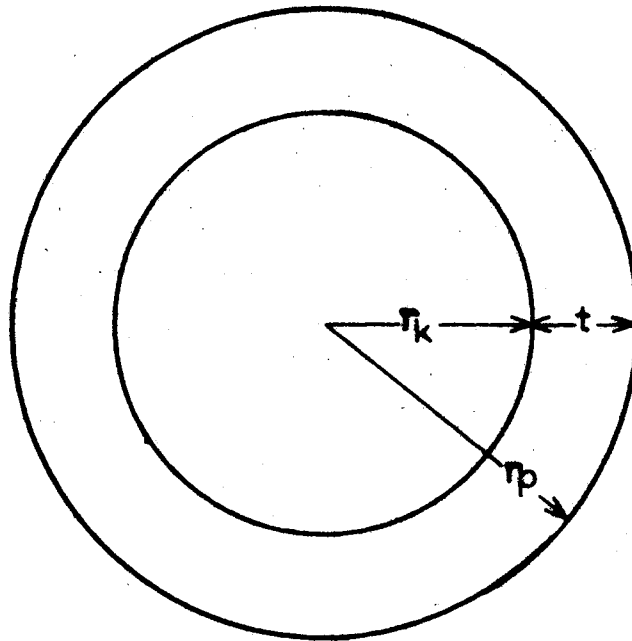
Figure 2. Cross Section of Cylindrical Model
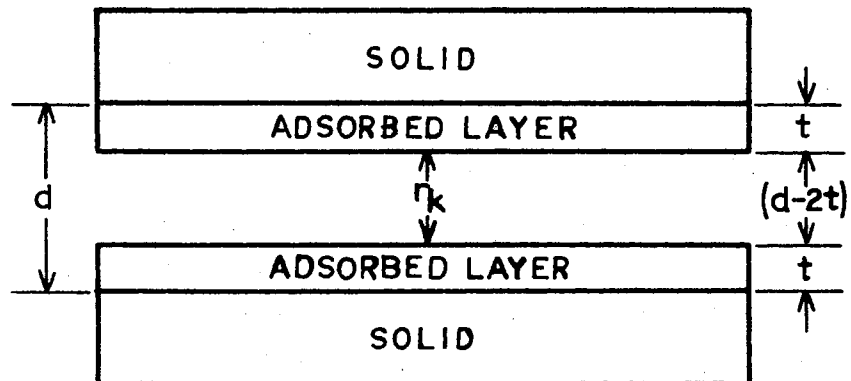
Figure 3. Cross Section of Parallel-Plate Model

and

$$r_k = -4.05/\log (P/P_o) \tag{50}$$

In the case of hydrogen adsorption the values of γ (1.91 dynes/cm), V_M (28.39 cm^3/mole of the liquid), T (20.22°K), and R (the same as previously) when substituted in Equation (48) yield:

$$r_k = -2.80/\log (P/P_o) \tag{51}$$

with the units on the Kelvin radius, r_k, in angstroms, A.

The layer thickness, t, can be evaluated by either of two methods, one proposed by Shull[53], and the other by De Boer[59,60,61].

Shull has taken the BET thicknesses and plotted the experimental values of the number of adsorbed layers against the relative pressure. The number of adsorbed layers is given as the ratio $(V_{ads.}/V_m)$, where $V_{ads.}$ is the volume adsorbed at any pressure and V_m is the volume corresponding to monomolecular coverage of the surface. In this manner an average adsorption isotherm is obtained. It is obvious that this method does not take into account capillary condensation. Using now the average isotherm the thickness of the adsorbed layer can be calculated as a function of the relative pressure if it is assumed that the thickness of the monolayer must be equal to the diameter of the adsorbate molecule.

De Boer points out that Shull's calculation of the t curve is inconsistent because of the fact that when computing the diameter of the adsorbate molecule Shull assumed a closest packing of spheres, while on the other hand, he assumed that the successive layers in multilayer adsorption are packed in such a way that each adsorbed molecule of the following layer is placed exactly on top of a same molecule of the pre-

vious layer.

Lippens, Linsen, and De Boer make the use of a statistical thickness necessary by assuming that both the adsorbed layer and the condensed liquid have the same density, which is taken as that of the liquid adsorbate; either nitrogen or hydrogen. They have defined t as:

$$t = \frac{X}{S} \cdot 10^4 \ A \qquad (52)$$

or

$$t = \frac{M \cdot V_{sp}}{22414} \cdot \frac{V_{ads.}}{S} \cdot 10^4 \ A \qquad (53)$$

where t is the statistical thickness of the adsorbed layer, X is the adsorbed volume in cm^3 of the liquid adsorbate, S is the specific surface area of the adsorbent in m^2/g, M is the molecular weight of the adsorbate, V_{sp} is the specific volume of the adsorbate in the liquid phase, and $V_{ads.}$ is the adsorbed volume of gas in cm^3 at S.T.P. per gram of adsorbent. The factor 10^4 is a consequence of the conversion into angstroms.

When the values for nitrogen (M = 28 g/mole, V_{sp} = 1.000/0.808 cm^3 per gram) are substituted into Equation (53) the result is:

$$t = (15.47) \cdot \frac{V_{ads.}}{S} \ A \qquad (54)$$

For hydrogen as the adsorbate M = 2 g/mole, V_{sp} = 1.000/0.071 cm^3 per gram, and Equation (53) becomes:

$$t = (12.67) \cdot \frac{V_{ads.}}{S} \ A \qquad (55)$$

The value of the surface area, S, is usually that obtained from the BET method which also gives the monolayer volume, V_m. For nitrogen and hydrogen as the adsorbates the BET surface areas are given by Equations (27) and (28), respectively. When substituted into Equations (54) and (55) the corresponding relations will be:

For nitrogen

$$t = (3.54) \cdot \frac{V_{ads.}}{V_m} \text{ A} \tag{56}$$

For hydrogen

$$t = (3.35) \cdot \frac{V_{ads.}}{V_m} \text{ A} \tag{57}$$

Thus, from nitrogen adsorption data either Equation (54) or (56) may be used to evaluate the multilayer adsorption thickness, t, while from hydrogen adsorption data either Equation (55) or (57) may be used to carry out the same calculations at the various equal increments of the relative pressure.

CHAPTER IV

THE ADSORPTION APPARATUS

General Considerations

With the theory of physical adsorption being already developed, it
is now necessary to consider an apparatus which will give the experi-
mental data for determining the adsorption isotherms and the surface area
of porous solids. Such data may be obtained either by volumetric or
gravimetric methods. The volumetric method is still, to date, the most
common method for determining the amount of gas adsorbed by measuring the
volume of gas taken up by the adsorbent. The simple gas adsorption ap-
paratus of Richardson[62] and Pease[63] has undergone many changes and im-
provements designed to increase accuracy and eliminate errors in measure-
ments.

The gravimetric method is also used to determine the amount of gas
adsorbed by measuring the increase in the weight of the adsorbent. This
is usually accomplished by the use of a sorption balance initially de-
veloped by McBain and Bakr[64]. Later developments and the application of
more sensitive vacuum microbalances, by Rhodin[65,66], have rendered in-
creased accuracy to this method.

The experimental data of this study were obtained by the volumetric
method. Consequently, only such a volumetric gas adsorption apparatus
will be considered here. Gravimetric methods are outside the scope of
this investigation and will not be considered.

In order to determine the surface area from the BET theory it is
necessary to obtain data which will enable one to make a plot of
$(P/P_o)/V_{ads.}(1 - P/P_o)$ versus (P/P_o). Therefore, the quantities needed
to determine a particular point are: the equilibrium pressure, P, of the
adsorbed phase, the volume, $V_{ads.}$, of gas adsorbed at the pressure P, and
the vapor pressure, P_o, of the adsorbate at the temperature at which ad-
sorption is carried out. Thus, an adsorption apparatus must be capable
of measuring an amount of gas before adsorption, then determining the
amount of gas remaining in the gaseous phase. Since several points are
required, the apparatus must be able of altering the pressure by chang-
ing the amount of gas (or volume) so that a series of points can be ob-
tained as a function of pressure. If other properties of the sample are
needed, such as the pore structure in this study, it will be necessary
to obtain adsorption data over a wide range of pressures, from close to
zero up to the vapor pressure of the adsorbate. In addition, the vapor
pressure must be measured simultaneously, although independently, of the
actual adsorption data of volume adsorbed and pressure, since P_o depends
entirely upon the temperature at which adsorption takes place.

In order to determine accurately the amount of gas which is not ad-
sorbed at equilibrium it is necessary to know precisely the "dead space"
surrounding the adsorbent particles. For this reason the apparatus must
have as small a free volume as possible. This dead-space volume is usu-
ally determined from calibration with helium at the temperature of ad-
sorption. In addition, since the gas pressure depends strongly upon
temperature, the temperature of various parts of the apparatus is moni-
tored by placing thermometers at appropriate points.

A large number of adsorption systems which satisfy the above re-

quirements have been described in the literature[29,32,67]. Such apparatuses consist of two major components, the adsorption system containing the gas burette, sample chamber, and manometer, and some auxiliary equipment such as the high vacuum system, gas purification system, gas reservoirs, low temperature bath, the vapor pressure manometer, and a furnace for degassing the sample.

The present apparatus was designed and constructed by Rutledge, Kohnke, and Cunningham[68]. It includes the vapor pressure "thermometer" patterned after Farkas and Melville[69], the gas purification system after Barr and Anhorn[70], and the gas handling system after Constabaris, Singleton and Halsey[71]. It differs significantly, however, from previous apparatuses[70,71] in the design of the gas burette and the manometer. The latter utilizes a simple electrical contact indicator originally described by Mills[72] for adjusting the mercury levels at a fixed reference point.

Barr and Anhorn[70] and Constabaris et al.[71] give a detailed description of design and construction and their material will not be reproduced here. The apparatus of Rutledge, Kohnke, and Cunningham[68], with the changes in gas burette and manometer design, is shown diagrammatically in Figure 4.

The Adsorption System

The gas burette consists of five bulbs which are connected in parallel, in contrast to the standard design in which the bulbs are connected in series. This way each bulb can be filled or emptied independently of the others and with five bulbs it is possible to obtain as many as 32 points, instead of only six with the bulbs is series, before the system
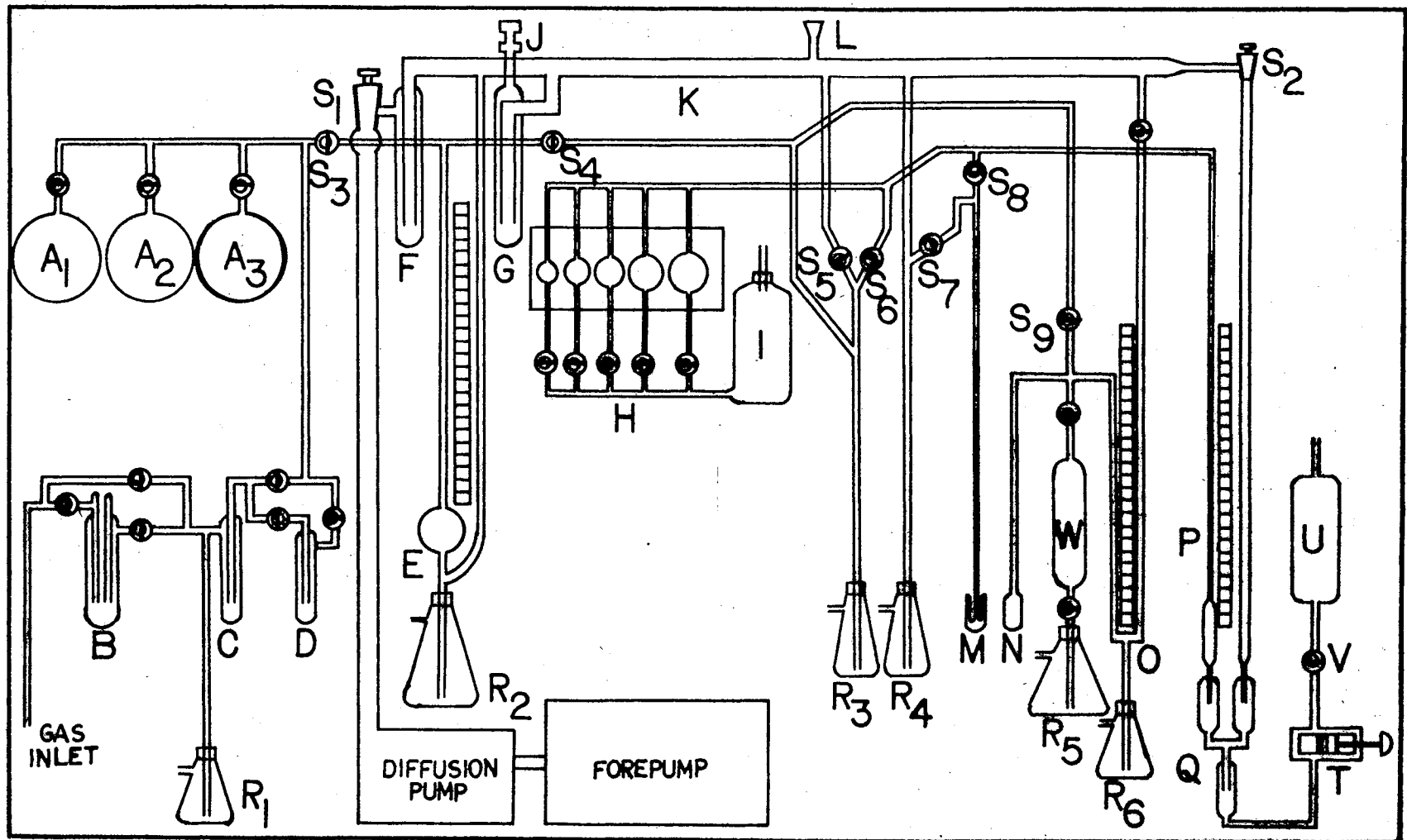
Figure 4. Complete Diagram of the Adsorption Apparatus

Legend for Figure 4

A_1, A_2, A_3 . . Gas storage bulbs for helium, nitrogen, and hydrogen

B . . . . Hot copper trap (350°C)

C . . . . Glass-bead trap (78°K)

D . . . . Silica gel trap (78°K)

E . . . . Toeppler pump

F, G. . . . . . Liquid nitrogen traps

H . . . . Gas burette

I . . . . Mercury reservoir for burette bulbs

J . . . . Cold cathode vacuum tube

K . . . . High vacuum manifold

L . . . . Hastings vacuum gauge

M . . . . Sample bulb

N . . . . Vapor pressure cold bulb

O . . . . Vapor pressure manometer

P . . . . Constant volume manometer

Q . . . . Filter bulbs for main manometer

T . . . . Level adjust for main manometer

U . . . . Mercury reservoir for main manometer

V . . . . Valve for mercury flow into manometer

W . . . . Pressurizing pump for vapor pressure device

S_1 to S_9. . . Isolation stopcocks

R_1 to R_6. . . Mercury reservoirs

is recharged with gas. The volume of each bulb is very nearly twice as large as the volume of each preceeding bulb. The actual volumes of the various bulbs in the burette were determined before the apparatus was assembled by measuring the mass of mercury required to fill each bulb between two reference marks and then calculating the volume from the density of mercury at the appropriate temperature. Starting with the smallest bulb these volumes are equal to 6.994, 15.538, 31.686, 66.904, and 125.806 cm^3, respectively. A water bath is placed around the bulbs and a thermometer is used to monitor the temperature.

The manometer is built so that the pressure side is always at the same level for all the readings. This way a constant volume is maintained in the adsorption system. The mercury level is adjusted approximately by applying pressure or vacuum at the top of the stainless steel mercury reservoir. The finer adjustment is accomplished by means of a small O-ring sealed piston as indicated on the electron ray tube of the contact indicator. A wooden case with a glass front encloses the manometer. The mercury levels become more distinct by a fluorescent light behind the mercury columns and shining through a vertically movable slotted panel. A precision meter bar in graduations of a tenth of a centimeter is placed between the manometer columns for the pressure measurements. The height of both mercury levels is obtained by a cathetometer located about six feet from the manometer and capable of reading to a thousandth of a centimeter. The temperature of the area surrounding the manometer is read on a thermometer placed in the wooden casing.

The adsorption bulb or sample holder must be designed in such a way as to have as low a free volume as possible. The sample bulb used with the present apparatus was constructed with the above requirement in mind.

It is located at point M of Figure 4. The figure also shows that the seal above the sample must be made far enough away from it in order to avoid excess heating of the sample.

The Auxiliary Equipment

The high vacuum system consists of the main manifold at K (see Figure 4) with the two liquid nitrogen traps at F and G. The latter functions as the cold trap for the "Cold Cathode Vacuum Tube" at J. The main stopcock, S_1, isolates the system from the oil diffusion pump and the forepump.

The gas reservoirs can store at the same time as many as three different gases at a pressure of about one atmosphere as regulated by the overflow bubbler at R_1. The purification traps are used primarily for the removal of oxygen and moisture from the adsorbate gases before they are admitted into the storage bulbs. The Toeppler pump at E is employed to transfer gas into the adsorption system at a known pressure obtained from the auxiliary manometer incorporated into the pump.

The vapor pressure thermometer consists of a simple manometer, a mercury bulb used to pressurize the gas, and a bulb located adjacent to the sample at N in the low temperature bath. By exerting pressure on the gas until it partially liquefies in N the vapor pressure of the adsorbate can be read directly from the manometer.

The degassing of the adsorbent to clean its surface consists of the usual procedure of heating the sample under high vacuum. This is accomplished by a small copper tube furnace large enough to go over the sample tube and controlled by a variac. The outgassing temperature is obtained by a mercury thermometer placed between the sample bulb and the furnace.

Baths for the Liquid Refrigerants

When the apparatus is used to obtain the nitrogen adsorption iso-
therm of the stannic oxide gel a liquid nitrogen bath is employed to
keep the sample at the proper temperature. A wide-mouth Dewar flask is
used to hold the liquid nitrogen. The flask is placed in a protective
brass jacket with port windows and it is strip-silvered so that the
liquid level can be measured and used subsequently in the determination
of the free volume in the adsorption bulb. For this reason the level of
the liquid refrigerant is to be kept as constant as possible. In order
to maintain the temperature of the bath constant a loose-fitting cover
with holes to admit the sample bulb and the vapor pressure thermometer
bulb may be used very effectively.

In the particular case when the apparatus is used to determine the
hydrogen adsorption isotherm of the sample at the temperature of the
liquid hydrogen a modification of the low temperature bath is necessary
because of the change in refrigerants. Liquid hydrogen is quite danger-
ous if not properly handled. Therefore, a system of double Dewars was
constructed which was completely closed to the atmosphere in the room
and vented to the outside. The double-Dewar arrangement is protected by
a brass cylindrical jacket with port windows, as previously, for observ-
ing the liquid level. The complete system is shown in Figure 5.

The outside Dewar contains liquid nitrogen and the inside one liquid
hydrogen. Both inner and outer Dewars are strip-silvered and the un-
silvered strip runs the total length of the column. The brass cylindri-
cal jacket may be completely airtight, if necessary, and O-ring seals
may be used. The inner Dewar is supported from the top, as shown in
Figure 5, and it is vacuum-tight so that no hydrogen gas can escape to
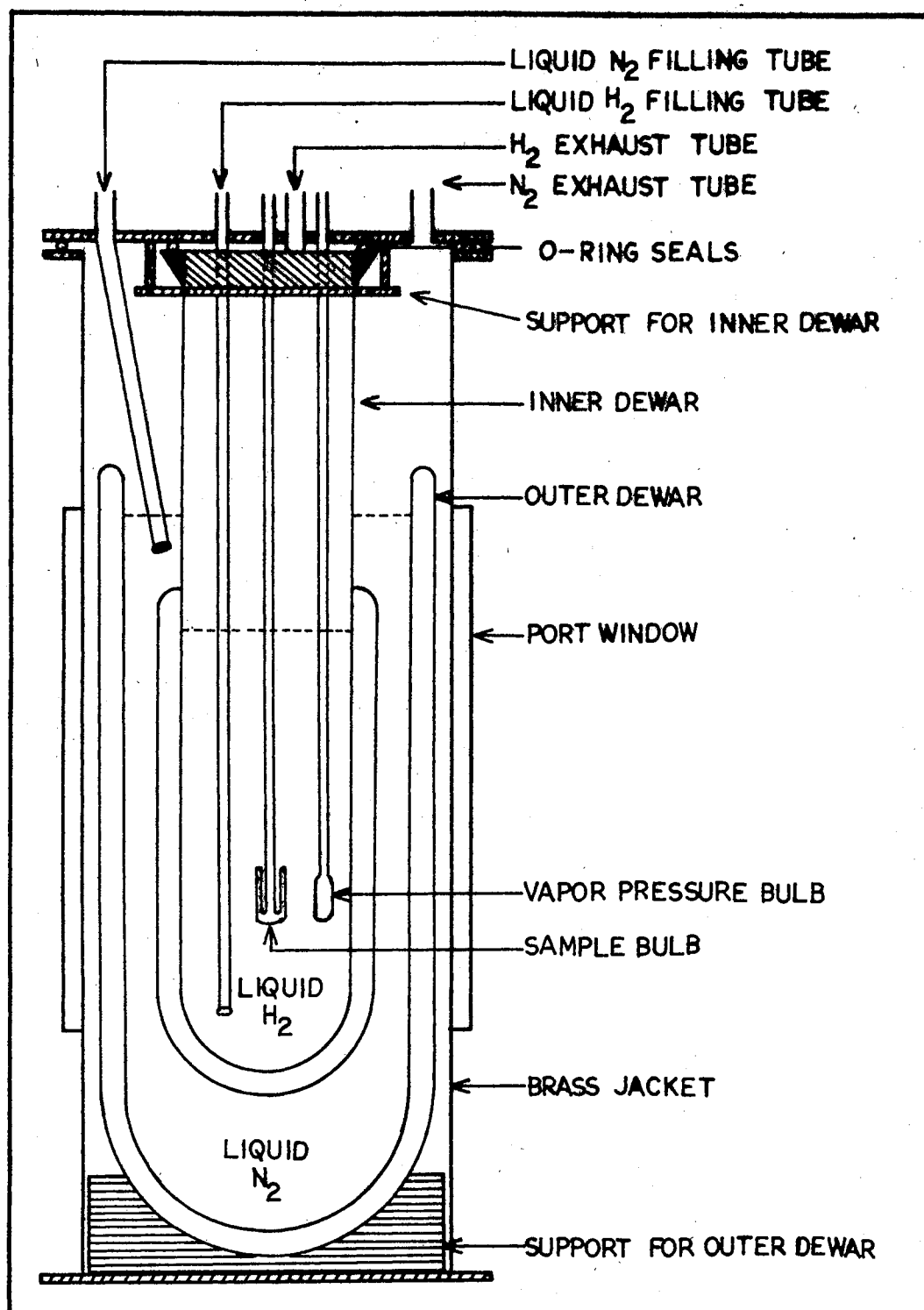
Figure 5. Liquid Hydrogen Bath

the room during evaporation of the liquid. A special flexible liquid hydrogen transfer tube is used to fill the inner Dewar. All evaporating liquid is vented to the outside through the "Hydrogen Exhaust Tube".

In addition to the various components of the apparatus shown in Figure 4 an auxiliary manifold is employed for raising and lowering the mercury levels in the reservoirs R_2 through R_6. This is accomplished by connecting one side of the manifold to a compressed gas cylinder (usually nitrogen) for raising the levels and the other to an auxiliary vacuum pump for lowering them.

With the exception of the manometer reservoir U which is made out of stainless steel, the rest of the adsorption apparatus is constructed out of pyrex glass tubing. The main vacuum manifold is made of 1" diameter pyrex tubing. The adsorption system consists of 2 mm standard capillary tubing so as to minimize the free volume. The remaining tubing is nearly all 10 mm pyrex with the exception of the constant volume manometer. Its complete right side and the bottom part of the left side where the zero reference point is located are constructed of the same piece of 1/2" precision bore tubing in order to reduce meniscus effects to a minimum. The three gas reservoirs are constructed from 6-liter Florence flasks.

CHAPTER V

THE EXPERIMENTAL TECHNIQUE

Start-up Procedure of the Adsorption Apparatus

The adsorption apparatus already described and presented in Figure 4 was designed to be of a permanent nature. At first glance the entire system appears quite complicated. It is, however, quite simple since it consists of several completely isolated or semi-isolated components each of which is of the simplest design and can be used very easily.

After the sample is weighed, placed in the adsorption bulb and attached to the system at M the first task is to test the capacity of the completed apparatus to hold a high vacuum. The mercury level in all the reservoirs is kept at the lowest position. In the five bulbs of the gas burette the mercury in container I is adjusted until it reaches the lower reference marks of the five capillaries just above the stopcocks. In the main manometer the mercury remains in the reservoir U with the valve leading to the two columns (valve V) kept closed. All other stopcocks remain opened except the main stopcock, S_1, which is used to isolate all the parts of the apparatus from the vacuum pumps. This stopcock is kept closed.

The fore-pump is then switched on and the main stopcock is opened just slightly and with great caution. The mercury should start rising very slowly in all the reservoirs except, of course, in the bulbs of the burette and in the columns of the constant volume manometer. When the

highest allowable levels are reached the stopcock is closed and the mercury is lowered back down to the original levels in the reservoirs. This is accomplished through the auxiliary manifold which at this point should be operating on vacuum from the secondary pump. This process of opening and closing the main stopcock is repeated until no more rise is observed in the mercury levels. When this is complete the liquid nitrogen traps at F and G are filled and the oil diffusion pump is switched on and regulated by a variac. The pressure readings are obtained first by a "Hastings Vacuum Gauge" and then by a "Miller Cold Cathode Vacuum Gauge" from the "Cold Cathode" vacuum tube attached on the main manifold at J. If no leaks are present the pressure should be lowered to 10^{-7} or 10^{-8} Torr in about 36 hours.

With the manometer evacuated up to the valve V of the mercury reservoir U it is necessary at this point to fill the manometer columns up to the zero reference mark with mercury. The valve is opened slowly and cautiously and the mercury is let to fill the filter bulbs at Q and then adjusted at zero reference with the O-ring piston at T and the electrical contact indicator. The zero reference point can be located on the meter scale by taking several cathetometer readings until reproducible measurements are obtained.

Filling the Gas Reservoirs

It is now necessary to fill the gas reservoirs with the three desired purified gases, helium, nitrogen and hydrogen. The gas reservoirs and the purification system are isolated from the other parts by closing the appropriate stopcock, S_3. The hot copper trap B is maintained at $350^\circ C$ while the glass-bead trap C and the silica gel trap D are at liquid

nitrogen. The hot copper is used to remove all but the last few hundredths of a percent of the oxygen contained as impurity in the helium and nitrogen gases. Removal of oxygen from the hydrogen gas is accomplished by passing the hydrogen through a catalytic purifier (Hydrogen Deoxo Purifier) and not through the hot copper trap which in this case is bypassed. The two cold traps are used to remove moisture from all three gases.

One by one the three reservoirs are filled with helium (A_1), nitrogen (A_2), and hydrogen (A_3). In each case before the next gas is admitted into a storage bulb the system is evacuated to remove the previous gas from the traps and the gas tubing. The depth of the relief tube (overflow bubbler) at R_1 regulates the maximum pressure at which the gas may be stored in a reservoir. This maximum pressure is about one atmosphere.

The degassing of the sample may proceed simultaneously with the filling of the storage bulbs since evacuation of the rest of the system continues. The sample is usually heated up to about $200^{\circ}C$ by means of the small copper tube furnace under vacuum (about 10^{-7} Torr) for approximately two hours. This is generally sufficient to drive off adsorbed water vapor which is the only substance likely to cause any trouble.

Calibration With Helium

The apparatus is now ready for calibration with helium. Starting at the left of Figure 4 the mercury in R_2 is raised to fill up the bulb of the Toeppler pump E by employing the auxiliary manifold connected to the pressurized gas cylinder. In reservoir R_3 the mercury is raised to just below the connection leading to the Toeppler pump and the gas res-

ervoirs. Stopcock S_5 is closed, thus eliminating the vacuum pumps.
Stopcock S_6, for filling the main adsorption system, remains opened.
The mercury in reservoir R_4 is raised to a position just above stopcock
S_7, which is then closed. The mercury will remain at that position
throughout the experiment. Stopcock S_8, leading to the sample bulb, and
S_9, used to isolate the vapor pressure system, are closed.

With the manometer set at the zero reference point helium gas is
admitted into the adsorption system from reservoir A_1. The level of
mercury in the left arm of the Toeppler pump will descent and a rise
will be observed in the right arm. This gives an approximate measure of
the amount of helium introduced into the system. Caution must be exer-
cised not to lower the mercury below the joint of the Toeppler pump be-
cause the gas will be drawn by the vacuum pump through the right arm and
will be lost. Also, mercury may bubble into the manifold. The level in
reservoir R_3 will descent and again no gas should escape. It is advisa-
ble to let just enough gas into the system so that the pressure in the
main manometer will be about two to three centimeters when the left arm
is adjusted to the zero reference point. Now all five burette bulbs are
filled with helium. After the reference adjustment is complete the
manometer reading is taken with the cathetometer. Five more pressure
readings are taken by successive filling of the burette bulbs with mer-
cury starting with the largest one.

The gas is then returned to the bulbs by withdrawing the mercury
and the sample stopcock S_8 is opened. Six more manometer readings are
taken as before. Thus, a total of twelve pressure readings may be ob-
tained, six with the sample stopcock closed and six with the stopcock
opened. The helium gas is then evacuated from the system and a few more

reference checks may be taken.

It is worth noting that the calibration may be carried out with the sample bulb either at room temperature, at liquid nitrogen, or at liquid hydrogen. Also, after each manometer reading, the temperature of the burette bulbs, room, manometer, and sample must be obtained, as well as the level of the liquid refrigerant in the bath.

<center>Adsorption and Desorption Data</center>

After all the helium has been evacuated the apparatus is ready for the main adsorption run. The sample stopcock is closed. If the nitrogen adsorption isotherm is to be determined, nitrogen gas is admitted into the system from reservoir A_2 by the same procedure as in the case with helium. The sample and vapor pressure bulbs are maintained at the temperature of liquid nitrogen. If hydrogen gas is the desired adsorbate, then it is transferred into the system from reservoir A_3 with the bulbs kept at the temperature of liquid hydrogen. In each particular case the vapor pressure thermometer assembly is filled with the proper gas (nitrogen or hydrogen) at the corresponding temperature.

The vapor pressure system, which is already evacuated, is filled with gas as follows: the Toeppler pump contains gas at a pressure of about three-fourths of an atmosphere, stopcock S_6 is closed so that the burette and manometer are isolated, the mercury in the vapor pressure manometer O is raised to its highest possible point, and the stopcock just below the pressurizing bulb W is kept closed while that just above W remains open. Stopcock S_9 is slowly opened and the gas enters bulb W. At the same time the mercury level in the left arm of the manometer is pushed down and caution must be exercised not to bubble the gas through

the right arm and into the manifold. After bulb W is filled stopcock S_9 is closed and the mercury in the manometer is raised again. By applying pressure to the mercury in the reservoir of the pressurizing pump the gas is pushed into the vapor pressure bulb N and the manometer O. When the pressure is about atmospheric, as indicated by the manometer, the gas in the vapor pressure bulb will start to liquefy. If, by allowing more gas into the bulb N, no change is observed in the mercury levels of the manometer then it means that the point of measuring the vapor pressure has been reached.

The burette bulbs being filled with the adsorbate gas and the sample stopcock closed a pressure reading is taken, then followed by two or three more readings by pushing mercury into each appropriate bulb and forcing a known amount of gas into the manometer. The gas is then returned to the bulbs and the stopcock S_8 of the sample is opened. At this point adsorption is in progress. Before every pressure reading the adsorbate is allowed to come to equilibrium with the solid surface for about three minutes. Similar readings are obtained until the burette bulbs are emptied of gas and filled with mercury. It is necessary at this point to admit more of the adsorbate into the system. Therefore, the sample is again isolated, the mercury withdrawn from the bulbs, and several pressure measurements obtained in order to determine the new amount of gas. The sample stopcock is opened and adsorption proceeds as previously. More readings are taken and more adsorbate gas admitted into the system until the equilibrium pressure, P, of the adsorbed phase reaches a value nearly equal to the vapor pressure, P_o, of the adsorbate. In other words, adsorption is discontinued when the relative pressure P/P_o reaches a value close to unity.

After adsorption is complete it is customary to obtain the desorption isotherm in order to determine the presence or absence of hysteresis. With the sample stopcock opened adsorbate is removed from the surface in the amount dictated by the filling of each burette bulb. When the point is reached at which all bulbs are filled with gas the sample is isolated and adsorbate is withdrawn from the adsorption system by opening stopcock S_5. Pressure readings are taken to determine the amount of gas remaining in the system. All bulbs are then filled with mercury, the sample stopcock is opened, and gas is removed from the surface and into the burette by withdrawing the mercury from the bulbs. This process is repeated until desorption is complete and then the entire system is evacuated.

During adsorption, as well as desorption, the temperature of the burette bulbs, room, manometer, sample and vapor pressure bulbs must be obtained after every manometer pressure reading. Measurement of the vapor pressure and the level of the liquid in the bath are also necessary. The low temperature bath must be recharged with refrigerant from time to time so as to be maintained at as much a constant level as possible.

The shut-down procedure is quite simple. The liquid nitrogen dewars are removed from the traps, and so is the bath, thus allowing the two traps and the sample to reach room temperature. The stopcock of the main manifold leading to the vacuum pumps is closed and all the mercury levels in the various reservoirs are raised. Air is then allowed to enter the lines from the "Gas Inlet" of the purification system. The mercury levels will descend until they reach their lowest constant position. At this point the system is at atmospheric pressure. The pumps are

switched off and the main stopcock S_1 is opened thus bringing the entire adsorption apparatus to normal atmosphere.

<center>Materials Used</center>

The stannic oxide (SnO_2) used in this study is prepared in the form of the gel. Stannic oxide gels were an object of study in the period from 1915 to 1932 under the name of stannic acids. Such compounds were prepared as early as 1898 by Zsigmondy[73]. Subsequent preparations of the gel under the name of stannic hydroxide abound in the literature[74,75,76,77,78]. The method used in preparing the gel for this study is closely similar to that reported by Goodman and Gregg[79]. It is based upon the hydrolysis of stannic ethoxide and the gel obtained is considered to be "ion free".

For the preparation of the gel clean metallic sodium is slowly dissolved in a large excess of absolute ethyl alcohol. To the resulting solution of sodium ethoxide in alcohol the proper amount of an alcoholic solution of anhydrous stannic chloride is added. The mixture is refluxed for approximately 36 hours, resulting in the formation of stannic ethoxide (stannic tetraethylate) in the alcohol solution and sodium chloride precipitate. The mixture is filtered to remove the precipitated sodium chloride which is insoluble in alcohol. The filtrate containing the stannic ethoxide is poured into an excess of distilled water from which the SnO_2 gel precipitates slowly. The gel is let to settle and the supernatant liquid is removed by siphoning. The precipitate is washed repeatedly with distilled water in order to remove chloride ions and then it is dried overnight at $110^{\circ}C$.

The preparation of the gel is carried out in three steps which may

be represented in equation form as follows:

$$4 \ C_2H_5OH + 4 \ \underline{Na} \longrightarrow 4 \ C_2H_5ONa + 2 \ H_{2(g)}$$

$$4 \ C_2H_5ONa + SnCl_4 \longrightarrow Sn(OC_2H_5)_4 + 4 \ \underline{NaCl}$$

$$Sn(OC_2H_5)_4 + x \ H_2O \longrightarrow \underline{SnO_2 \cdot nH_2O} + 4 \ C_2H_5OH + y \ H_2O$$
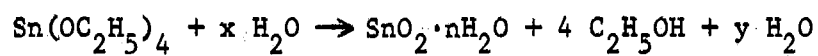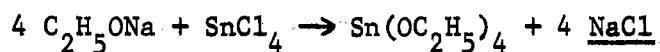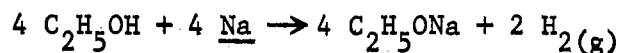
In the above equations the ethyl alcohol and water used are in excess.

For the calibration and adsorption experiments high grade helium and nitrogen gases were used from the regular compressed gas cylinders. They were further purified when passed through the purification train, as described earlier in this chapter. For hydrogen adsorption "Ultra Pure" hydrogen gas was used which was obtained from the Matheson Company. The liquid hydrogen refrigerant was obtained from Linde, Division of Union Carbide, Amarillo, in a special 50-liter liquid hydrogen dewar. Linde also provided the transfer tube.

CHAPTER VI

THE TREATMENT OF THE DATA

Analysis of the Adsorption Data

Having already obtained the data in the manner discussed in Chapter
V it is now necessary to present the method by which they can be conven-
iently analyzed. Such an analysis could present some difficulties and
it is the purpose of this Chapter to clarify a number of points, discuss
the concepts of certain corrections utilized, and introduce a convenient
and concise method by which the data can be treated.

Before a detailed discussion is presented it is advisable to define
a system of units to express the data and the results. For consistency
with other work in this field volumes are measured in cm^3, pressures in
cm of mercury, and temperatures in degrees Kelvin. Thus, the most con-
venient unit for an amount of gas is cm^3 at S.T.P. With this convention
it is proper to consider an amount of gas as a volume.

The P-V-T relations are obtained from the ideal gas law which is
normally valid at low pressures and ordinary temperatures. The only two
exceptions occur with nitrogen and hydrogen at their corresponding liquid
temperatures in the adsorption bulb. The deviation from ideality, how-
ever, can be rectified by introducing a correction factor when necessary
without disrupting the overall scheme of analysis. By applying the ideal
gas law the amount V of a gas at S.T.P. in a volume V_i at temperature T_i

and pressure P_i is given by:

$$V = V_i \cdot \frac{P_i}{76} \cdot \frac{273.16}{T_i} \qquad (58)$$

or

$$V = [V_i \cdot \frac{273.16}{76}] \cdot \frac{P_i}{T_i} \qquad (59)$$

Usually it is convenient to define the quantity in brackets as a "volume factor", f_i, as:

$$f_i = V_i [\frac{273.16}{76}] \qquad (60)$$

Thus, for any amount of gas in the system for which the pressure and temperature have been determined, V at S.T.P. is given by:

$$V = f_i [P_i/T_i] \qquad (61)$$

and the total amount of gas contained in "n" different volumes is:

$$V_{total} = \sum_{i=1}^{n} (f_i) [P_i/T_i] \qquad (62)$$

The volume of gas in the adsorption system can be easily evaluated provided enough information is known. Referring to Figure 4 it can be seen that different portions of the system are at different temperatures. This makes it necessary to consider each portion, with its corresponding volume, separately. The adsorption system in the present case consists of four different volumes: 1) V_1, the volume of the gas burette consist-

ing of the five calibrated bulbs, 2) V_2, the volume of the connecting capillary to the manometer and the sample isolation stopcock, S_8, 3) V_3, the volume of the capillary between stopcock S_8, the mercury level above stopcock S_7, and the liquid nitrogen or liquid hydrogen level in the sample dewar, and 4) V_4, the free volume in the sample bulb up to the level of the liquid refrigerant.

When the sample stopcock S_8 is closed volumes V_1 and V_2 are always under the same pressure, hence $P_1 = P_2$. Similarly, $P_3 = P_4$. With S_8 open all the volumes are under the same pressure. Temperature gradients may exist in some portion of each volume. Usually, they are either small enough to be neglected or the associated volume is small leading to a correspondingly small error. This is true in the case of V_3 where a temperature change of over $200^{\circ}C$ exists. However, a small error in calculating f_3 will be compensated for by calibration appearing as a change in the value of f_4.

In the course of an adsorption experiment three of the volumes (V_2, V_3, and V_4) remain unchanged. Only volume V_1, which is the independent variable, changes. From the design of the gas burette it is possible to have as many as 32 changes in volume V_1. Thus, it is convenient to construct a table of the 32 possible values of V_1 and the corresponding values of the volume factor f_1 with the associated bulb settings. Such a table is shown in Appendix B. Also included in the appendix is the calculation of the volume of each of the five bulbs of the gas burette.

The data for both the calibration and the main adsorption run will be taken with the sample stopcock S_8 either opened or closed and with a known volume of gas (possibly zero) in V_3 and V_4 in the latter case. When S_8 is open the pressure is the same for all four volumes and the

total volume of gas in the system for the $\underline{i}$th point is given by:

$$(V_{total})_i = [\frac{(f_1)_i}{(T_1)_i} + \frac{f_2}{(T_2)_i} + \frac{f_3}{(T_3)_i} + \frac{f_4}{(T_4)_i}] P_i \tag{63}$$

In the second case with S_8 closed the last two terms in Equation (63) will be constant (possibly zero).

During the analysis of the data the manometer must be corrected to standard readings because of temperature, local gravity, and meniscus effects. Meniscus effects may be omitted since both sides of the mano- meter are constructed of the same precision bore tubing which reduces these effects to a minimum. The temperature and local gravity correc- tions may be combined and a table representing local conditions may be constructed. Such a table[80] consists of the temperature and the cor- responding correction factor by which the measured pressure must be multiplied in order to give the true pressure. Both the equilibrium pressure of the adsorbed phase, P, and the vapor pressure, P_o, are cor- rected at the appropriate temperature. These correction factors range from 0.99543 at 20°C to 0.99359 at 31°C.

At the beginning of calibration with helium the sample stopcock is closed and the system is governed by Equation (64), i.e.,

$$(V_{total})_i = [\frac{(f_1)_i}{(T_1)_i} + \frac{f_2}{(T_2)_i}] P_i = constant \tag{64}$$

which is obtained from Equation (63) with the last two terms on the right set equal to zero, since there is no gas in volumes V_3 and V_4.

In Equation (64) the term $[(f_1)_i/(T_1)_i] P_i$ is equal to the volume $(V_1)_i$ in the bulbs. By knowing the temperature of the burette bulbs,

$(T_1)_i$, at every P_i this volume can be calculated from:

$$(V_1)_i = [(f_1)_i/(T_1)_i] \, P_i \qquad (65)$$

which holds true regardless as to whether the sample stopcock is opened or closed.

Rearrangement of Equation (64) yields:

$$\frac{(f_1)_i}{(T_1)_i} \cdot P_i = (V_1)_i = (V_{total})_i - \frac{f_2}{(T_2)_i} \cdot P_i \qquad (66)$$

from which if a plot of $[(f_1)_i/(T_1)_i] \cdot P_i$ or $(V_1)_i$ versus P_i is made will give a straight line the slope of which is $-(f_2)/(T_2)_i$ and f_2 may be determined. Actually f_2 is not necessary. It is the value of $f_2/(T_2)_i$ which is needed to calculate $(V_2)_i$ at the various P_i's from:

$$(V_2)_i = [f_2/(T_2)_i] \, P_i \qquad (67)$$

The quantity f_3 and subsequently $f_3/(T_3)_i$ must be calculated from geometrical data. This is accomplished by measuring the length of the 2 mm I.D. standard capillary tubing from the sample stopcock to the level of the refrigerant and then determining its volume. The value of f_3 is obtained from the general Equation (60) in the form:

$$f_3 = V_3 \cdot (273.16/76) \qquad (68)$$

and then $f_3/(T_3)_i$ can be calculated with $(T_3)_i$ being the room temperature. The volume $(V_3)_i$ is then given by:

$$(V_3)_i = [f_3/(T_3)_i] \, P_i \qquad (69)$$

With the sample stopcock open the value of f_4 or $f_4/(T_4)_i$ is calculated from Equation (63) in the form:

$$[\frac{(f_1)_i}{(T_1)_i} + \frac{f_2}{(T_2)_i} + \frac{f_3}{(T_3)_i}] \, P_i = (V_{total})_i - \frac{f_4}{(T_4)_i} \cdot P_i \tag{70}$$

or

$$(V_1)_i + (V_2)_i + (V_3)_i = (V_{total})_i - \frac{f_4}{(T_4)_i} \cdot P_i \tag{71}$$

If the left hand side of Equation (71), $[(V_1)_i + (V_2)_i + (V_3)_i]$, is plotted against P_i a straight line will result the slope of which is equal to $-f_4/(T_4)_i$ and from which f_4 can be obtained. The value of the volume $(V_4)_i$ is then calculated from:

$$(V_4)_i = [f_4/(T_4)_i] \, P_i \tag{72}$$

All the volume factors are determined in this manner and the calibration is complete.

In analyzing the adsorption data the volume of gas introduced into the system is determined with the sample stopcock closed, and it is the sum of $(V_1 + V_2)$. When the system is recharged with gas the total volume is given by the sum of all four volumes plus the volume of gas adsorbed, $V_{ads.}$, on the sample, as:

$$V_{total} = V_1 + V_2 + V_3 + V_4 + V_{ads.} \tag{73}$$

The volume of gas adsorbed is given by the difference between the total volume of gas placed in the system and the amount remaining in the gas phase for the ith point as measured by the sum of $(V_1)_i + (V_2)_i +$

$(V_3)_i + (V_4)_i$. Thus:

$$(V_{ads})_i = V_{total} - [(V_1)_i + (V_2)_i + (V_3)_i + (V_4)_i] \qquad (74)$$

The amount of gas in the sample bulb at the temperature of the liquid refrigerant deviates from ideality so the necessary correction must be made to the pressure before the volume $(V_4)_i$ can be evaluated. In the case of N_2 adsorption at liquid nitrogen the measured pressure is multiplied by the correction factor $(1 + 0.05P/76)$ obtained by Emmett and Brunauer[35,36]. The corrected volume would then be:

$$(V_4)_i = \frac{f_4}{(T_4)_i} \cdot P_i \cdot (1 + \frac{0.05\ P_i}{76}) \qquad (75)$$

For hydrogen adsorption, on the other hand, at liquid hydrogen the correction to the pressure is found to be $(1 + 0.077P/76)$ and the corrected volume, $(V_4)_i$, is given by:

$$(V_4)_i = \frac{f_4}{(T_4)_i} \cdot P_i \cdot (1 + \frac{0.077\ P_i}{76}) \qquad (76)$$

In order to obtain the adsorption isotherm the data are plotted as volume adsorbed, $V_{ads.}$, against the relative pressure, P/P_o.

The surface area from the BET theory is determined from the plot of $(P/P_o)V_{ads.}(1 - P/P_o)$ versus P/P_o in accordance with Equations (24) and (27) or (28) of Chapter II. The BET constant c can be evaluated next and the "net" heat of adsorption is obtained from Equation (30).

The tabular form for taking and analyzing the adsorption data is given in Appendix C.

From the analysis of the data the volume of gas adsorbed is given in cm^3 at S.T.P. for the specific amount of adsorbent used. For highly porous solids 0.2 to 0.5 g is a convenient sample size. Both adsorption isotherms are obtained with the same amount of SnO_2 gel. The weight of the sample used is 0.3574 grams. The volume adsorbed is then converted to cm^3 at S.T.P. per one gram of adsorbent and plotted against P/P_o to give the standard adsorption isotherms.

Evaluation of the Pore-Size Distribution Curves

The data from the BET nitrogen and hydrogen adsorption isotherms along with the corresponding surface areas are used to compute the pore-size distributions of stannic oxide gel. The pores in SnO_2 are assumed to be "slit-shaped" instead of circular so the parallel-plate model of De Boer and co-workers[58,59,60,61] is employed as representing a more realistic physical picture. This model has already been developed mathematically in Chapter III. At this point only a brief explanation of the treatment of the data will be presented.

The standard adsorption-desorption isotherms are plotted on an expanded scale and then divided into equal increments of the relative pressure. (When equations are used in the subsequent discussion, the equation appearing first refers to the nitrogen adsorption isotherm while that appearing second refers to the hydrogen adsorption isotherm). The volume of gas adsorbed in cm^3 per gram of adsorbent corresponding to each of the pressure increments is read from the graph and used to calculate the values of the statistical thickness, t, from Equations (54) or (55). The values of the Kelvin radius, r_k, are calculated from Equations (50) and (51), where P/P_o values are taken as the relative pres-

sure increments. To evaluate the pore-wall separation, d, at each P/P_o Equation (47) is employed. The liquid volumes are computed by multiplying the values of $V_{ads.}$ by 0.001548 for nitrogen and by 0.001266 for hydrogen. This factor is simply the ratio of the gas density to the liquid density of the adsorbate and it is used to convert the volume of gas in cm^3 at S.T.P. to the volume of liquid in cm^3 at its normal boiling point. For nitrogen the density of the gas is 0.0012506 g/cm^3 and that of the liquid is 0.808 g/cm^3. For hydrogen the gas and liquid densities are 0.0000899 g/cm^3 and 0.071 g/cm^3, respectively[81].

The volume of liquid desorbed between two consecutive pressure increments is given ΔX_{x_i} from Equation (39); it is, however, obtained by progressive subtraction of each liquid volume from the succeeding one. ΔX_{x_i} represents the uncorrected volume distribution for physical adsorption and it is used to calculate the corrected volume of liquid desorbed. To do so, it is necessary first to evaluate the two correction factors R_{x_i} and R'_{x_i} from Equations (42) and (43), respectively.

Computation of the corrected liquid volume ΔV_{x_i}, the cumulative pore volume $\Sigma \Delta V_{x_i}$, the area ΔS_{x_i} of the group of pores of mean width d_{x_i}, and the cumulative pore area $\Sigma \Delta S_{x_i}$ must be made from the bottom to the top, from the largest to the smallest group of pores.

Evaluation of ΔV_{x_i} is made from Equation (44). For the very last (first from the bottom) group of pores, which are also the largest in size this equation becomes:

$$\Delta V_{x_i} = R_{x_i} \cdot \Delta X_{x_i} \qquad (77)$$

For the other pores the complete equation is used and the cumulative area $\Sigma \Delta S_{x_{i-1}}$ of all the pores of mean width larger than $d_{(x_i + \Delta x)}$ is employed to calculate the correction to the volume of the next lower group of pores of mean width d_{x_i}, etc. The surface area of a group of pores at any x_i is given by Equation (33) rearranged to yield:

$$\Delta S_{x_i} = \frac{2 \Delta V_{x_i}}{d_{x_i}} \cdot 10^4 \qquad (78)$$

The presence of the factor 10^4 in Equation (78) is necessary in order to express ΔS_{x_i} in m^2/g, because ΔV_{x_i} is given in cm^3/g and d_{x_i} in angstroms, A. Consequently, when ΔV_{x_i} is computed the units on $\Sigma \Delta S_{x_{i-1}}$ have to be converted to the original units; therefore, $\Sigma \Delta S_{x_{i-1}}$ is now multiplied by a factor of 10^{-4}.

The cumulative pore volume $\Sigma \Delta V_{x_i}$ and the cumulative pore area $\Sigma \Delta S_{x_i}$ are obtained by the progressive summing of ΔV_{x_i} and ΔS_{x_i}, respectively, from the bottom to the top.

The differential pore-volume and pore-area distribution curves are calculated by dividing all the ΔV_{x_i}'s and ΔS_{x_i}'s, respectively, by the Δd's over which they were determined. Values of Δd at any x_i are obtained from Equation (45). The results are often presented as distribution curves by plotting $\Delta V/\Delta d$ or $\Delta S/\Delta d$ against d_{x_i}. These curves indicate the location of the pore-volume and pore-area maxima and also the range of the pore-wall separation in which most of the adsorption occurs.

It is usually convenient to present pore-size distribution calculations in a tabular form. Such a table will consist of 16 columns and it

is shown in Appendix D.

It was mentioned previously that some quantities were calculated by starting at the bottom of the table (or with the largest group of pores) and proceeding to the top (or towards the smallest group of pores). Such references are made to the tabular form of Appendix D.

CHAPTER VII

EXPERIMENTAL RESULTS

Surface Area

Analysis of the adsorption data according to the discussion in
Chapter VI and the tabular form of Appendix C will give first the adsorp-
tion isotherms and then the BET specific surface areas of the stannic
oxide gel.

For the nitrogen adsorption isotherm at $78^{\circ}K$ the sample consisted
of 0.3574 g of the gel. Degassing was accomplished by heating the sam-
ple at $200^{\circ}C$ and 10^{-8} torr for approximately two hours. Table I shows
the adsorption results in terms of the volume of nitrogen gas adsorbed
in cm^3 at S.T.P. per one gram of SnO_2 gel at the corresponding relative
pressure. The data in this table represent the results of one complete
run (adsorption and desorption). They agree very well with at least two
previous experimental isotherms obtained by Rutledge, Kohnke, and Cun-
ningham[68] and by the author[82]. The nitrogen adsorption isotherm is shown
in Figure 6. This is a Brunauer Type I or Langmuir isotherm with no
hysteresis. The BET plot shown in Figure 7 deviates from linearity at
relative pressures above 0.20. Application of the linear form of the BET
equation to the adsorption isotherm yields a value of the monolayer
volume, V_m, equal to 39.18 cm^3 of N_2 gas at S.T.P. per gram of adsorbent.
The slope of the linear BET plot in Figure 7 is 0.02546 g/cm^3 while the
intercept is 0.00006 g/cm^3. The BET specific surface area is evaluated

TABLE I

VOLUME OF NITROGEN GAS ADSORBED ON SnO_2 GEL AND SURFACE COVERAGE

P/P_o	$V_{ads.}$	θ
0.0072	32.08	0.819
0.0101	33.33	0.851
0.0128	34.48	0.880
0.0157	35.16	0.897
0.0174	35.64	0.910
0.1391	48.16	1.229
0.1804	50.14	1.280
0.2101	51.45	1.313
0.2288	52.14	1.331
0.2383	52.53	1.341
0.2850	54.11	1.381
0.4300	56.30	1.437
0.6910	57.81	1.476
0.8012	58.00	1.480
0.9912	58.55	1.494
0.5257	57.24	1.461
0.3495	55.48	1.416
0.2564	53.11	1.356
0.2183	51.69	1.319
0.1947	50.85	1.298
0.1936	50.79	1.296
0.1683	49.59	1.266
0.1553	49.28	1.258
0.1467	48.59	1.240
0.1308	47.63	1.216
0.0921	45.06	1.150
0.0581	42.15	1.076
0.0355	39.27	1.002

$V_{ads.}$ is expressed in cm^3 at S.T.P. per 1 g of adsorbent.
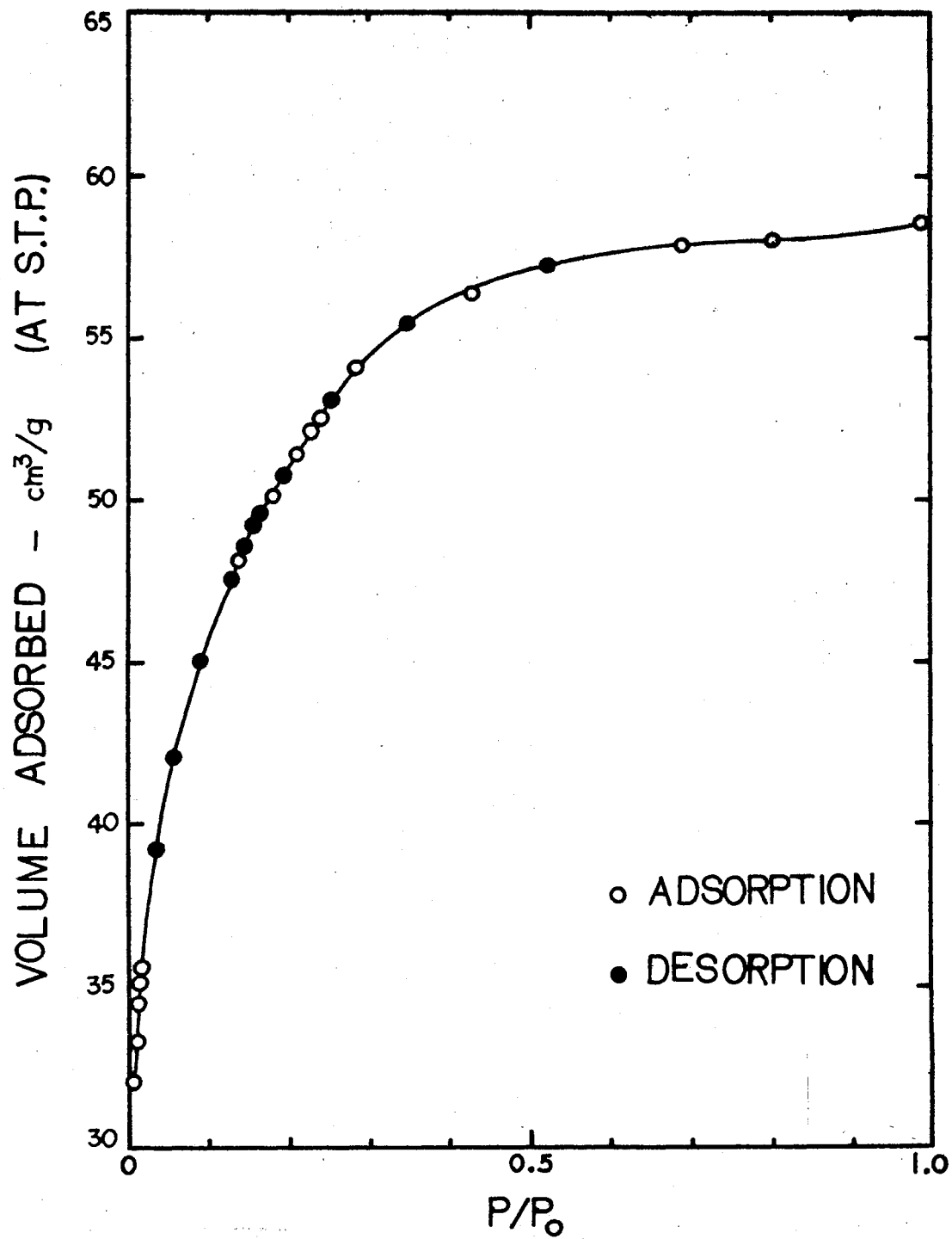
Figure 6. Nitrogen Adsorption Isotherm of SnO_2 Gel at $78^{\circ}K$
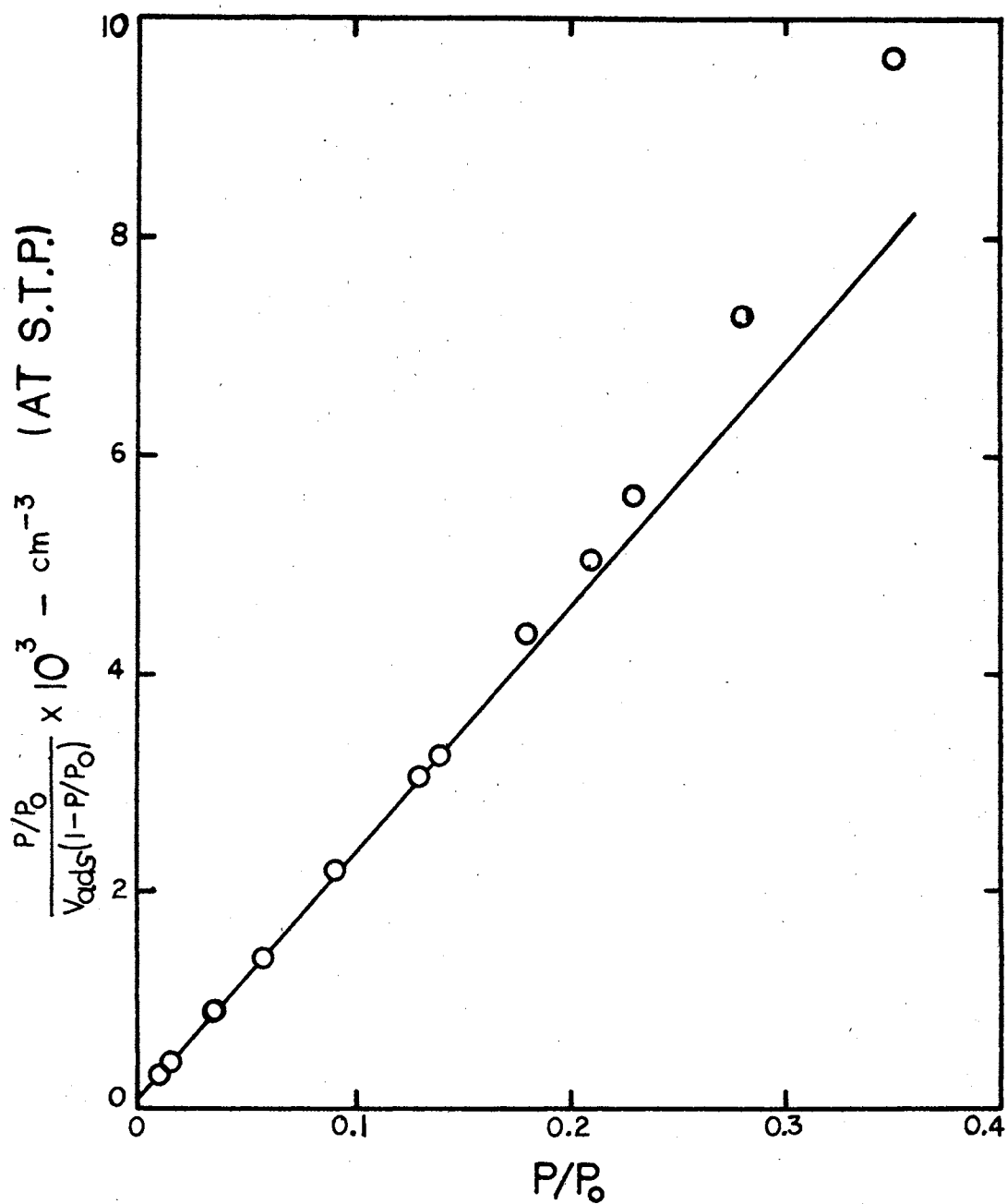
Figure 7.   Linear BET Plot for Surface Area Calculation of
SnO$_2$ Gel From Nitrogen Adsorption Isotherms
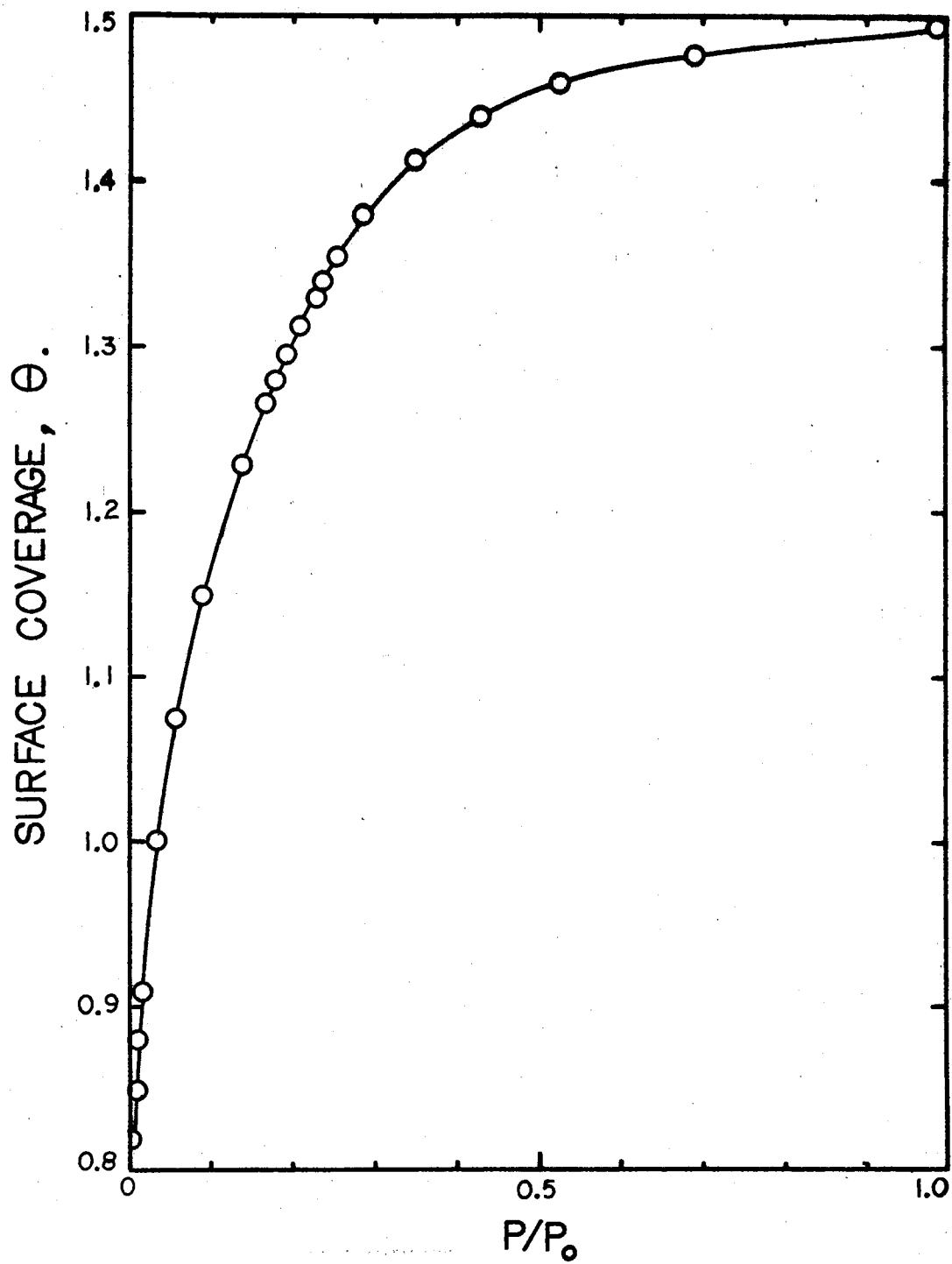
Figure 8.   Surface Coverage of SnO$_2$ Gel vs Relative Pressure of Nitrogen Gas

to be 171.2 m^2/g from Equation (27) as:

$$(S_{BET})_{N_2} = 4.37 \times 39.18 = 171.2 \ m^2/g \tag{79}$$

This value compares very well with those of 173 m^2/g and 172 m^2/g reported by Rutledge, Kohnke, and Cunningham[68] and by Goodman and Gregg[79], respectively, for similarly treated stannic oxide gel.

In addition, the fraction of the surface, θ, covered by the adsorbate is calculated from the equation below:

$$\theta = \frac{V_{ads.}}{V_m} \tag{80}$$

where the symbols have their usual meaning. Values of the surface coverage are shown in Table I and plotted against P/P_o in Figure 8.

In obtaining the hydrogen adsorption isotherm at $20.2^{\circ}K$ the weight of the SnO_2 gel used was the same as previously, i.e., 0.3574 g, and the sample was pretreated in the same manner with degassing taking place at $200^{\circ}C$ and 10^{-8} torr for two hours. The adsorption results are shown in Table II. It should be mentioned that two complete hydrogen adsorption-desorption isotherms were obtained experimentally for reproducibility and as a check of the data. The results of each run were plotted on the same graph and when the curve was drawn all points were located almost exactly on this curve. For this reason experimental points were taken from both runs in such a way as to fill spaces on the isotherm where the pressure increments happened to be too large. Thus, Table II includes data taken from two experimental adsorption isotherms. The hydrogen adsorption isotherm is presented in Figure 9 and it is shown to be a Lang-

TABLE II

VOLUME OF HYDROGEN GAS ADSORBED ON SnO_2 GEL AND SURFACE COVERAGE

P/P_o	$V_{ads.}$	θ
0.0086	59.59	0.909
0.0116	60.88	0.929
0.0130	61.65	0.940
0.0161	62.84	0.959
0.0201	63.98	0.976
0.0618	70.76	1.079
0.0704	71.46	1.090
0.1110	74.36	1.134
0.1630	76.93	1.174
0.1826	78.00	1.190
0.2142	79.07	1.206
0.2319	79.48	1.212
0.2717	80.22	1.224
0.3621	81.74	1.247
0.5504	83.45	1.273
0.7303	84.42	1.288
0.9441	86.08	1.313
0.9662	86.78	1.324
0.8666	85.34	1.302
0.7302	84.43	1.288
0.5506	83.39	1.272
0.3621	81.70	1.246
0.2216	79.00	1.205
0.1946	78.18	1.193
0.1796	77.63	1.184
0.1533	76.65	1.169
0.1273	75.75	1.156
0.1192	74.97	1.144
0.0822	72.61	1.108
0.0562	70.55	1.076
0.0527	69.98	1.068

$V_{ads.}$ is expressed in cm^3 at S.T.P. per 1 g of adsorbent.
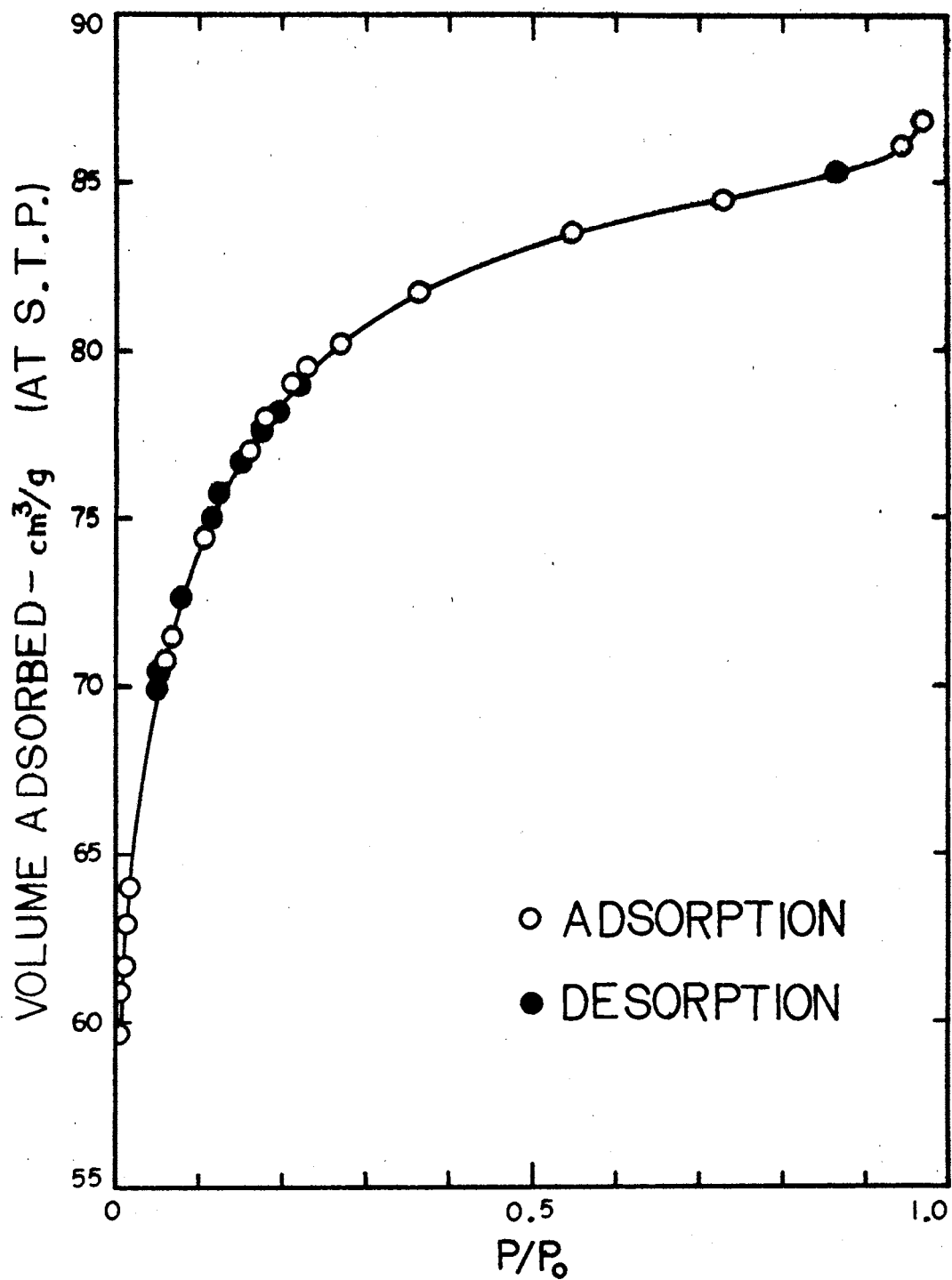
Figure 9. Hydrogen Adsorption Isotherm of SnO_2 Gel at 20.2°K

73

muir or Brunauer Type I isotherm without hysteresis. The BET plot of

Figure 10 deviates from linearity at relative pressures above 0.20. The

slope of this line is 0.015240 g/cm^3 and the intercept is 0.000015 g/cm^3.

The BET monolayer volume, V_m, as calculated from Equation (24) is 65.55

cm^3/g at S.T.P. The specific surface area of the gel has a value of

247.8 m^2/g as evaluated from Equation (28) in the form:

$$(S_{BET})_{H_2} = 3.78 \times 65.55 = 247.8 \ m^2/g \qquad (81)$$

Comparisons in this case are impossible since no value of the specific

surface area of stannic oxide gel from H_2 adsorption data is available

in the literature. Values of the surface coverage for hydrogen adsorp-

tion, as computed from Equation (80), are included in Table II and

plotted against P/P_o in Figure 11.

The value of the BET constant c is calculated from both the slope

and the intercept of the linear plots and the monolayer volume, V_m. From

the slope the equation for c is:

$$c = \frac{1}{1 - sV_m} \qquad (82)$$

while from the intercept:

$$c = \frac{1}{IV_m} \qquad (83)$$

In the case of N_2 adsorption the average value of c is 425 and that

from H_2 adsorption is 1030.

The net heat of adsorption, $E_1 - E_L$, and the heat of adsorption in

the first layer, E_1, can be obtained from Equation (30) rearranged as:
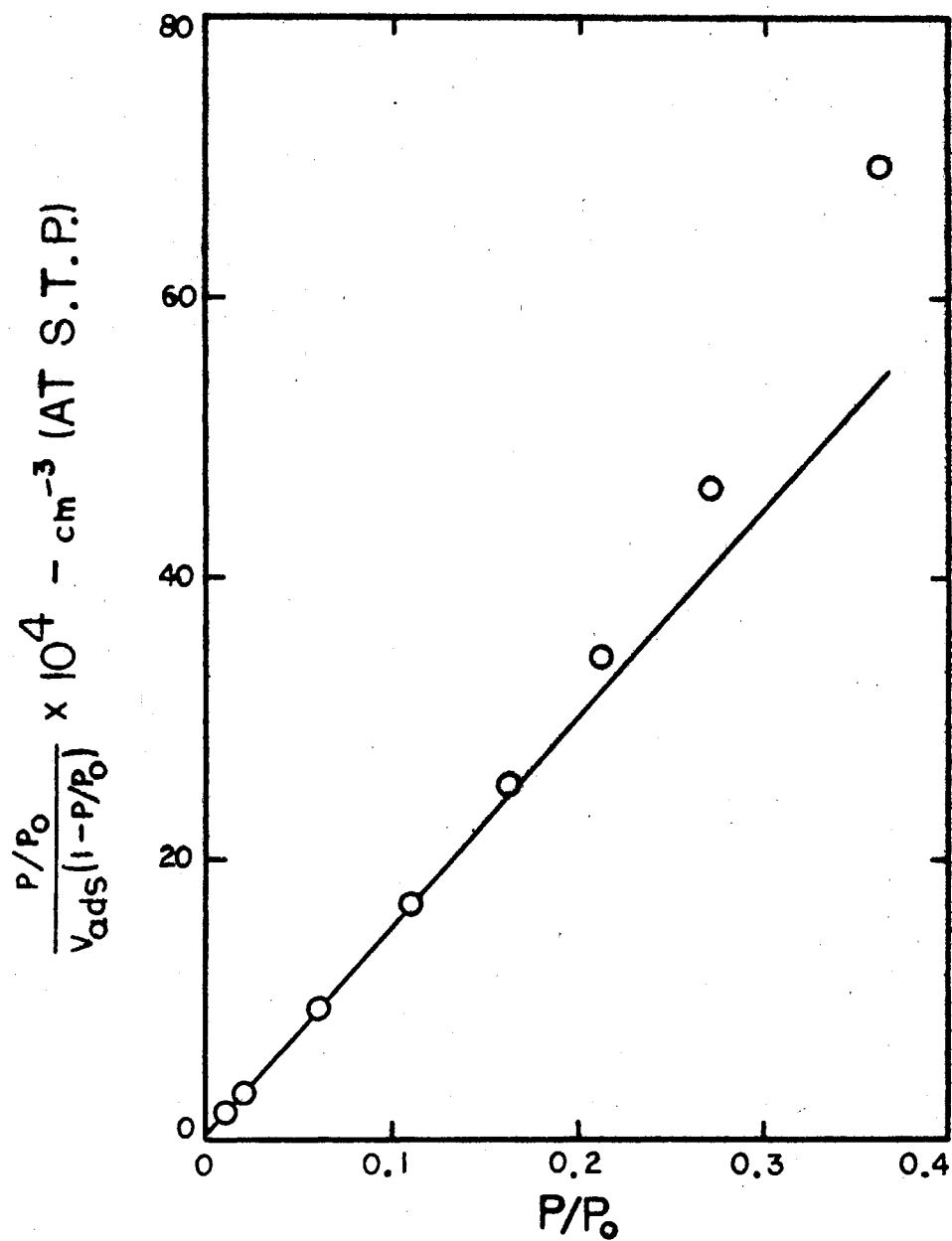
Figure 10. Linear BET Plot for Surface Area Cal-
culation of SnO_2 Gel From Hydrogen
Adsorption Isotherm
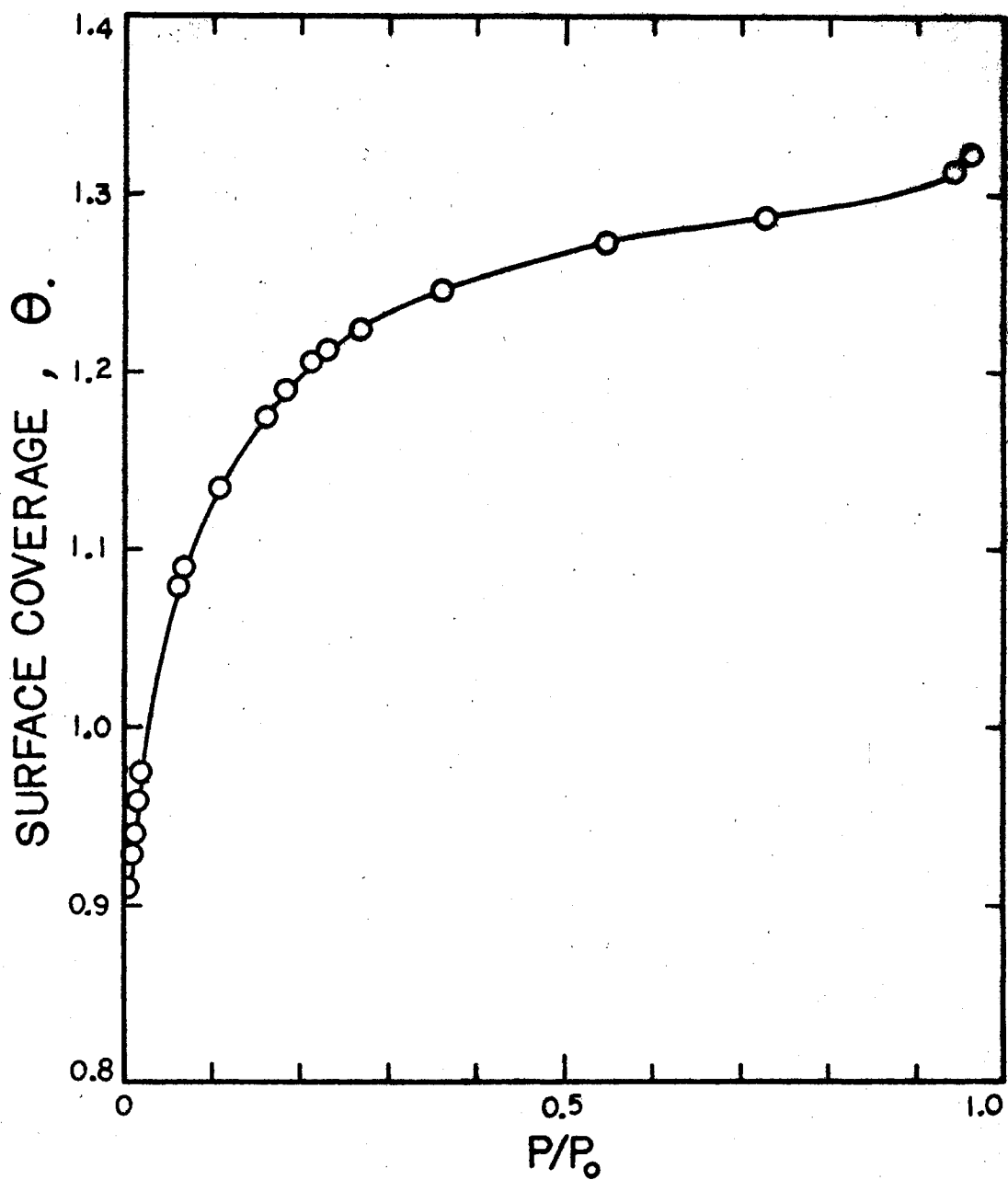
Figure 11.   Surface Coverage of SnO_2 Gel vs Relative Pressure
of Hydrogen Gas

$$E_1 - E_L \;=\; 2.303 \; RT \; \log c \tag{84}$$

For nitrogen with T = 78°K and c = 425 (R = 1.987 cal/deg·mole) the quantity $E_1 - E_L$ has a value of 940 cal/mole. The heat of liquefaction, E_L, for N_2 is 1330 cal/mole, therefore, E_1 will be 2270 cal/mole.

In the case of H_2 as the adsorbate T = 20.2°K, c = 1030, so $E_1 - E_L$ will be equal to 278 cal/mole. The heat of liquefaction for H_2 is 216 cal/mole, consequently, E_1 will have the value of 494 cal/mole.

Since heats of adsorption are exothermic the "net" heat of adsorption and the heat of adsorption in the first layer should be represented by a negative sign. It is customary, however, to report these values without a sign and with the understanding that heat is liberated during the adsorption process. Otherwise, they may be looked upon as heats of desorption. In addition, it should be pointed out that such heats of adsorption obtained from the isotherms are only approximate and in general lower than those measured calorimetrically because of the over-simplified assumptions of the BET theory.

It has already been mentioned that the stannic oxide gel exhibits a Brunauer Type I or a Langmuir isotherm with no hysteresis in the two cases of N_2 and H_2 adsorption. The validity of the Langmuir isotherm can be tested quite simply. Starting with Equation (1) of Chapter II and Equation (80) of this Chapter the Langmuir equation can be written in the form:

$$\frac{V_{ads.}}{V_m} \;=\; \frac{bP}{1 + bP} \tag{85}$$

or

$$\frac{P}{V_{ads.}} = \frac{1}{bV_m} + \frac{P}{V_m}$$ (86)

Plotting $P/V_{ads.}$ versus P a straight line is obtained having a slope $1/V_m$ and intercept $1/bV_m$. The value of V_m can then be evaluated from the slope. Table III lists the values of P, $V_{ads.}$, and $P/V_{ads.}$ for both N_2 and H_2 isotherms. The corresponding linear plots of the Langmuir equation are shown in Figures 12 and 13. It is evident from these plots that deviation from linearity occurs at pressures above that at which the volume adsorbed exceeds the volume of a monolayer. Such behavior should be expected, however, by considering the value of V_m from the BET theory. At lower pressures the Langmuir equation is quite valid. Its application to the adsorption data in this range of pressures yields values of the monolayer volume, V_m, and the specific surface area, S, which are in excellent agreement with those obtained from the BET equation. For nitrogen adsorption calculation of V_m and S gives values of 39.06 cm^3/g and 170.7 m^2/g, respectively. The corresponding values of V_m and S for hydrogen adsorption are 64.87 cm^3/g and 245.2 m^2/g.

Having completed the calculations dealing with the adsorption data the various surface parameters of stannic oxide gel may now be tabulated for ease of reference and comparisons. The results are listed in Table IV for both N_2 and H_2 adsorption.

Pore-Size Distributions

The analysis of the adsorption results for the evaluation of the pore-size distributions of stannic oxide gel is carried out in the manner discussed in Chapter VI and Appendix D. Since the calculations are lengthy and extended table space is required such computations will not

TABLE III

LANGMUIR TREATMENT OF THE ISOTHERMS

N$_2$ ADSORPTION			H$_2$ ADSORPTION		
P (cm)	V$_{ads.}$ (cm^3/g)	P/V$_{ads.}$	P (cm)	V$_{ads.}$ (cm^3/g)	P/V$_{ads.}$
0.543	32.08	0.0169	0.615	59.59	0.0103
0.757	33.33	0.0227	0.823	60.88	0.0135
0.966	34.48	0.0280	0.937	61.65	0.0152
1.177	35.16	0.0335	1.164	62.84	0.0185
1.305	35.64	0.0366	1.451	63.98	0.0227
10.477	48.16	0.2175	4.466	70.76	0.0631
13.584	50.14	0.2709	5.071	71.46	0.0710
15.820	51.45	0.3075	7.992	74.36	0.1075
17.232	52.14	0.3305	11.736	76.93	0.1525
17.945	52.53	0.3416	15.446	79.07	0.1953
21.464	54.11	0.3967	16.720	79.48	0.2104
32.381	56.30	0.5752	19.560	80.22	0.2438
52.030	57.81	0.9000	26.073	81.74	0.3190
60.330	58.00	1.0402	39.627	83.45	0.4748
74.641	58.55	1.2748	52.579	84.42	0.6228
			67.973	86.08	0.7897
39.584	57.24	0.6915	69.565	86.78	0.8016
26.314	55.48	0.4743			
19.309	53.11	0.3635	62.396	85.34	0.7312
16.435	51.69	0.3179	52.575	84.43	0.6227
14.678	50.85	0.2886	39.643	83.39	0.4754
14.578	50.79	0.2870	26.068	81.70	0.3191
12.688	49.59	0.2558	15.952	79.00	0.2019
11.712	49.28	0.2376	14.012	78.18	0.1792
11.059	48.59	0.2276	12.928	77.63	0.1665
9.866	47.63	0.2071	11.037	76.65	0.1440
6.941	45.06	0.1540	8.585	74.97	0.1145
4.380	42.15	0.1039	5.915	72.61	0.0815
2.676	39.27	0.0681	4.055	70.55	0.0575
			3.796	69.98	0.0542
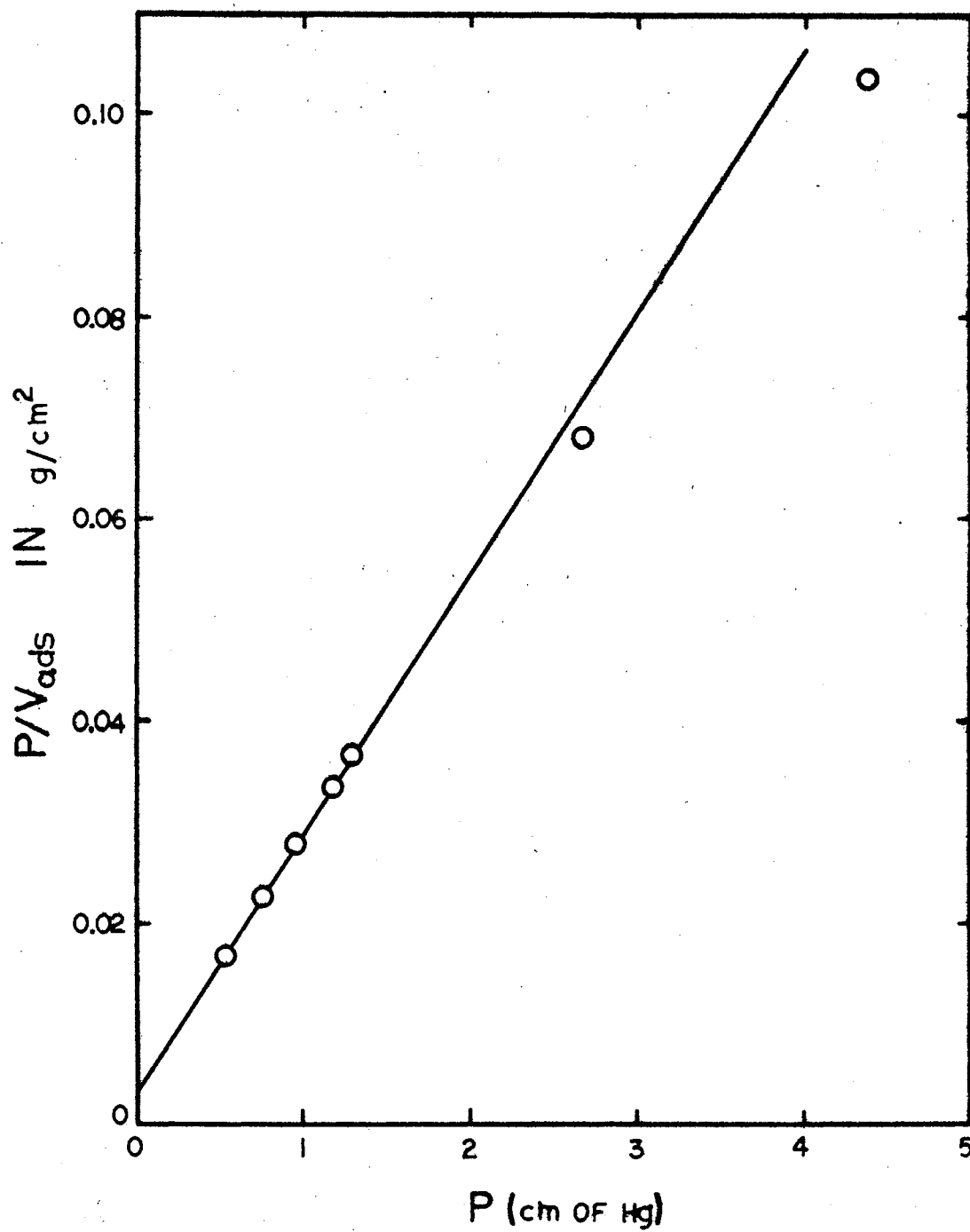
Figure 12. Adsorption Isotherm of Nitrogen on SnO_2 Gel
Plotted According to the Langmuir Equation
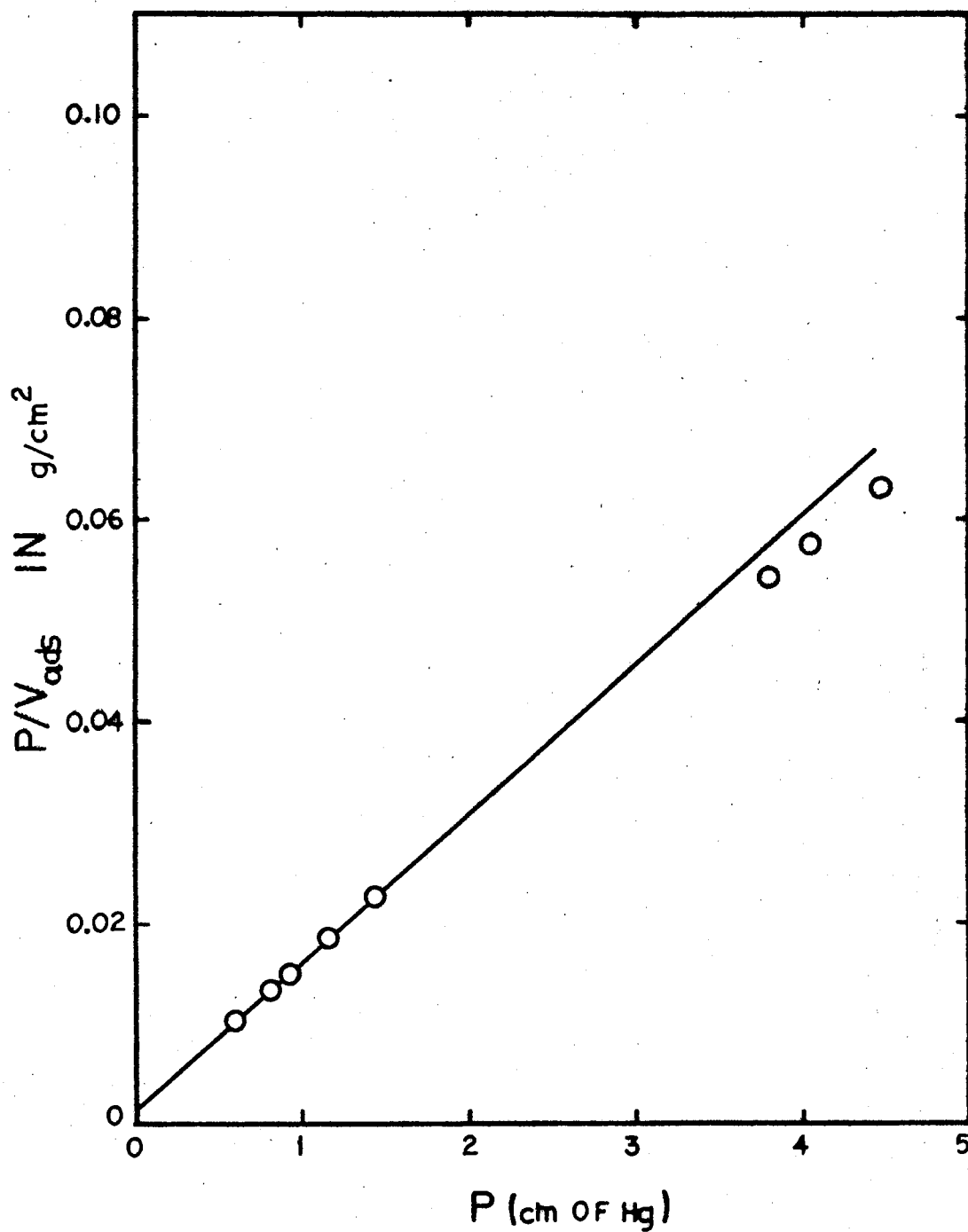
Figure 13. Adsorption Isotherm of Hydrogen on SnO_2 Gel
Plotted According to the Langmuir Equation

TABLE IV

SURFACE PARAMETERS OF STANNIC OXIDE GEL FROM THE
NITROGEN AND HYDROGEN ADSORPTION ISOTHERMS

Surface Parameter	N_2 Adsorption	H_2 Adsorption
	Bet Theory	
V_m	39.18 cm^3/g	65.55 cm^3/g
S	171.2 m^2/g	247.8 m^2/g
c	425	1030
$E_1 - E_L$	940 cal/mole	278 cal/mole
E_L	1330 cal/mole	216 cal/mole
E_1	2270 cal/mole	494 cal/mole
	Langmuir Isotherm	
V_m	39.06 cm^3/g	64.87 cm^3/g
S	170.7 m^2/g	245.2 m^2/g

be carried out here. Only the necessary results will be presented. A detailed discussion, including sample calculations, was carried out by this investigator[82] in a previous study.

Table V gives selected values of the cumulative pore-volume, cumulative pore-area, differential pore-volume, and differential pore-area distributions with the corresponding values of the pore-wall separation, d, for stannic oxide gel from the nitrogen adsorption isotherm. Plots of these distributions against d_{x_i} are represented in Figures 14, 15, 16, and 17, correspondingly.

It is necessary at this point to indicate that the size of the smallest possible pore will be equal to or greater than the diameter of the nitrogen molecule which is taken as 4.30 A. Therefore, the smallest group of pores will contain those pores that have an average pore-wall separation larger than the size of the nitrogen molecule but smaller than the size of the smallest pore contained in the group immediately above.

The differential distribution curves of Figures 16 and 17 show that most of the adsorption takes place primarily in pores of wall separation between about 5 A and 20 A. When calculations are completed the value of the cumulative pore-area $\Sigma \Delta S$ should be in good agreement with the total surface area computed from the BET method. From the third column of Table V it can be seen that $\Sigma \Delta S$ is equal to 168.6 m^2/g.

The pore-size distribution results obtained from a similar treatment of the hydrogen adsorption isotherm are presented in Table VI. The corresponding cumulative pore-volume, cumulative pore-area, differential pore-volume, and differential pore-area distribution curves are shown in Figures 18, 19, 20, and 21, respectively. Again, the size of the smallest pore is limited by the size of the hydrogen molecule the diameter of

TABLE V

CUMULATIVE PORE-VOLUME AND CUMULATIVE PORE-AREA

DIFFERENTIAL PORE-VOLUME AND PORE-AREA DISTRIBUTIONS

FOR STANNIC OXIDE GEL FROM THE NITROGEN ADSORPTION ISOTHERM

d	$\Sigma\Delta V$	$\Sigma\Delta S$	$\Delta V/\Delta d$	$\Delta S/\Delta d$
4.30	--------	------	0.000000	0.000
5.06	0.090650	168.59	0.002930	11.666
6.57	0.086130	150.59	0.004460	13.603
7.24	0.081025	135.01	0.006025	16.653
7.66	0.078151	127.06	0.006613	17.260
8.27	0.074398	117.39	0.006955	16.819
8.95	0.069188	105.03	0.007750	17.327
9.24	0.066840	99.78	0.007952	17.220
9.91	0.061221	87.88	0.008170	16.488
10.48	0.056612	78.74	0.008326	15.897
11.11	0.051294	68.81	0.008243	14.846
11.74	0.046614	60.53	0.007940	13.532
12.75	0.038791	47.59	0.007349	11.530
13.59	0.032540	37.99	0.006808	10.017
14.38	0.027282	30.40	0.006178	8.589
14.90	0.024147	26.07	0.005705	7.658
15.41	0.021251	22.22	0.005292	6.868
16.18	0.017299	17.17	0.004571	5.650
16.94	0.014071	13.24	0.003922	4.631
17.98	0.010304	8.88	0.002667	2.966
18.51	0.008965	7.40	0.002154	2.328
19.32	0.007339	5.67	0.001492	1.544
19.88	0.006590	4.90	0.001066	1.073
20.46	0.005982	4.29	0.001000	0.977
21.08	0.005385	3.71	0.000917	0.870
22.08	0.004516	2.90	0.000805	0.729
22.80	0.003950	2.39	0.000703	0.529
23.56	0.003508	2.01	0.000546	0.463
24.38	0.003089	1.65	0.000432	0.354
25.26	0.002730	1.36	0.000350	0.277
26.21	0.002422	1.12	0.000275	0.210
27.24	0.002167	0.93	0.000212	0.156
28.36	0.001949	0.77	0.000163	0.115
29.61	0.001769	0.64	0.000116	0.080
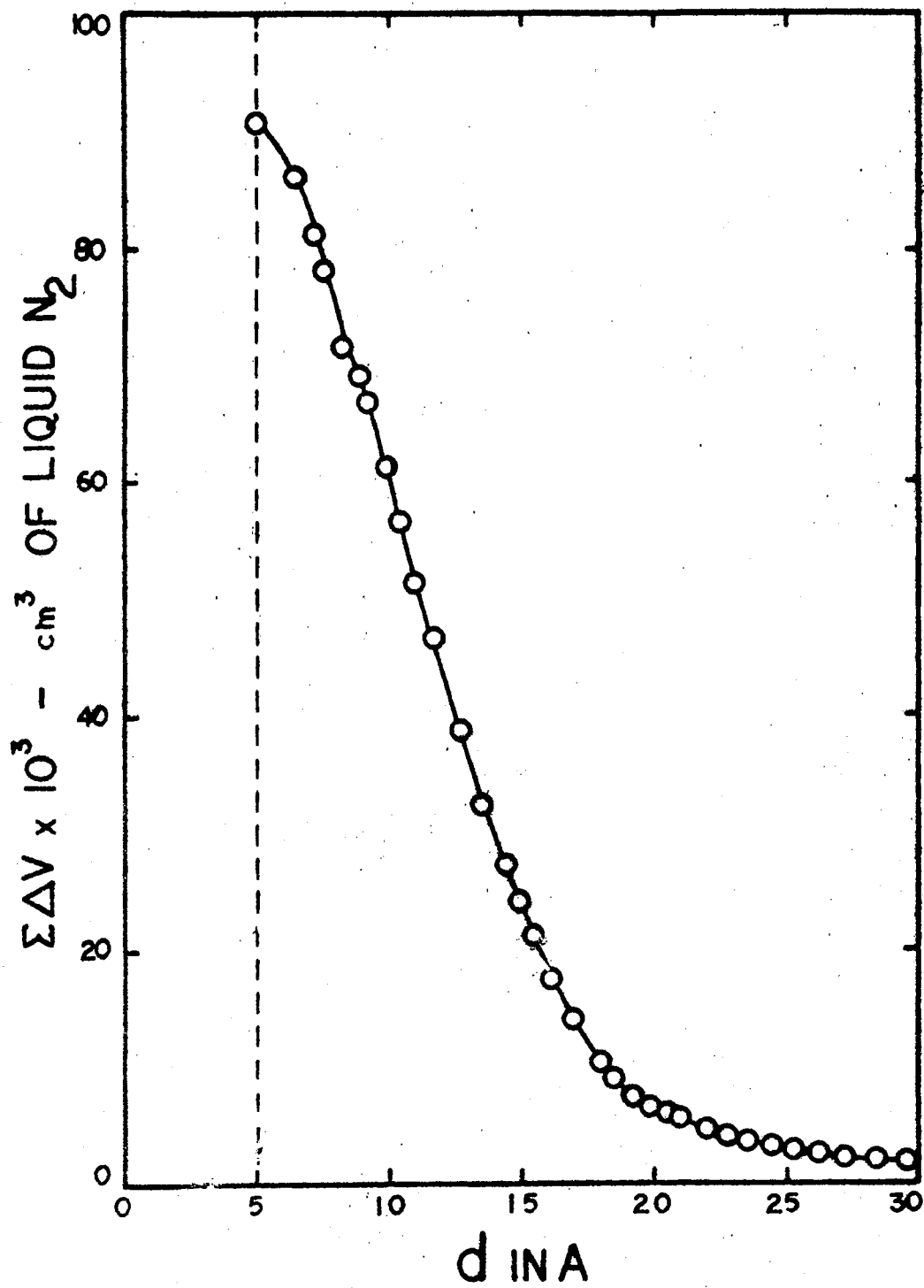
Figure 14. Cumulative Pore-Volume Curve for SnO_2 Gel From N_2 Adsorption Isotherm

285

Figure 15. Cumulative Pore-Area Curve for SnO_2 Gel From N_2 Adsorption Isotherm

Figure 16. Differential Pore-Volume Distribution Curve
for SnO_2 Gel From N_2 Adsorption Isotherm

Figure 17. Differential Pore-Area Distribution Curve for
SnO_2 Gel From N_2 Adsorption Isotherm

TABLE VI

CUMULATIVE PORE-VOLUME AND CUMULATIVE PORE-AREA

DIFFERENTIAL PORE-VOLUME AND PORE-AREA DISTRIBUTIONS

FOR STANNIC OXIDE GEL FROM THE HYDROGEN ADSORPTION ISOTHERM

| d	$\Sigma\Delta V$	$\Sigma\Delta S$	$\Delta V/\Delta d$	$\Delta S/\Delta d$
3.80	--------	------	0.00000	0.000
4.61	0.109160	246.40	0.00345	14.951
6.55	0.103508	221.87	0.00865	26.414
7.02	0.091406	184.92	0.01408	40.155
7.28	0.086871	171.99	0.01475	40.543
7.48	0.083581	162.95	0.01602	42.849
8.19	0.072221	133.57	0.01679	41.003
8.53	0.066135	118.85	0.01679	39.377
8.94	0.058990	102.35	0.01655	37.014
9.30	0.052883	88.87	0.01617	34.775
9.40	0.051120	85.08	0.01591	33.854
9.61	0.047787	78.03	0.01560	32.472
9.70	0.046274	74.88	0.01531	31.557
9.84	0.044835	71.92	0.01480	30.094
10.18	0.039639	61.44	0.01377	27.063
10.34	0.037394	57.03	0.01346	26.045
10.49	0.035307	52.99	0.01286	24.515
10.83	0.031171	45.17	0.01117	20.622
11.33	0.025894	35.57	0.00929	16.387
11.81	0.021717	28.29	0.00746	12.618
12.44	0.017462	21.22	0.00563	9.058
12.91	0.014900	17.15	0.00453	7.022
13.23	0.013503	15.00	0.00396	5.994
13.72	0.011631	12.20	0.00315	4.591
14.24	0.010131	10.04	0.00247	3.473
14.98	0.008467	7.74	0.00185	2.467
15.78	0.007143	6.01	0.00140	1.782
16.44	0.006353	5.02	0.00106	1.284
17.17	0.005673	4.20	0.00085	0.993
18.56	0.004719	3.13	0.00054	0.585
19.52	0.004249	2.63	0.00041	0.423
20.61	0.003831	2.21	0.00030	0.293
21.43	0.003578	1.96	0.00024	0.221
22.81	0.003250	1.66	0.00022	0.194
24.43	0.002934	1.39	0.00016	0.127
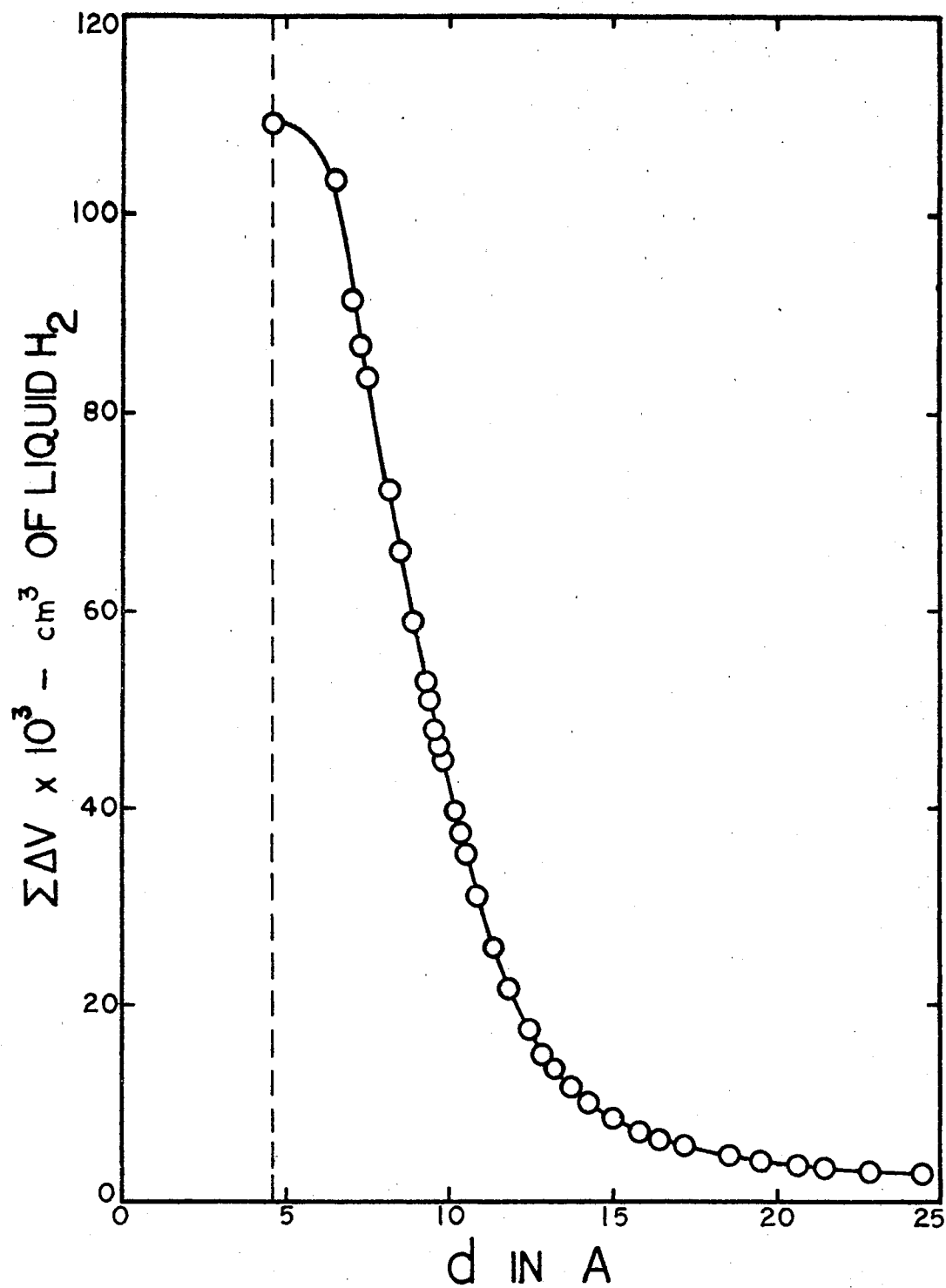
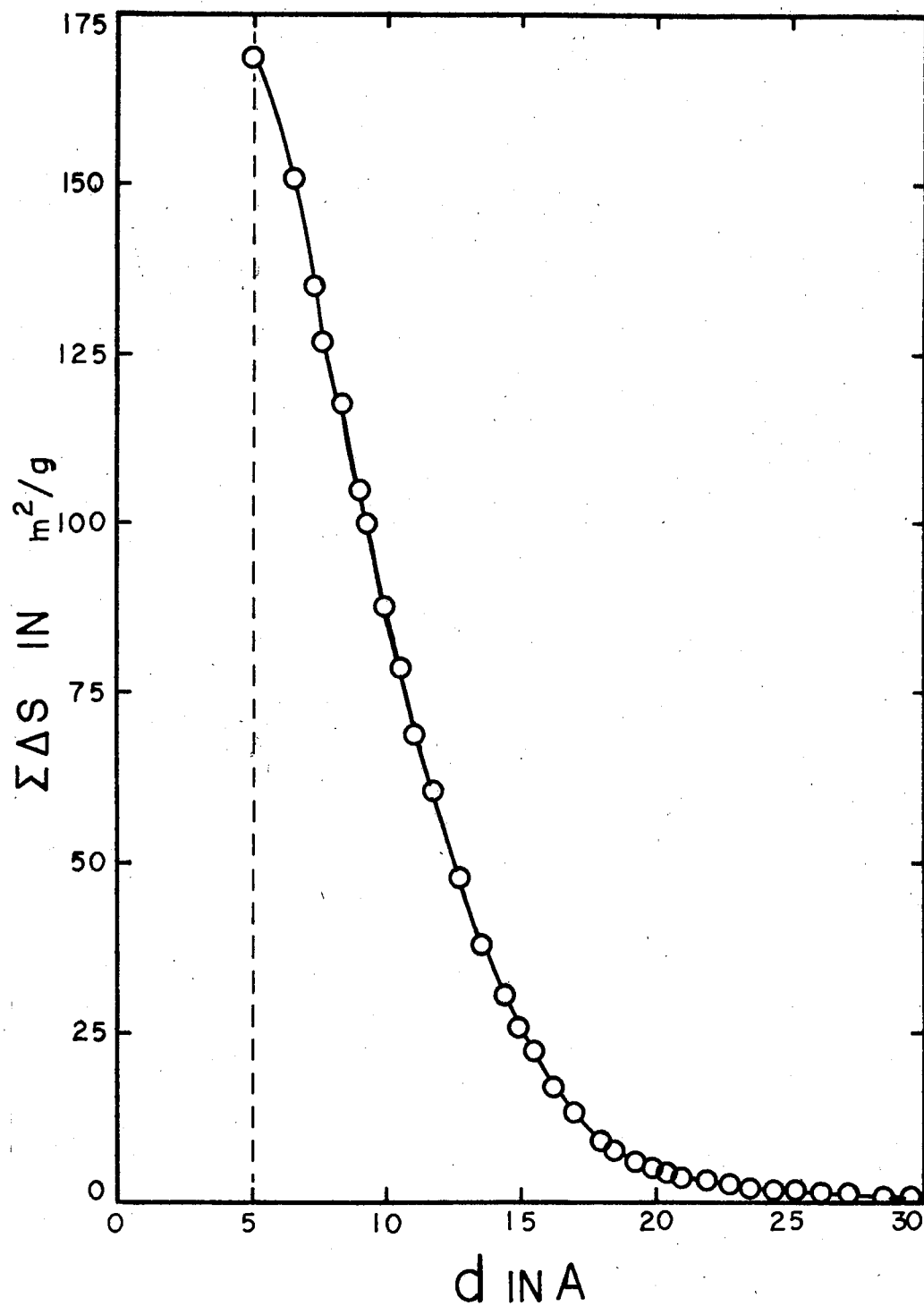Figure 18. Cumulative Pore-Volume Curve for SnO_2 Gel From H_2 Adsorption Isotherm
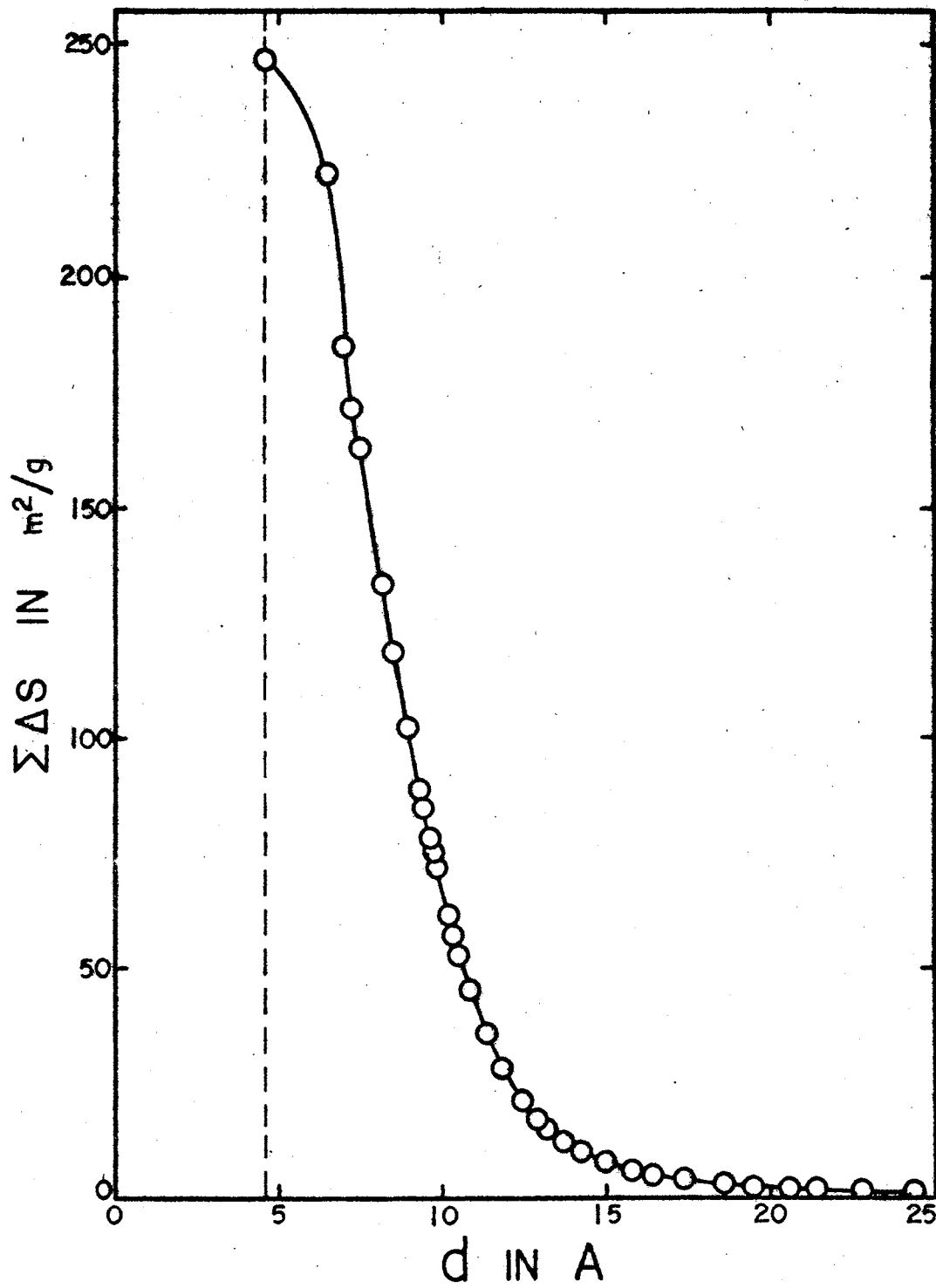
Figure 19. Cumulative Pore-Area Curve for SnO_2 Gel From H_2
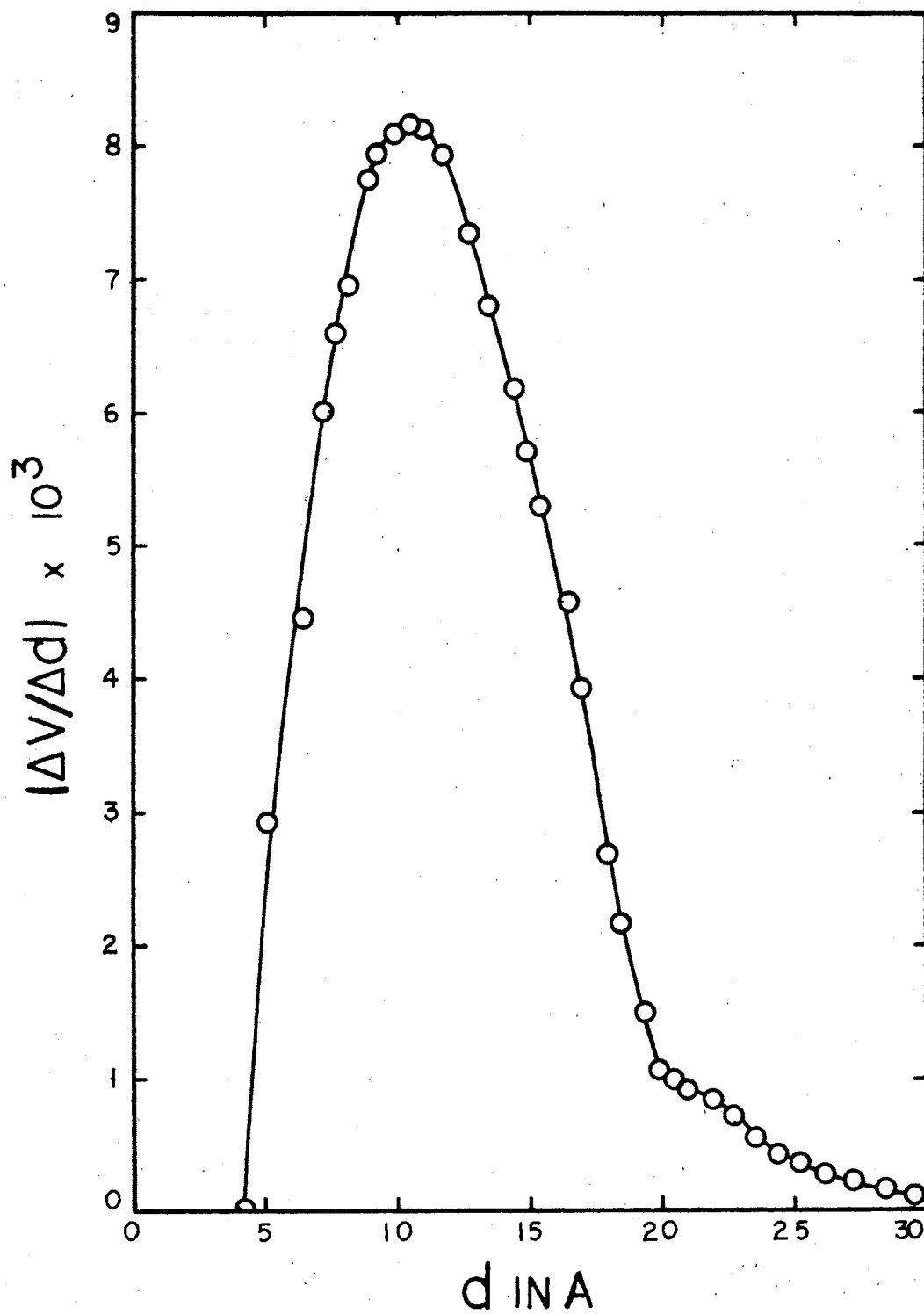Adsorption Isotherm

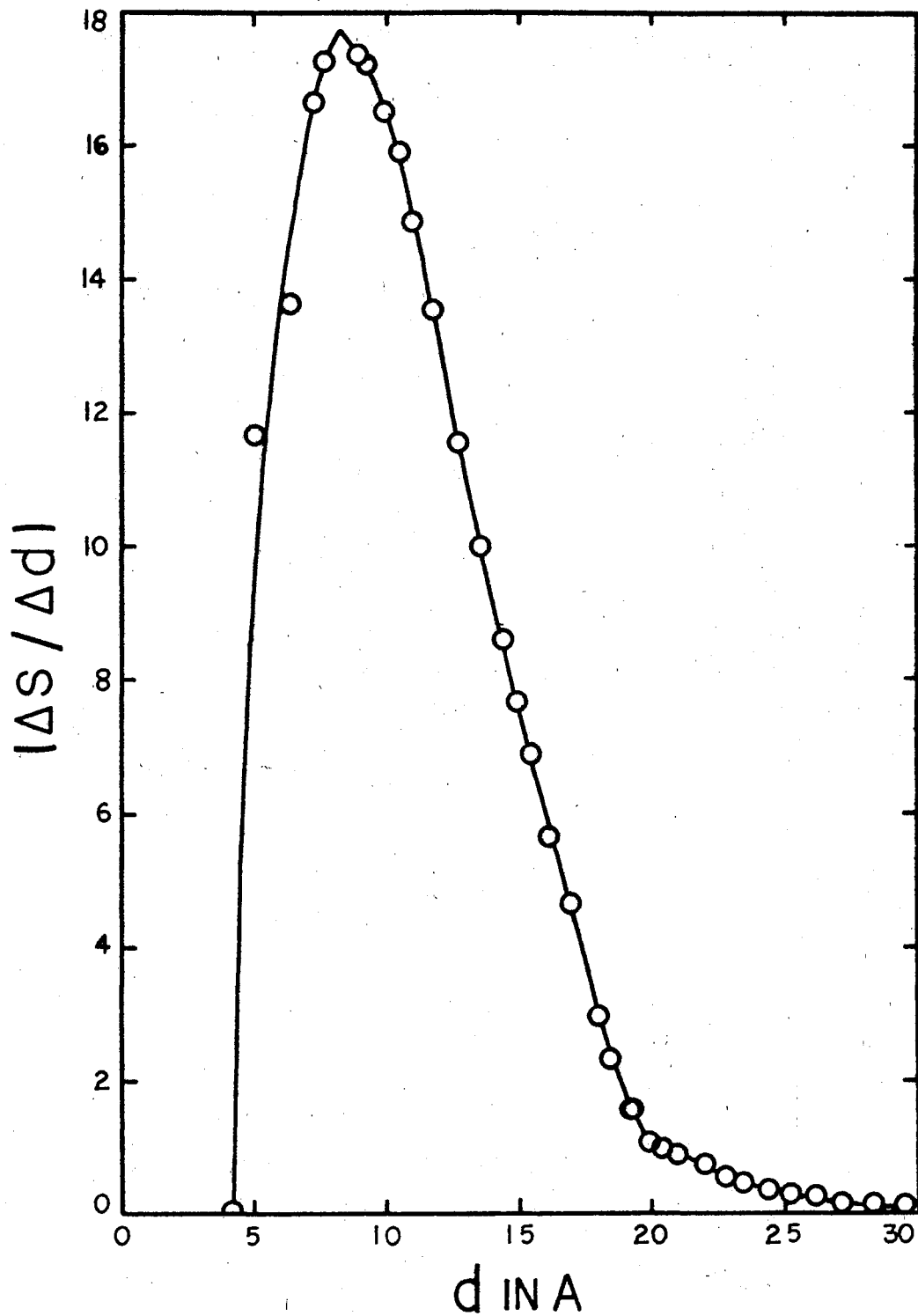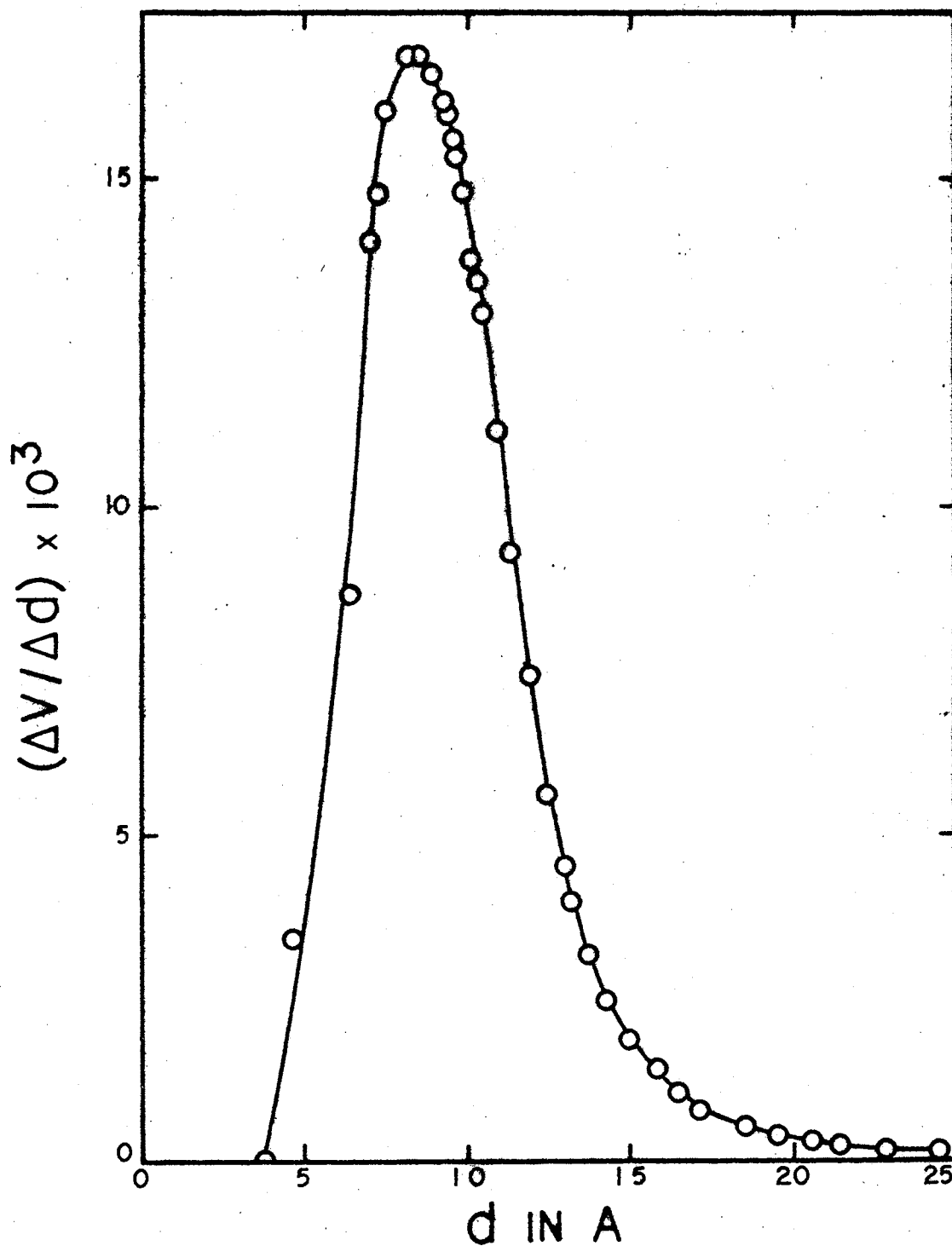Figure 20. Differential Pore-Volume Distribution Curve for SnO$_2$ Gel From H$_2$ Adsorption Isotherm
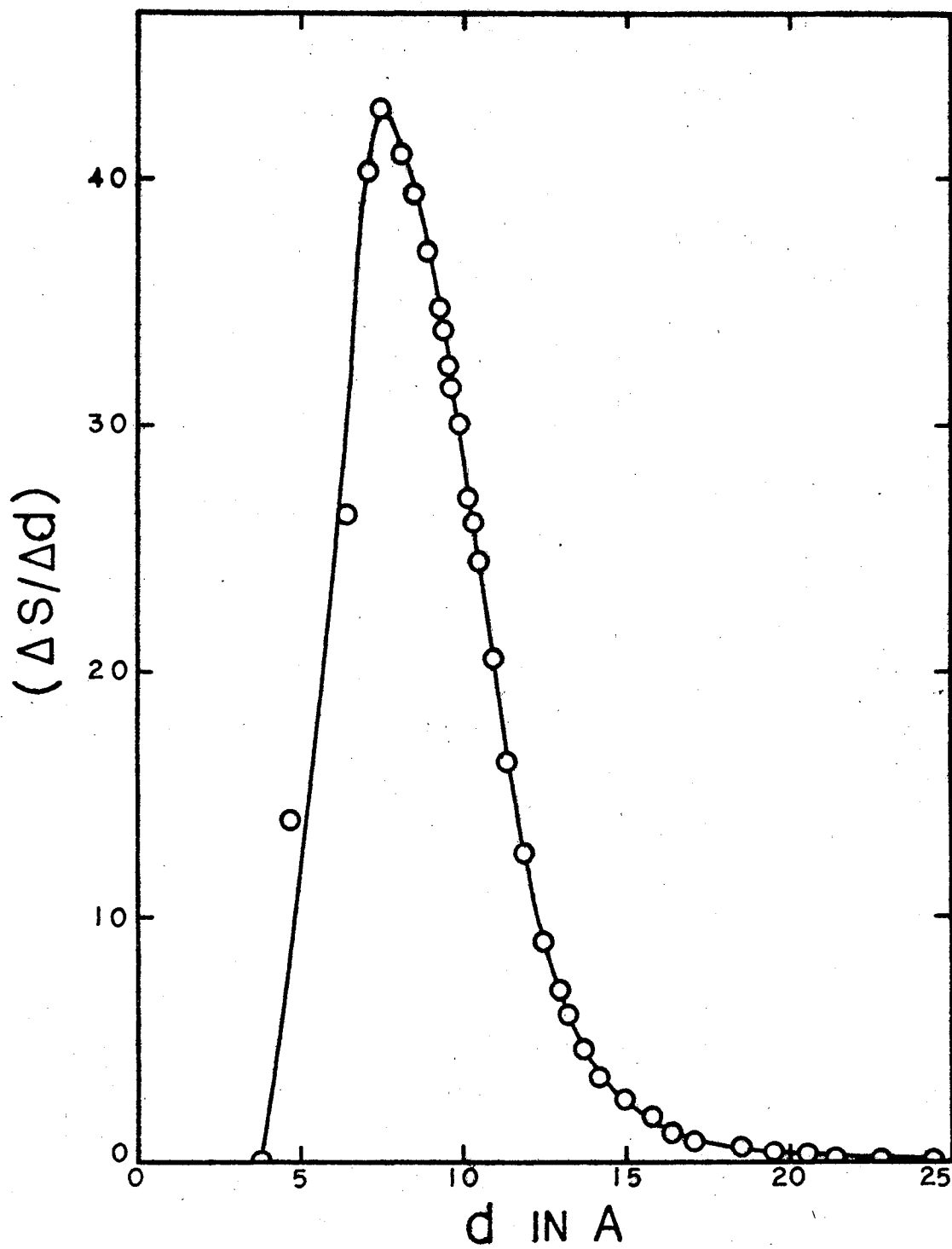
Figure 21. Differential Pore-Area Distribution Curve for
SnO_2 Gel From H_2 Adsorption Isotherm

which is taken as 3.80 A. The differential distribution curves of

Figures 20 and 21 show the range of pore-size for which adsorption is

the largest. The pore-wall separation ranges between about 4 A to about

15 A. The cumulative pore-area, as taken from Table VI, has a value of

246.4 m^2/g and compares very well with that obtained from the BET.

CHAPTER VIII

DISCUSSION OF RESULTS AND CONCLUSIONS

Gels, in general, have a highly porous structure and as such they are expected to exhibit a large surface area. The shape of their adsorption isotherms is expected to be strongly dependent upon pore and capillary effects.

The stannic oxide gel exhibits adsorption isotherms whose shape is similar for both nitrogen and hydrogen adsorption. They were already labeled as Brunauer Type I or Langmuir type isotherms without hysteresis. The Langmuir isotherm presupposes a monomolecular adsorbed layer which in this case would not be entirely correct. Calculation of the surface coverage indicates that adsorption exceeds a monolayer although by not more than half a layer as seen from Tables I and II. We shall return to the discussion of the isotherms later in the Chapter when dealing with considerations of pore structure.

The determination of surface area is always a function of the size of the particular adsorbate molecule used. Larger molecules, invariably, give smaller surface area values because of their inability to penetrate into the narrowest pores of the adsorbent. Considering the molecular diameters of nitrogen (4.30 A) and hydrogen (3.80 A) it is expected that the specific surface area of the stannic oxide gel will have a larger value when calculated from hydrogen adsorption than nitrogen. Correspondingly, the volume of gas necessary for monomolecular coverage of

94

the surface, V_m, and the total volume of gas adsorbed, $V_{ads.}$, will be larger for hydrogen than nitrogen. The values obtained for these three parameters from each adsorbate are qualitatively consistent with the differences in the size of the two gases used. Comparison between Tables I and II shows that the volume of hydrogen gas adsorbed on the gel is considerably larger than that of nitrogen gas adsorbed on the same surface. In addition, Table IV represents a comparison of the values of V_m and S, showing that for hydrogen adsorption $V_m = 65.55$ cm^3/g and S = 247.8 m^2/g are larger than the corresponding values of $V_m = 39.18$ cm^3/g and S = 171.2 m^2/g for nitrogen adsorption.

The value of 171.2 m^2/g for the BET surface area of the gel with N_2 gas as the adsorbate has already been compared with those values obtained by Goodman and Gregg[79] (172 m^2/g) and by Rutledge, Kohnke, and Cunningham[68] (173 m^2/g) and the agreement is remarkably good. Further confidence is placed on this value since Goodman and Gregg arrived at the same surface area by using a gravimetric method in contrast to the volumetric method of the present investigation. As no value for the surface area of the gel from hydrogen adsorption is available in the literature it can be concluded that its value of 247.8 m^2/g is quite reasonable.

It was felt that the validity of the above results from the BET theory could be checked to a certain extent if the adsorption data were treated according to the Langmuir equation. This assumption may be justified for the reason that the isotherms are of the Langmuir type and the equation should be applicable up to pressures where the adsorbed volume is equal to the monolayer volume as obtained from the BET. Whereas the BET is a multimolecular adsorption theory and the Langmuir equation applies to monolayer adsorption only it is possible to fit the latter

theory to the low pressure parts of the isotherms. With this in mind calculations were carried out and the results of the Langmuir theory are shown in Table III and Figures 12 and 13. As expected, the theory is valid only up to pressures of two to three centimeters of Hg, in contrast to the BET which holds true up to equilibrium pressures of 18 to 20 cm of Hg. The Langmuir values of V_m (equal to 39.06 cm^3/g for nitrogen and 64.87 cm^3/g for hydrogen) and S (170.7 m^2/g and 245.2 m^2/g for nitrogen and hydrogen, respectively) are in very good agreement with those of the BET method.

Approximate heats of adsorption are calculated from the BET equation and shown in Table IV. It is well known that heats of adsorption are comparable to heats of liquefaction. The values of the net heat of adsorption, $E_1 - E_L$, of nitrogen and hydrogen on the SnO_2 surface are 940 and 278 cal/mole, respectively, and they are indeed of the same order as the heats of liquefaction, E_L (1330 cal/mole of nitrogen and 216 cal/mole of hydrogen). The heat of adsorption in the first layer, E_1, is 2270 cal/mole for N_2 and 494 cal/mole for H_2. These values are of the right order of magnitude for the heats of physical adsorption of nitrogen and hydrogen. Brunauer[32] points out that isosteric and calorimetric heats of adsorption of nitrogen on various oxide catalysts at liquid nitrogen range from 2700 to 4600 cal/mole. In the case of hydrogen adsorption on gel and oxide surfaces at liquid air temperatures values of the heat of adsorption range between 1000 and 2000 cal/mole. More recent studies[83,84] on the adsorption of hydrogen on alumina at liquid nitrogen have produced experimentally determined heats of adsorption between 700 to 1050 cal/mole. Adsorption of hydrogen at the temperature of liquid hydrogen would be expected to give values of E_1 lower than 700 cal/mole.

Thus, results of the heats of adsorption obtained in this study are in general agreement, although slightly lower, than the experimentally determined isosteric and calorimetric heats of physical adsorption.

Brunauer et al.[31] have shown that the relative magnitude of the heat of adsorption E_1 and the heat of liquefaction E_L dictate the shape of the adsorption isotherm in the low relative pressure region. If the attractive forces in the adsorbent-adsorbate system are greater than those between the adsorbate molecules in their liquid state then E_1 will be greater than E_L and the isotherm at low pressures will be concave to the relative pressure axis. If, on the other hand, E_L is greater than E_1, then the isotherm will be convex to the pressure axis. The nitrogen and hydrogen adsorption isotherms of Figures 6 and 9 are both concave to the relative pressure axis indicating that E_1 should be larger than E_L, in each case. This basic premise is correct since, by looking at the results of Table IV, one can verify that E_1 is indeed larger than E_L for both adsorption systems.

Adsorption of gases at the temperature of the corresponding liquid is, in general, multimolecular and the pore structure of the adsorbent is of great importance in multimolecular adsorption. Narrow pores fill at lower relative pressures; wider pores fill at higher pressures; at the saturation pressure all pores are filled. The size of the pore limits the number of layers that can be adsorbed within it. These statements are true whether adsorption beyond the first layer is interpreted in terms of the theory of multimolecular adsorption or the capillary condensation theory.

Consideration of the shape of the nitrogen and hydrogen adsorption isotherms leads to the observation that the pores in the stannic oxide

gel should be quite narrow since they fill at a very low relative pressure as indicated by the steepness of the isotherms during the early stages of adsorption. Hysteresis upon desorption is absent because adsorption and desorption take place to and from the same meniscus. In addition, as the pressure is increased, after all pores are filled, the isotherm hardly rises indicating that contributions from any free surface are insignificant.

Part of this investigation is devoted to the mathematical evaluation of pore-size distributions to determine that the high porosity of the SnO_2 gel arrived at from theoretical considerations of the shape of the adsorption isotherms is in complete agreement with the computational results. Capillary condensation constitutes the basis of such calculations. The simultaneous occurrence of multimolecular adsorption is entirely separated from capillary condensation. In the methods of evaluation of pore-size distributions it is necessary to exclude multilayer adsorption. This is accomplished by the correction factors introduced into the calculations.

The results for the pore-size distribution of SnO_2 gel from the nitrogen adsorption isotherm are shown in Table V. Figures 14 and 15 represent the cumulative pore-volume and pore-area distributions while Figures 16 and 17 represent the differential pore-volume and pore-area distribution curves. The latter curves show the range in pore size in which most of the adsorption takes place. Definite breaks in the curves occur at a value of the pore-wall separation, d, approximately equal to 20 A. No significant amount of gas is adsorbed by pores wider than 20 angstroms. The lower limit of the pore size is taken as the molecular diameter of the nitrogen molecule equal to 4.30 A. The volume adsorbed

in pores of size between 4.30 and 20 A makes up the largest part of the total volume adsorbed by the gel.

The value of the cumulative pore-area obtained by this method is 168.6 m^2/g and, as expected, it shows a remarkable agreement with the BET result of 171.2 m^2/g.

Pore-size distribution results from hydrogen adsorption are listed in Table VI and the corresponding plots of the cumulative and differential distribution curves appear in Figures 18, 19, 20, and 21. Analysis of the plots shows that the largest adsorption takes place in pores ranging in size between 3.80 A, the molecular diameter of hydrogen, and about 15 A. The total surface area of the gel of 246.4 m^2/g obtained from Table VI compares remarkably well with the value of 247.8 m^2/g from the BET method.

Comparison of the distribution curves obtained from the N_2 isotherm with those obtained from the H_2 shows that the latter curves have been slightly displaced to lower values of the pore-wall separation. This is to be expected since the H_2 molecules, being smaller than the N_2 molecules, can penetrate into narrower pores. Even smaller pores are present in this adsorbent but their filling is impossible owing to the limitations imposed by the molecular size of the adsorbate gases. It is concluded, therefore, that the largest fraction of the surface is located in pores up to four or five molecular diameters wide. At higher values of the pore-wall separation the curves reach the d-axis asymptotically indicating that wider pores are present, although their contribution to the total surface area is quite small.

The differential pore-volume distribution curves of Figures 16 and 20 show that the pore-volume maxima occur at pore-sizes of 10 to 11 A

for nitrogen and 8 to 9 A for hydrogen. Values then of approximately 10.5 and 8.5 A may be taken as the mean pore-wall separations of stannic oxide gel corresponding to nitrogen and hydrogen as the adsorbates.

In conclusion, the results of the BET multimolecular adsorption theory, relating to monolayer volumes and specific surface areas for the SnO_2 gel, are considered to be the best obtainable knowing the simplified assumptions of the theory. At low relative pressures the Langmuir monomolecular adsorption theory is also found to be valid. The BET heats of adsorption are, at best, only in semi-quantitative agreement with experiment, although they do well in explaining the shapes of the adsorption isotherms in the low relative pressure region.

The shapes of the hydrogen and nitrogen adsorption isotherms, Brunauer Type I or generalized Langmuir isotherms, are used very effectively to explain the highly porous structure of the SnO_2 gel. It is not possible, however, to believe that adsorption would take place only as a monomolecular film, as suggested by the Langmuir shaped isotherms, on a surface which microscopically should be similar to a surface exhibiting multilayer adsorption. In this case the theory of capillary condensation as proposed by Pierce and Smith[51] is definitely more reasonable. Thus, in this situation, one should not probably depend too heavily on a parameter such as surface area as calculated by the BET method. Instead, it would be preferable to speak of the "adsorptive capacity" of a solid adsorbent, or some other parameter linked with its capability to adsorb or condense a particular gas on its surface.

The theory of capillary condensation gives an excellent picture of the mechanism of physical adsorption as applied to this highly porous gel. The calculations carried out on pore-size distributions give a

quantitative picture of the size (up to 20 A in pore-wall separation) and the structure (slit-shaped capillaries) of the pores in SnO_2 gel which constitute the largest part of its surface. The application of the parallel-plate model to the pores of the gel gave excellent results in the total volume adsorbed and the total surface area of the adsorbent. It is, therefore, concluded that it represents a good physical picture of the pores in the SnO_2 gel.

Objections may be raised as to the choice of the parallel-plate model in the evaluation of pore-size distributions. Two other possible models could have been employed. In the first, capillaries may be represented by an equivalent system of cylindrical pores. It is hard, however, to believe that all the pores in an adsorbent should have such an ordered circular shape. Results of a previous study[82] in which distribution calculations were carried out for nitrogen adsorption on the SnO_2 gel, based on the model of circular pore-radii, were proven unsatisfactory because of disagreements in the total volume adsorbed and the total surface area.

In the second model it can be assumed that the walls of the capillary may often be convergent instead of being parallel. The capillaries are then represented by a system of conical or V-shaped pores. In this case another parameter, the angle of the conical pore, would enter into the calculations of pore-size distributions. This angle would make the computations extremely complicated.

CHAPTER IX

THE INFRARED AND LASER-RAMAN SPECTRA

OF STANNIC OXIDE GEL

This part of the investigation is devoted to the study of the stannic oxide gel surface by infrared and Laser-Raman spectroscopic techniques. The spectra to be obtained will deal with the bare surface of the gel to the extent that no gases will be adsorbed. Only surface hydroxyls and adsorbed water, present from the preparation of the gel, will be of interest. In addition, the effect of dehydration will be studied by the same methods.

Before the spectral results are introduced a discussion of the spectroscopic techniques in the study of surfaces and adsorption will be presented. Also included in this chapter will be a literature survey of the spectra of adsorbed hydrogen to serve as a preliminary review to the suggestions for further study of the next chapter.

The Infrared Spectra of Adsorbed Molecules

Infrared spectroscopy can be used to obtain information as to the various functional groups which are structurally attached to the surface, the molecular structure of the adsorbed species, the nature of the adsorption site, and the type of interaction between the surface and the adsorbate molecules. Raman spectra may be used to supplement the infrared since vibrations which are infrared inactive can appear in the Raman.

The surface of the stannic oxide gel, like all other oxide sur-faces[85], is expected to be hydrated or hydroxylated as a result of its preparation from aqueous solution and due to atmospheric water vapor. For example, all the different forms of silica and alumina[86] carry on their surface so called "structural water" in the form of surface silanol ($\equiv$ Si—OH) or aluminol ($\equiv$ Al—OH) groups. The surface hydroxyl groups usually exist in various different states since they show infrared absorption bands at several distinct frequencies[27,28]. Each of these bands is characterized by its own frequency, intensity, and bandwidth. Changes which may occur in any one or in all three of these parameters, either with variation in temperature or in the presence and with various amounts of different adsorbed species, would indicate that the chemical environment of the surface structural groups has been altered.

Surface groups which are affected more readily and to a greater extent by adsorbed gases are the hydroxyl groups. The variation of their stretching frequencies as gases are adsorbed is larger than that of other types of functional groups because of their ability to undergo hydrogen bonding with the adsorbed molecules[87], and between each other if they are closely located on the surface[88,89].

The absorption band due to the stretching vibration of the hydroxyl group appears very clearly in the fundamental region at 3750 cm^{-1} in the infrared spectra of silica gel[90,91,92], Aerosil[24], and Cabosil[25]. This band has been assigned to completely "isolated silanol groups" or "free surface hydroxyl groups". When OH groups are close together and favorably oriented then hydrogen bonds can easily be formed between them. These "combined" or "hydrogen-bonded" hydroxyls produce absorption bands in the longer wavelength, lower frequency, part of the free hydroxyl

band. Studies by McDonald[25] on Cabosil silica showed a sharp band at 3747 cm^{-1} due to the isolated surface hydroxyls (silanol groups) and a broader band at 3660 cm^{-1} due to the hydrogen-bonded surface OH groups. Very similar bands were obtained for both the isolated and combined surface hydroxyls on other gel and oxide surfaces such as alumina[93,94], zinc oxide[95], chromium oxide[96], titanium dioxide[97,98,99], ferric oxide[100], nickel oxide[101], beryllium oxide[102], magnesium oxide[103], and germania[104].

When molecules are adsorbed on the surface they interact specifically with the surface free hydroxyl groups. These interactions are given in terms of the displacement of the OH band to lower frequencies after adsorption indicating the formation of hydrogen bonds between surface hydroxyls and adsorbate molecules. McDonald[24,25] has examined the spectra of Aerosil and Cabosil silica with a number of non-polar molecules adsorbed on the surface. Upon nitrogen adsorption at high coverage the 3750 cm^{-1} band disappeared and a new band appeared at 3725 cm^{-1} indicating that N_2 molecules are preferentially attached to the free OH groups on the surface and that all such sites were interacting with adsorbed nitrogen. Molecules that form stronger hydrogen bonds cause greater displacements of the free hydroxyl band.

Isotope effects on the surface can also be studied spectroscopically and results are shown to be compatible with expected isotopic shifts. When heavy water was adsorbed on Cabosil[25] the bands at 3750 and 3660 cm^{-1} of the free and hydrogen-bonded hydroxyls, respectively, decreased rapidly in intensity and new bands appeared at 2765 and 2600 cm^{-1}. The first band is attributed to free deuteroxyl groups and corresponds to the 3750 cm^{-1} band. The second band is due to OD groups which have replaced hydrogen-bonded OH groups contributing to the 3660 cm^{-1} band.

Infrared spectroscopy is capable of giving information concerning chemisorption and physical adsorption. Molecules that are physically adsorbed can be removed from the adsorbent surface and in so doing any spectroscopic evidence for physical adsorption will be destroyed. Chemisorbed substances, on the other hand, remain on the surface and their bands will be present in the spectrum. When ammonia, for instance, is adsorbed on porous glass[105] two pairs of IR absorption bands are observed, one at 3400-3320 cm^{-1} and the other at 3365-3280 cm^{-1}. The bands of the first high frequency set are due to the physically adsorbed NH_3 molecules which form hydrogen bonds with the OH groups of the surface and they disappear readily after evacuation. The bands of the second low frequency set are due to chemisorbed ammonia, the molecules of which are coordinated to the surface by the lone pair electrons of the nitrogen, and they are still present after evacuation.

The effect of the surface on adsorbed molecules may be studied spectroscopically. Changes in the spectra of the adsorbed molecules themselves compare very closely with the spectra which result from a change in state, i.e., from the gas to the liquid or solid phases. The spectral changes that occur when molecules are condensed have been discussed by Herzberg[106]. Upon adsorption the rotational freedom of the molecules is lost and it is replaced by a restricted rotational freedom. The rotational fine structure of the bands is very nearly lost and a single peak usually appears which is shifted to frequencies lower than that of the gaseous molecules. The broadness of this band may be used to show the extent of restricted rotation in the adsorbed phase[107]. It is also quite possible that the molecular symmetry may be distorted during adsorption because of the asymmetric force field at the surface.

Thus, bands which are forbidden in the more symmetrical environment of the molecules, like for instance the gas phase, can appear in the spectrum after adsorption. Infrared forbidden bands have indeed been observed in the absorption spectrum of methane[26] and ethylene[108] physisorbed on porous glass. Therefore, distortion of the molecular skeleton produces a change in dipole moment during the vibration which gives rise to an absorption band in the infrared spectrum.

Infrared spectroscopy is used to give evidence of surface heterogeneity. If the surface exhibits active sites of various degrees, then several absorption bands will be produced in the spectrum of an adsorbed substance because independent surface species are held by different types of surface sites. In addition, as the coverage is increased changes occur in the intensity and frequency of certain bands. Surface hydroxyls are used as adsorption sites for molecules which form hydrogen bonds. Also, electron deficient (Lewis acid) and proton-donor (Bronsted acid) sites exist on the surface as shown by a number of investigators [109,110,111].

The Raman Spectra of Adsorbed Molecules

In contrast to the abundance of the infrared spectra of adsorbed molecules very few cases are recorded in the literature regarding their Raman spectra. Karagounis and Issa[112,113] investigated the Raman spectra of several cyclic organic compounds adsorbed on Aerosil silica and porous glass. They have found that new Raman lines appeared in the case of polycyclic aromatic compounds which posses a center of symmetry. The relatively large specific surface area of the adsorbents was a prerequisite in obtaining the Raman lines of the adsorbed compounds.

Laser Raman spectroscopy was applied to the study of a number of adsorption systems with silica[114,115,116], alumina[115,117], and titanium and magnesium oxides[115] as the adsorbents. The Laser Raman spectra of various adsorbates, such as halogens, nitriles, aldehydes, and hydrocarbons adsorbed on different oxide surfaces were reported by Hendra and Loader[118]. It was clearly shown in this study that the origin of the spectra was due to vibrations of the adsorbed species. The spectra of physisorbed molecules were quite similar to those of the liquid. Chemisorption, on the other hand, caused considerable changes both in frequency and intensity of the Raman bands.

Raman spectroscopy is advantageous over the infrared in so far as bands due to the solid adsorbents are not prominent in the spectrum. The method, however, is lacking in sensitivity to the extent that presently only high surface area solids and good Raman scatterers are used as adsorbents and adsorbates, respectively.

The Spectra of Adsorbed Hydrogen

The infrared spectrum of hydrogen adsorbed on porous silica glass at the temperature of liquid nitrogen was studied by Sheppard and Yates[26]. The fundamental vibrational stretching frequency of hydrogen gas is Raman active and occurs at 4160 cm^{-1}. Adsorbed H_2 shows an absorption band at 4131 cm^{-1} which is due to the distorting forces of the surface on the infrared inactive stretching vibration of the molecule. The shape of this band suggests that no free rotation of the adsorbed H_2 molecule takes place, or that free rotation may be present only about an axis perpendicular to the surface.

Eischens et al.[119] examined the chemisorption of hydrogen and deu-

terium on zinc oxide. At $30^{\circ}C$ and pressures up to 0.5 atm. adsorbed H_2 produces bands at 3496 and 1709 cm^{-1}. The first band is attributed to the oxygen-hydrogen stretching vibration of the OH groups, while the second one is due to the zinc-hydrogen stretching vibration of the ZnH or $(ZnH)^{+}$ groups. The bands of the surface OH groups or the OH groups within the bulk of the ZnO remained constant during adsorption, and they were used to distinguish the new OH groups produced by chemisorption.

When D_2 is chemisorbed on ZnO a band is produced at 2604 cm^{-1} which is assigned to the stretching vibrations of the new OD groups. A second band at 1232 cm^{-1} is due to the ZnD groups. No changes were observed in the OH bands of the background. Deuterium exchange was found to proceed faster for the OH groups and slower for the ZnH groups as shown by the decrease in intensity and frequency of the 3496 and 1709 cm^{-1} bands, respectively. The mechanism suggested by these investigators in the production of the ZnH surface species involves the splitting of H_2 (or D_2) molecules by the zinc-oxygen pairs of the surface:

$$ZnO + H_2 = ZnH + OH$$
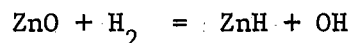
This type of reaction is strengthened by the fact that the bands at 3830, 3745, and 3412 cm^{-1} due to surface and internal hydroxyls did not change after adsorption. Such an observation would mean that the surface hydroxyls are not perturbed by the H_2 or D_2 molecules, and reaction should take place on some other type of sites, these being the Zn-O pairs.

Abrams and Sutherland[120] investigated the radiolysis of H_2 adsorbed on silica. A band appeared at 2284 cm^{-1} which is characteristic of the SiH_2 group. This surface species is quite stable since the band was present after evacuation at $450^{\circ}C$. The intensity of the Si-OH band re-

mained unchanged indicating that very little hydrogen dissociated during radiolysis.

The infrared spectra of hydrogen and deuterium on germania gel were studied by Low and co-workers[121]. Degassed germania showed bands at 3673 and 3550 cm^{-1} which were attributed to isolated Ge-OH groups and to hydrogen-bonded hydroxyl groups. Both bands were removed completely by evacuation at 500°C. Hydrogen adsorption on such a highly degassed sample exhibited bands at 3669 and 3550 cm^{-1} assigned to the same vibrations as previously. By degassing at 550°C all bands were removed entirely and the sample thus produced is known as a "reduced sample".

Hydrogen adsorption on reduced samples of germania gel showed a slightly different behavior. Bands were observed at 3550 cm^{-1}, as before, and at 2170 cm^{-1} assigned to the valence stretching vibrations of the surface Ge-H species. The absence of the 3673 cm^{-1} band indicates that isolated Ge-OH groups are probably nonexistent. Reduction of the germania surface almost completely eliminated their formation.

Deuterium adsorption gave similar results, except of course, the absorption bands were formed at lower frequencies. The bands observed at 2702, 2630, and 1540 cm^{-1} were attributed to the isolated Ge-OD sites, to the deuterium-bonded surface OD groups, and to the stretching vibration of the Ge-D species, respectively. Exchange reactions on the surface between hydrogen and deuterium (Ge-OH to Ge-OD and Ge-H to Ge-D) do take place, although some uncertainty exists as to their relative rates. It could be concluded, however, that exchange may proceed faster for the Ge-OH groups than the Ge-H species, in accordance with the exchange experiments performed on the surface of zinc oxide by Eischens and co-workers[119].

The Infrared and Laser-Raman Spectra of Stannic Oxide Gel

Preliminary infrared absorption spectra of SnO_2 gel were obtained at room temperature with a Beckman IR7 infrared spectrophotometer. The thickness of the sample used was less than 0.5 mm. Radiation losses due to scattering and absorption were the main problem in obtaining a measurable spectrum even at such low sample thicknesses. For this reason it became necessary to use an infrared beam condenser. In addition, the spectrum was obtained with relatively large slit widths.

The presence of surface hydroxyl groups and adsorbed water are of considerable interest in this study. Therefore, the infrared spectra were recorded in the high frequency region (between 3300 to 3800 cm^{-1}) where the vibrational absorption bands of water and surface hydroxyls occur. The sample was preheated at $120^{\circ}C$ in order to drive off excess water and then allowed to come to room temperature before the spectra were recorded.

The infrared absorption spectrum of SnO_2 gel under the above conditions is shown in Figure 22. A broad band appears in the spectrum in the region of the valence vibrations of the hydroxyl groups and adsorbed water, with three well characterized peaks at frequencies of 3740, 3660, and 3600 cm^{-1}. The sharp peak at 3740 cm^{-1} is assigned to the stretching vibration of the free hydroxyl groups of the surface, while the slightly broader band at 3660 cm^{-1} is due to the hydrogen-bonded surface OH groups. The band at 3600 cm^{-1} is attributed to water molecules which are hydrogen-bonded to surface hydroxyls. The broadening of this band towards lower frequencies (down to approximately 3340 cm^{-1}) is due to physically adsorbed water and due to water molecules in different environments, as it will be pointed out shortly.
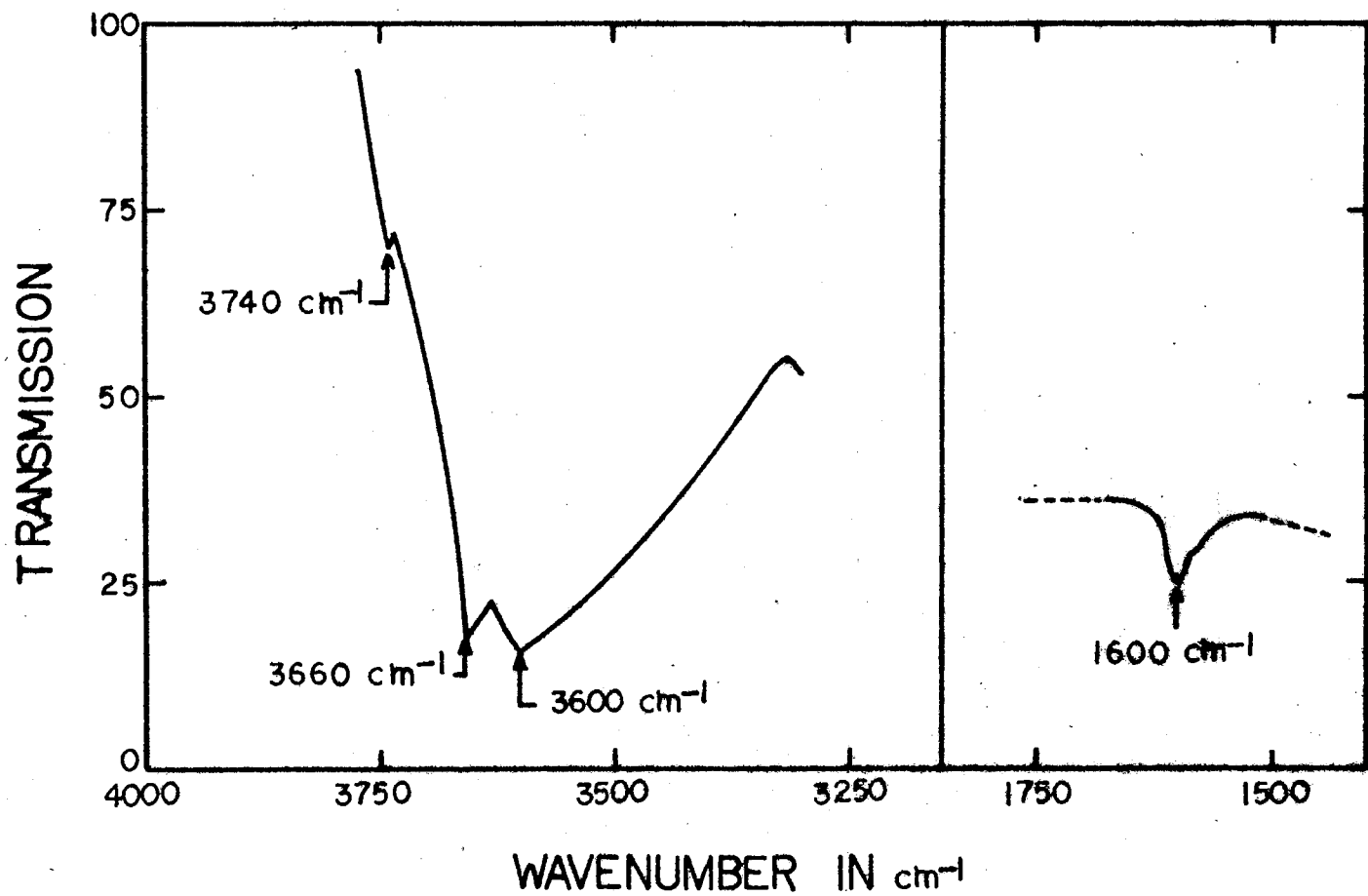
Figure 22. The Infrared Spectrum of SnO$_2$ Gel at Room Temperature

The assignment of these absorption bands was made by comparison with the spectra of hydroxyl groups and water on the surfaces of other gels, like silica[25] and alumina[94]. The 3740 cm^{-1} infrared band was assigned to the surface free Sn-O-H groups because such groups are characterized by sharp and narrow high frequency bands in the neighborhood of 3750 cm^{-1}. Hydroxyl groups which are hydrogen-bonded to each other
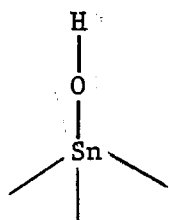
Free Surface OH Group   Hydrogen-bonded OH Groups
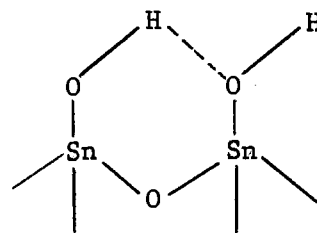
exhibit broader bands at lower frequencies than those of the free hydroxyls. Assignment of the 3660 cm^{-1} band to combined surface OH groups was made on this basis. Adsorbed water is expected to exist on the surface in various environments, i.e., as monomeric water hydrogen-bonded to surface hydrohyls, as clusters of water molecules forming a hydrogen-bonded network, and as internal water trapped within the stannic oxide gel globules or in the narrow pores of the adsorbent. The effect of such water molecules is manifested in the spectrum as a broadening and tailing off of the 3600 cm^{-1} band at lower frequencies.

In addition to the high frequency bands another one is observed in the infrared spectrum of the gel at 1600 cm^{-1}, as indicated in Figure 22. This absorption band is attributed to the vibrational bending mode of adsorbed water.

In as much as the infrared spectra of the SnO$_2$ gel were difficult

to obtain because of problems in scattering and absorption by the sample it became apparent that the use of Laser-Raman spectroscopy would produce more conclusive results as to the constitution of the gel surface. It can also serve as a check for the infrared absorption bands since the vibrations due to surface hydroxyls and adsorbed water are both infrared and Raman active.

The thickness of the sample was no longer a problem since, in this case, it is desirable to use relatively thick samples. Furthermore, the gel can be treated in place, by heating under vacuum, in order to remove adsorbed water from the surface. Removal of such water molecules should be demonstrated either by the complete absence or the decrease in intensity of certain vibrational bands in the spectrum.

The Raman spectra of SnO_2 gel were obtained with a Coherent Radiation Argon Ion Laser in the blue-green region of the visible spectrum with principal laser emission at 4880 A and 5145 A. The green line at 5145 A was used as the exciting line.

The sample, having a thickness of approximately 1.5 mm and length of 1 cm, was positioned in a conventional Raman optical cell so that the incoming radiation strikes the 1.5 mm edge and goes through its total length. The spectra are recorded from the radiation scattered by the flat surface of the sample at right angles to the incoming laser beam. The cell permits evacuation, as well as, in situ heating and then cooling of the gel with liquid nitrogen. Preheating of the sample was not carried out, in this case, so that excess water is still present on the surface.

Fluorescence of this material was quite intense so the sample had to be irradiated for about one hour at 1063 cm^{-1} or for longer periods,

if necessary, until the fluorescence decreased to a low tolerable level.

The Laser-Raman spectra of SnO_2 gel under varying conditions are represented in Figures 23(a) and (b). Figure 23(a) shows the Raman spectrum of the gel at room temperature. Distinct Raman shifts are located at 3740 and 3660 cm^{-1} with a broad band having maximum intensity at 3400 cm^{-1}. The band at 3600 cm^{-1} appears as a shoulder on this wide band. Assignment of the bands is made in accord with the infrared spectrum of the sample. It can be seen that the frequencies of the band maxima are very much the same in both the infrared and Raman. There may be an error of not greater than ±5 cm^{-1} in the numerical value of the band frequencies as read from the chart paper.

Free or isolated surface hydroxyls are responsible for the Raman shift at 3740 cm^{-1}, while OH groups combined through hydrogen bonding give rise to the band at 3660 cm^{-1}. Water molecules individually attached to surface hydroxyls produce the vibration at 3600 cm^{-1}. The broad band on either side of 3400 cm^{-1} is attributed, as with the infrared spectrum, to aggregates of H_2O molecules physically adsorbed on the surface with the individual molecules in the network held to each other by hydrogen bonds, to H_2O molecules held between the pore-walls of the gel, and to still other such molecules within the inner space of the adsorbent. Because different forces act on the molecules in the different environments their vibrations are displaced to lower frequencies thus causing the broadening of this absorption band.

Comparison between the infrared and Raman spectra indicates that the 3400 cm^{-1} band in the Raman is of higher intensity than in the infrared. This difference is due to the fact that the sample was preheated at 120°C before the infrared spectrum was recorded. The Raman
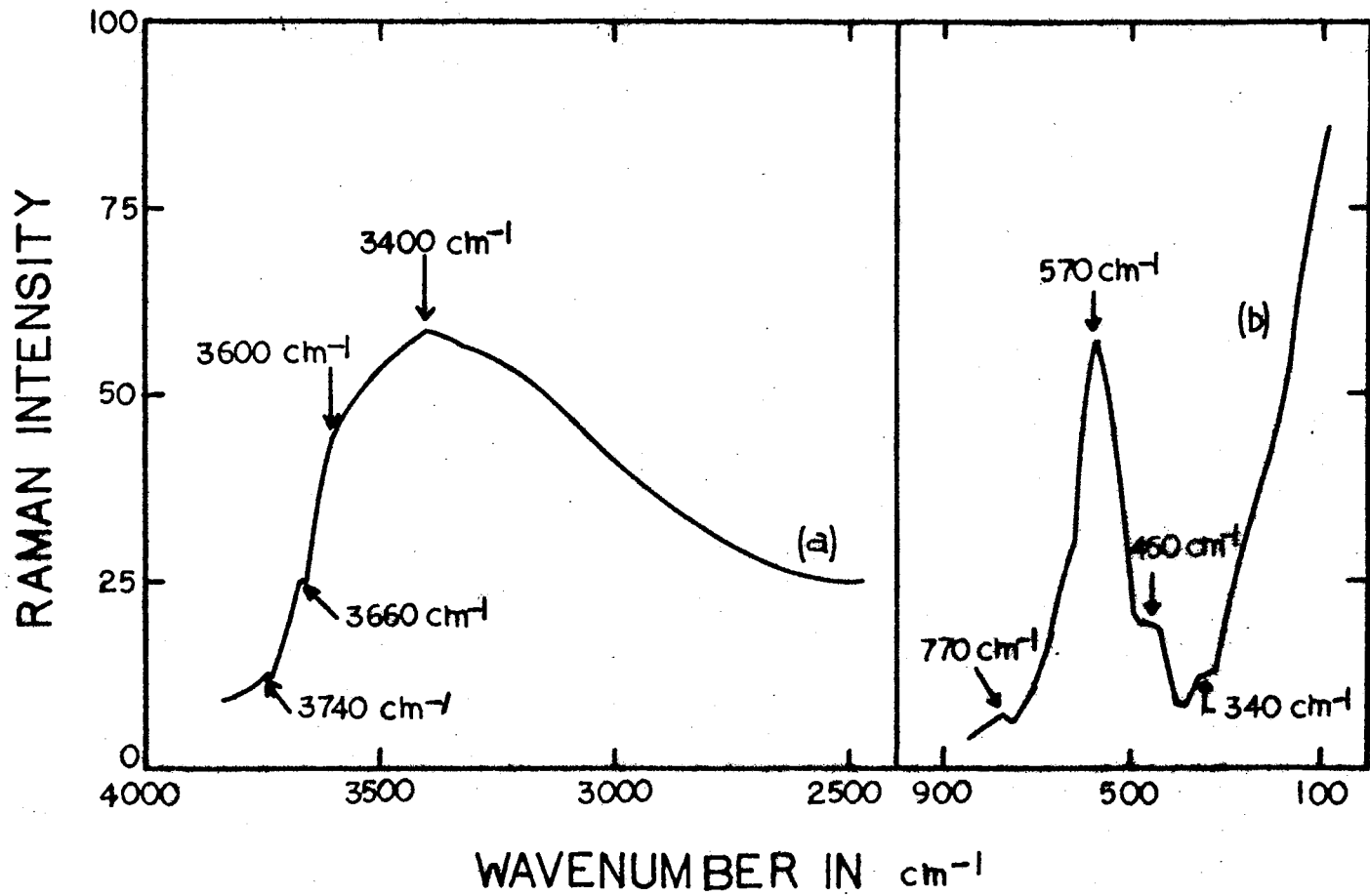
Figure 23.   The Laser-Raman Spectra of SnO_2 Gel; (a) At Room Temperature, (b) Lattice Vibrations at Room Temperature

spectrum was obtained with a nonpreheated sample, therefore, excess water was not removed from the surface. The presence of these adsorbed water molecules would increase the intensity of their corresponding band and this is indeed what is observed in the Raman spectrum.

Figure 23(b) shows the Raman spectrum of the gel in the range of 100 to 900 cm^{-1}. The bands in this region are attributed to the lattice or skeletal vibrations of the SnO_2 network. Since they are of no interest in this work their discussion is omitted. Assignment of these vibrations, however, can be made from the Raman spectra of stannic oxide single crystals reported in the literature by Katiyar et al.[122] and by Scott[123].

The Raman spectra of the gel represented in Figure 24 were taken at the temperature of liquid nitrogen after the sample was heated for several hours at 150°C with simultaneous evacuation at 1 x 10^{-5} Torr. The high background line of the spectrum is attributed to the fluorescence of the sample which appears to increase after the removal of adsorbed water. When attempts were made to decrease the fluorescence the sample charred at the point of incidence of the laser beam. For this reason the spectra were obtained with a lower beam intensity and with much of the fluorescence still present. The sample was cooled with liquid nitrogen in order to freeze the vibrations and also prevent it from charring.

The Raman bands in the semi-dehydrated sample at 3740 and 3660 cm^{-1} due to isolated and combined surface hydroxyls, respectively, appear to have intensified as compared with the corresponding bands of the hydrated gel of Figure 23(a). The broad band at 3400 cm^{-1} has decreased considerably in intensity and the peak has disappeared. This is an indication that a large number of adsorbed water molecules have been removed, due to
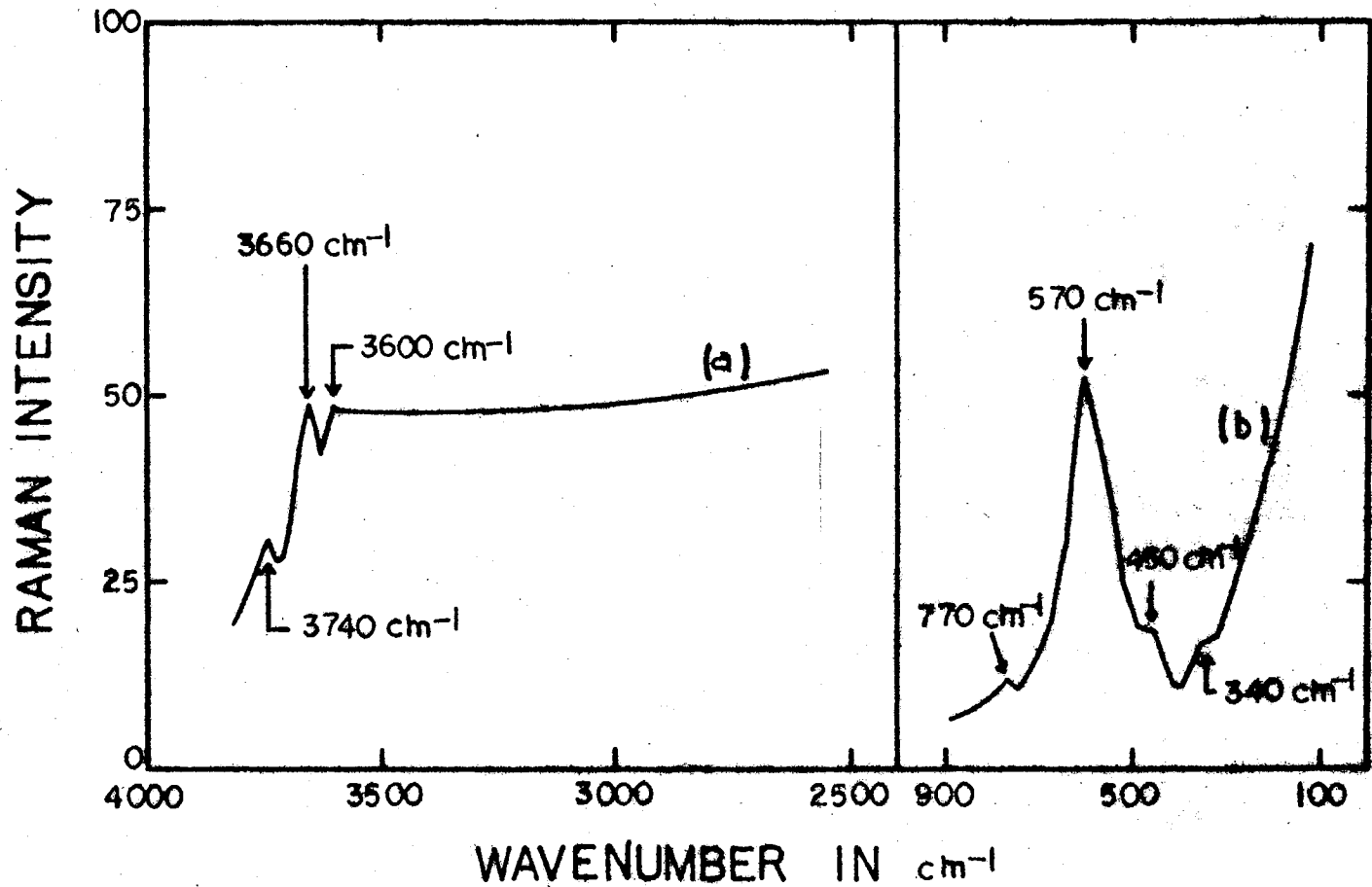
Figure 24. The Laser-Raman Spectra of SnO_2 Gel; (a) After Evacuation and Heating at 150°C. Spectra Taken at Liquid Nitrogen Temperature; (b) Lattice Vibrations at Liquid Nitrogen

evacuation and heating, giving way to an increase in the number of free and hydrogen-bonded surface OH groups, as seen by the increased intensities of their respective bands. The presence of the 3600 cm^{-1} absorption band shows that water is still present. Statements as to its intensity, however, cannot be easily made because of the high background due to fluorescence. This band may also include contributions from hydroxyl groups within the inner space and in the pores of the adsorbent. The vibrational frequencies of such hydroxyls would again be expected to be lower than those of the same groups on the surface (isolated or combined) because of the greater forces acting upon them.

In order to accomplish complete removal of water more severe treatment must be carried out on the sample. Removal of surface hydroxyls is even more difficult. McDonald[25] and Young[90], in their studies of silica gel, have shown that isolated surface hydroxyl groups remain on the surface even after heating the sample upto $900^{\circ}C$ under high vacuum for several hours. At higher temperatures the surface is usually destroyed because of sintering.

The lattice vibrations of the SnO_2 framework are shown in Figure 24(b). These bands arise from tin-oxygen fundamentals. The location of their frequency maxima and relative band intensities appear to be unchanged when compared with those of Figure 23(b).

The experimental results presented thus far establish the presence of hydroxyl groups and adsorbed water on the stannic oxide gel surface. The existence of free, combined, and inner hydroxyls is well accounted for from the experimental evidence of the spectra. In addition, water molecules in various force fields give rise to absorption bands and Raman shifts at the appropriate frequencies.

Water adsorption is primarily restricted to Sn-O-H sites on the surface of the gel as shown by the increase in intensity of both the isolated and combined hydroxyl bands in the Raman spectrum of the partially dehydrated sample. This conclusion may be strengthened by the fact that the tin-oxygen vibrations are virtually unchanged in going from the hydrated to the dehydrated sample. This is an indication that water does not adsorb on the remainder of the surface which is composed of tin and oxygen atoms.

CHAPTER X

SUGGESTIONS FOR FURTHER WORK

Spectroscopic Studies of the Adsorption
of Hydrogen on Stannic Oxide Gel

The investigation of hydrogen gas adsorption on the surface of
stannic oxide gel at liquid hydrogen with infrared and Raman techniques
will be a worthwhile study of the mechanism of adsorption, the nature of
adsorbed species, and the type of interaction between the surface and the
adsorbate molecules. Infrared spectroscopy will be limited by the thick-
ness of the sample. It is required that very thin samples must be used
so that absorption of radiation by the specimen will be reduced to a
minimum. In the case of Laser-Raman the thickness of the sample will not
be a limiting factor. As a matter of fact, it will be advantageous to
use thicker gel specimens in the Raman so that scattering of the radia-
tion will be increased and larger amounts of hydrogen gas can be adsorb-
ed on the surface. In this case more intense spectra will be recorded.
It would appear, at this point and from the results of Chapter IX, that
Raman spectroscopy would have a decided advantage over the infrared.

Hydrogen adsorption can be studied under various degrees of surface
coverage. For this reason the necessary data have already been obtained.
Values of the fraction of the surface covered up to a pressure of one
atmosphere were presented in Table II and Figure 11.

Of great interest will be the adsorption of deuterium gas on the

SnO_2 gel. The same spectroscopic methods will be employed in this case, as well. This wouldbe an excellent investigation of the exchange reactions between hydrogen and deuterium on the surface.

<div align="center">The Experimental Method-Refrigeration</div>
<div align="center">System and Miniature Cryostat</div>

The study of hydrogen adsorption on the surface of stannic oxide gel at the temperature of liquid hydrogen is to be carried out spectroscopically in a specially designed cryostat which is used to cool the sample down to the desired temperature. The cryogenic temperature of liquid hydrogen is achieved by the open-cycle Joule-Thomson expansion of gaseous hydrogen. For hydrogen gas to liquefy it must be below its inversion temperature. For this reason nitrogen gas is used which by expansion and liquefaction brings the hydrogen below its inversion temperature. The Joule-Thomson refrigerator employed for this purpose is a Miniature Cryostat obtained from Air Products and Chemicals, Inc. The Cryotip system consists of the Heat Exchanger, Model Number AC 2-110, the Dewar and Radiation Shield, Model Number WMX-1, the Control Panel, OC-22, including the cold trap coil, the Flexlines, and the Nitrogen and Hydrogen High Pressure Regulators. The schematic diagram for the complete system is shown in Figure 25.

Refrigeration systems of this kind were designed and developed by Geist and Lashmet[124] for the temperature range $4.2^{\circ}K$ to $200^{\circ}K$. White and Mann[125] designed miniature cryostats for Matrix-Isolation studies. Infrared work at low temperatures using such cryostats was carried out by Barnes and Hallam[126], by Hermann[127], and by King[128].

The operation of the Cryo-Tip Heat Exchanger will not be presented
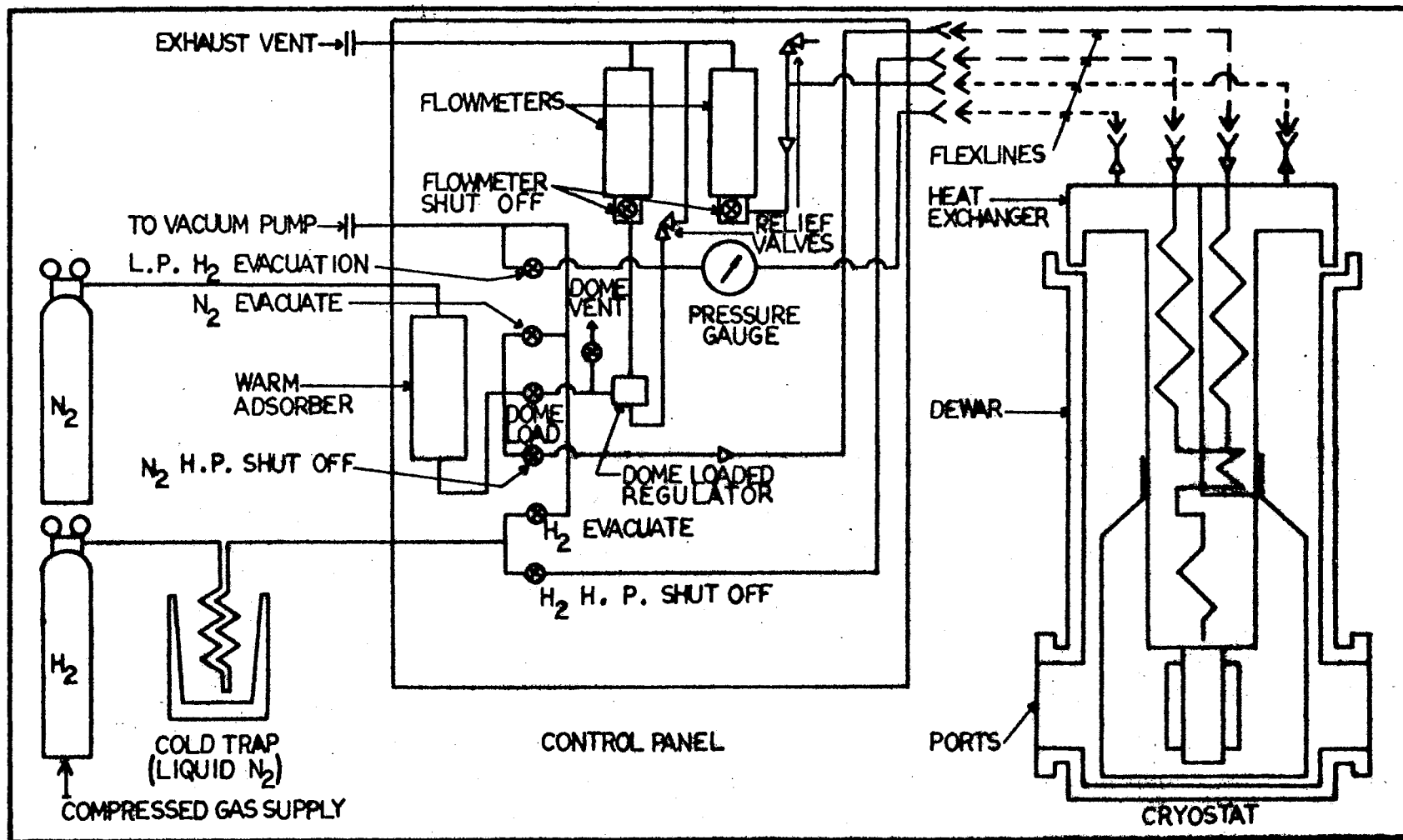
Figure 25. Complete System Schematic Flow Diagram for Miniature Cryostats

here. Operating instructions for the apparatus were provided by Air Products and Chemicals, Inc.[129] and helpful suggestions may be found in the literature just presented. Certain modifications, however, are necessary for the application of the cryostat to spectroscopic studies of adsorbed molecules. These include modifications in the sample holder and gas delivery system to the sample, as well as construction of the necessary vacuum system and auxiliary equipment.

For adsorption studies the sample compartment must be vacuum-tight so that the amount of the adsorbate gas can be measured. Since the cryostat was originally designed for matrix-isolation studies it became necessary to change the sample holder in order to fit the experimental needs of this investigation. Such an optical transmission cell was constructed out of brass and mounted onto the liquid hydrogen station of the heat exchanger. A side-view of the new cell is shown in Figure 26. The sample is held in place between two indium gaskets and a brass washer. Good thermal conduction to the sample is maintained by the use of "High Conductivity Grease" at all points of attachment. The sodium chloride windows are then inserted and firmly attached to the cell with the two cylindrical screws, as shown in the Figure. In order to insure high vacuum in the sample compartment a number of sealants are presently being tried which must perform well at the temperature of liquid hydrogen and maintain a good vacuum-tight seal between the brass sample holder and the sodium chloride windows. Such attempts have so far been unsuccessful. A copper-constantan thermocouple is attached to the cell with indium solder for monitoring the temperature of the sample. The cell compartment is evacuated through the "Evacuation Port" which also serves as the adsorbate gas delivery tube.
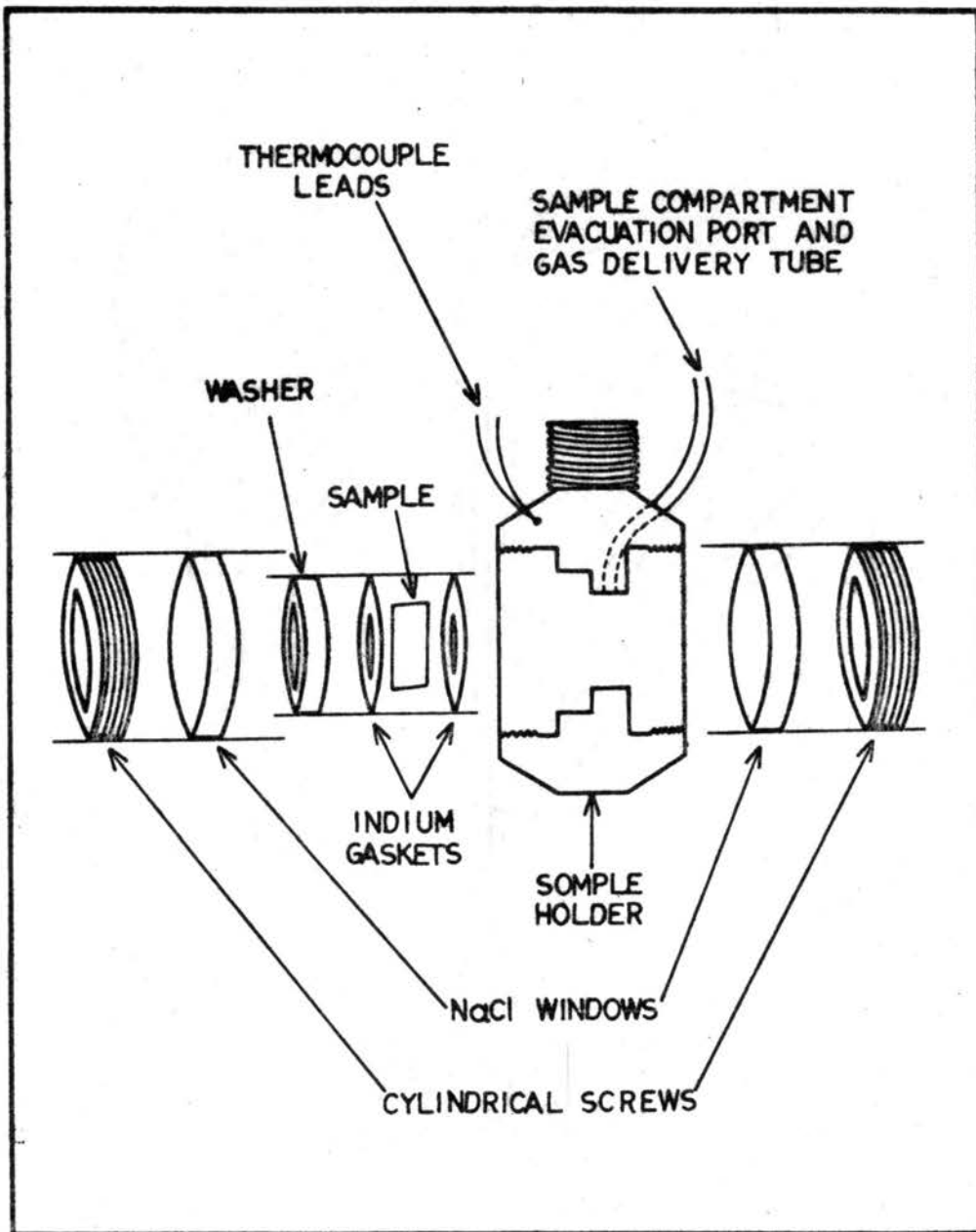
Figure 26. Sample Holder

The above cell has been constructed for infrared work. In the case of the Raman construction of a vacuum tight specimen holder should not present any problems. Such a cell may consist of pyrex glass instead of sodium chloride windows. It could be made to fit the liquid hydrogen heat station of the exchanger with a glass-to-metal seal. In this manner leaks should be eliminated.

The modified heat exchanger is shown in Figure 27. The gas is delivered to the sample through the thin stainless steel tubing which is subsequently connected to copper tubing of the same size leading to the sample holder. In order to minimize direct conductive heat leak the copper tubing is wrapped around the exchanger several times and soft soldered on the outside of the housing. This change necessitated a new liquid nitrogen radiation shield of larger diameter in order to accommodate the copper tubing. The Figure also shows the thermocouple leads wrapped around the bottom plug of the heat exchanger for heat leak minimization. General Electric GEVAC vacuum leak sealer is used to hold the wires onto the shaft.

The hydrogen gas delivery system is shown diagrammatically in Figure 28. The heavy lines indicate copper tubing connections; the thin lines indicate the glass part. The various sections can be isolated through valves No. 1, 2, 3, and 4, and the vacuum stopcock. The H_2 gas bulb is filled on an auxiliary vacuum system with "Ultra Pure" hydrogen to approximately 1.5 atm. and attached to the system as shown in the Figure. During evacuation of the sample the stopcock remains closed, while valves 2, 3, and 4 are open to the vacuum. Pumping continues until a vacuum of 1×10^{-6} torr or better is achieved. When it is necessary to admit the adsorbate gas into the sample cell compartment valve No. 2 is closed and
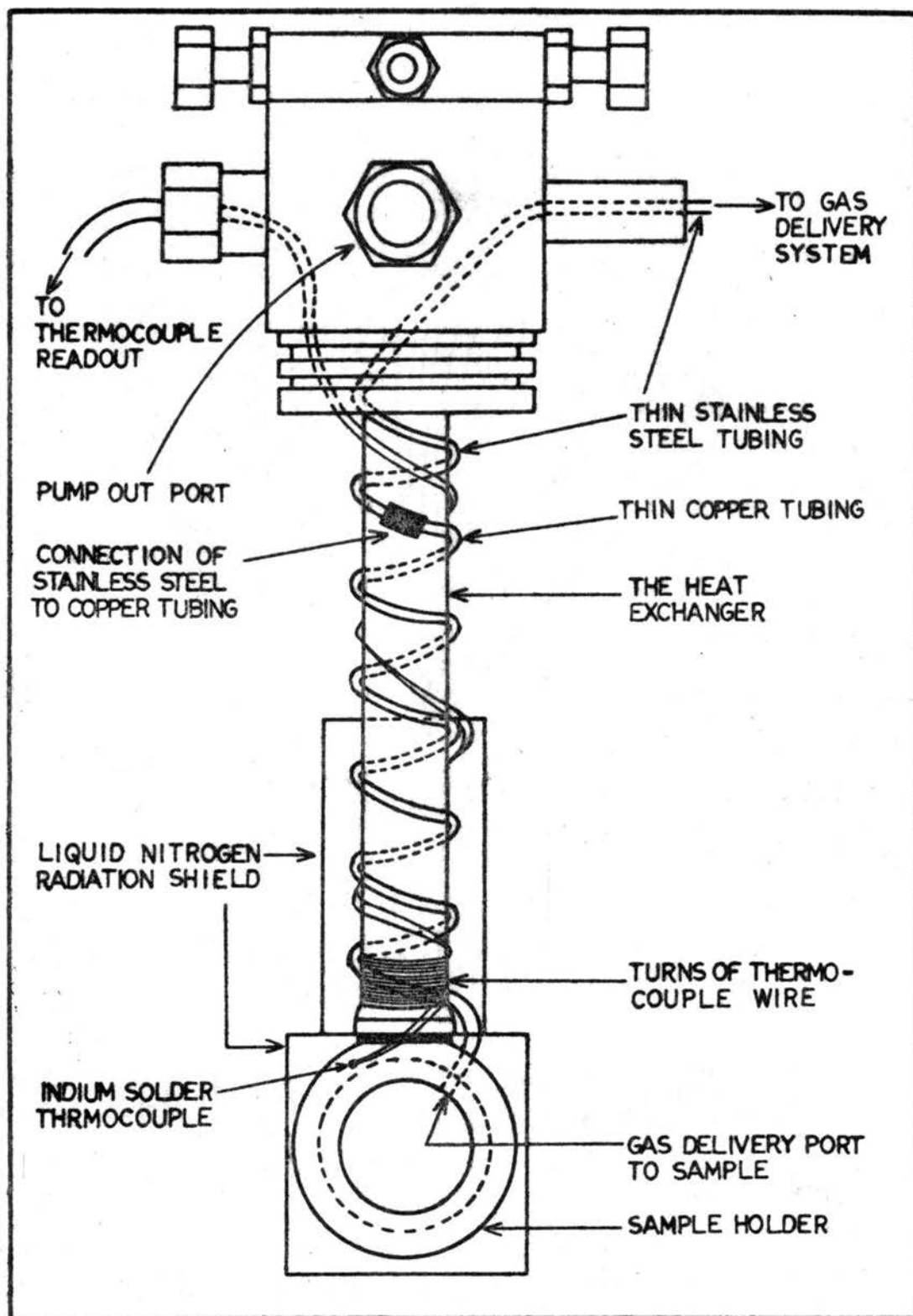
Figure 27. The Modified Heat Exchanger
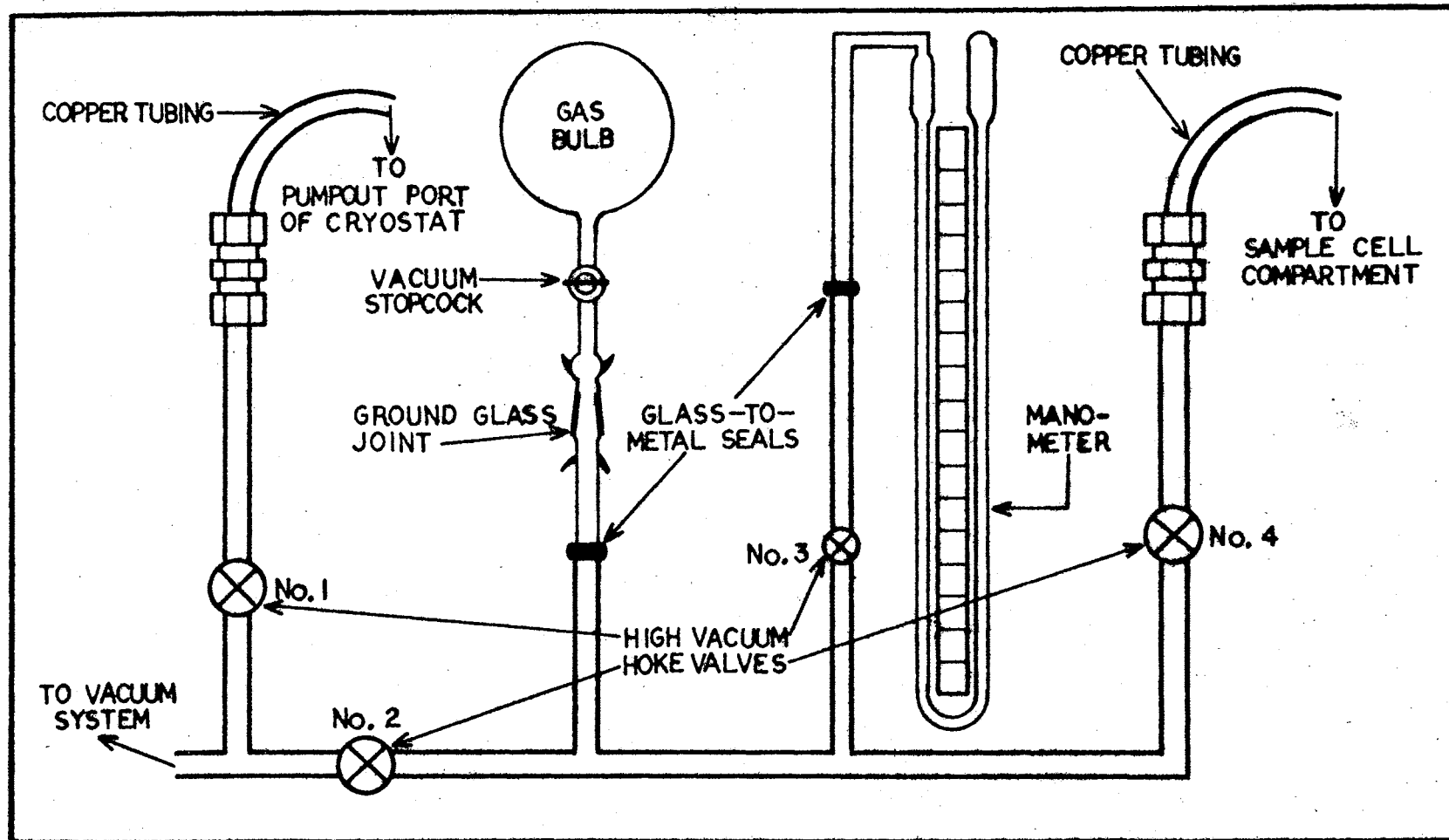
Figure 28. The Gas Delivery System

gas is transferred from the bulb to the specimen holder through the stopcock and valve No. 3. The desired amount of gas is measured by the mercury manometer. A slight increase in the temperature of the sample holder is observed during adsorption. After a minute or two the temperature reaches equilibrium and the manometer pressure is read. Valves No. 3 and 4 are closed and the spectra may be taken. Larger amounts of gas can be introduced into the cell in this manner and the spectra can be obtained at varying degrees of surface coverage. The fraction of the surface covered may be interpolated from the tables of Chapter VII (Table II) since the pressure at which adsorption occurs is known.

The vacuum system consists of two vacuum lines, each isolated by a high vacuum valve. The first line is connected to the pump-out port of the cryostat and the gas delivery system (see Figure 28). The second line is connected to the vacuum port of the control panel for evacuation of the inlet lines. A "Hastings" vacuum tube and a glass "Cold Cathode" vacuum tube are connected to each line so that measurements of the pressure in the system can be made both with a "Hastings Vacuum Gauge" and with a "Miller Cold Cathode Vacuum Gage". A port is provided on the brass jacket of the liquid nitrogen trap for attaching a helium leak detector. The system is helium tested for leaks after evacuation using such a detector, obtained from Mikros, Inc., Division of Varian Associates.

For convenience and ease of operation all the parts of the complete system are mounted onto a mobile instrument cabinet. Four demountable panels are used. The bottom panel contains the electrical outlets. The vacuum system is attached to the inside and the gas delivery system to the outside of the second panel. The third one is the cryostat control

panel and the fourth contains the pressure measuring devices. The fore-
pump is placed on the floor of the cabinet and a fan is mounted on the
top for good air ventilation.

For prolonged operation of the cryostat, as required in this study,
it is necessary to use a number of nitrogen and hydrogen gas cylinders
connected in series through a manifold. As many as four cylinders can
be connected to each manifold and an empty cylinder can be replaced
quite easily during operation. The cylinders are mounted in place on
two mobile racks, one for the nitrogen and the other for the hydrogen
gas cylinders and manifold. In this way the complete assembly (cabinet
and racks) can be rolled and moved to any desired location.

BIBLIOGRAPHY

1. Langmuir, I., J. Am. Chem. Soc., **38**, 2221 (1916).

2. Langmuir, I., J. Am. Chem. Soc., **40**, 1361 (1918).

3. Langmuir, I., J. Am. Chem. Soc., **54**, 2798 (1932).

4. Polanyi, M., Vehr. Deut. Physik, Ges., **16**, 1012 (1914); **18**, 55 (1916).

5. Polanyi, M., Z. Elektrochem., **26**, 371 (1920).

6. Goldmann, F. and Polanyi, M., Z. Phys. Chem., **132**, 321 (1928).

7. Polanyi, M. and Welke, K., Z. Phys. Chem., **132**, 371 (1928).

8. Polanyi, M., Z. Elektrochem., **35**, 431 (1929).

9. De Boer, J. H. and Zwikker, C., Z. Phys. Chem., **B3**, 407 (1929).

10. Brunauer, S., Emmett, P. H., and Teller, E., J. Am. Chem. Soc., **60**, 309 (1938).

11. Wheeler, A., Presentations at Catalysis Symposia, Gibson Island, AAAS Conferences, June 1945 and June 1946.

12. Wheeler, A., Catalysis, Emmett, P. H., ed., Vol. **2**, Reinhold, New York (1955).

13. Buswell, A. M., Krebs, K., and Rodebush, W. H., J. Am. Chem. Soc., **59**, 2603 (1937).

14. Terenin, A. N., Zh. Fiz. Khim., **14**, 1362 (1940); C. A., **35**, 38837 (1941).

15. Yaroslavskii, N. G. and Terenin, A. N., Dokl. Akad. Nauk SSSR, **66**, 885 (1949); C. A., **43**, 7343h (1949).

16. Yaroslavskii, N. G., Zh. Fiz. Khim., **24**, 68 (1950); C. A., **44**, 4786g (1950).

17. Yaroslavskii, N. G. and Karyakin, A. V., Kokl. Akad. Nuak SSSR, **85**, 1103 (1952); C. A., **47**, 967g (1953).

18. Kurbatov, L. N. and Newimin, G. G., Dokl. Akad. Nauk SSSR, **68**, 341 (1949); C. A. **44**, 435f (1950).

19. Sidorov, A. N., Dokl. Akad. Nauk SSSR, 95, 1235 (1954); C. A., 49, 8703b (1955).

20. Nikitin, V. A., Sidorov, A. N., and Karyakin, A. V., Zh. Fiz. Khim., 30, 117 (1956); C. A., 50, 9095e (1956).

21. Sidorov, A. N., Zh. Fiz. Khim., 30, 995 (1956); C. A., 51, 12656h (1957).

22. Babushkin, A. A. and Uvarov, A. V., Dokl. Akad. Nauk SSSR, 110, 581 (1956); C. A., 51, 12657g (1957).

23. Eischens, R. P. and Pliskin, W. A., Advances in Catalysis, Vol. X, p. 1, Academic Press, Inc., New York (1958).

24. McDonald, R. S., J. Am. Chem. Soc., 79, 850 (1957).

25. McDonald, R. S., J. Phys. Chem., 62, 1168 (1958).

26. Sheppard, N. and Yates, D. J. C., Proc. Roy. Soc., A238, 69 (1956).

27. Little, L. H., Infrared Spectra of Adsorbed Molecules, Academic Press, Inc., London, New York (1966).

28. Hair, M. L., Infrared Spectroscopy in Surface Chemistry, Marcel Dekker Inc., New York (1967).

29. Young, M. D. and Crowell, A. D., Physical Adsorption of Gases, Chapter I, Butterworths, Washington (1962).

30. Trapnell, B. M. W., Chemisorption, Chapter I, Butterworths, London (1955).

31. Brunauer, S., Deming, L. S., Deming, W. E., and Teller, E., J. Am. Chem. Soc., 62, 1723 (1940).

32. Brunauer, S., The Adsorption of Gases and Vapors, Vol. I, Physical Adsorption, Princeton University Press, Princeton (1945).

33. Wilkins, F. J., Proc. Roy. Soc., A164, 496 (1938).

34. Rowley, H. H. and Innes, W. B., J. Phys. Chem., 45, 158 (1941).

35. Emmett, P. H. and Brunauer, S., J. Am. Chem. Soc., 59, 1553 (1937).

36. Brunauer, S. and Emmett, P. H., J. Am. Chem. Soc., 59, 2682 (1937).

37. Lamb, A. B. and Coolidge, A. S., J. Am. Chem. Soc., 42, 1146 (1920).

38. Halsey, G. D., J. Chem. Phys., 16, 931 (1948).

39. Halsey, G. D., Advances in Catalysis, Vol. IV, p. 259, Academic Press, Inc., New York (1952).

40. Hill, T. L., J. Chem. Phys., 17, 106 (1949); 17, 590 (1949); 17, 668 (1949).

41. McMillan, W. G. and Teller, E., J. Chem. Phys., 19, 25 (1951).

42. McMillan, W. G. and Teller, E., J. Phys. Chem., 55, 17 (1951).

43. Davis, R. T. and DeWitt, T. W., J. Am. Chem. Soc., 70, 1135 (1948).

44. Kington, G. L., Beebe, R. A., Polley, M. H., and Smith, W. R., J. Am. Chem. Soc., 72, 1775 (1950).

45. Kington, G. L. and Aston, J. G., J. Am. Chem. Soc., 73, 1934 (1951).

46. Harkins, W. D. and Jura, G., J. Chem. Phys., 11, 431 (1943).

47. Zsigmondy, R., Z. Anorg. Chem., 71, 356 (1911).

48. McGavack, J., Jr. and Patrick, W. A., J. Am. Chem. Soc., 42, 946 (1920).

49. Cohan, L. A., J. Am. Chem. Soc., 60, 433 (1938).

50. Carman, P. C., J. Phys. Chem., 57 56 (1953).

51. Pierce, C. and Smith, R. N., J. Phys. Chem., 57, 64 (1953).

52. Barrett, E. P., Joyner, L. G., and Halenda, P. P., J. Am. Chem. Soc., 73, 373 (1951).

53. Shull, C. G., J. Am. Chem. Soc., 70, 1405 (1948).

54. Shull, C. G., Elkin, P. B., and Roess, L. C., J. Am. Chem. Soc., 70, 1410 (1948).

55. Oulton, T. D., J. Phys. Colloid. Chem., 52, 1296 (1948).

56. Anderson, R. B., J. Catal., 3, 50 (1964).

57. Innes, W. B., Anal. Chem., 29, 1069 (1957).

58. De Boer, J. H., Proceedings of the Tenth Symposium of the Colston Research Society Held in the University of Bristol, The Structure and Properties of Porous Materials, Butterworths, London (1958).

59. De Boer, J. H. and Lippens, B. C., J. Catal., 3, 38 (1964).

60. Lippens, B. C., Linsen, B. G., and De Boer, J. H., J. Catal., 3, 32 (1964).

61. Lippens, B. C. and De Boer, J. H., J. Catal., 3, 44 (1964).

62. Richardson, L. B., J. Am. Chem. Soc., 39, 1829 (1917).

63. Pease, R. N., J. Am. Chem. Soc., 45, 1196 (1923).

64. McBain, J. W. and Bakr, A. M., J. Am. Chem. Soc., 48, 690 (1926).

65. Rhodin, T. N., J. Am. Chem. Soc., 72, 4343 (1950); 72, 5691 (1950).

66. Rhodin, T. N., Advances in Catalysis, Vol. V, p. 39, Academic Press Inc., New York (1953).

67. Joy, A. S., Vacuum, 3, 254 (1953).

68. Rutledge, J. L., Kohnke, E. E., and Cunningham, C. M., Interim Report SS-2, NASA Grant NsG609, Research Foundation, Oklahoma State University, Stillwater, Oklahoma, December 1965.

69. Farkas, A. and Melville, H. W., Experimental Methods in Gas Reactions, p. 104, McMillan, London (1939).

70. Barr, W. E. and Anhorn, V. J., Scientific and Industrial Glass Blowing and Laboratory Techniques, p. 257, Instruments Publishing Co., Pittsburgh (1949).

71. Constabaris, G., Singleton, J. H., and Halsey, G. D., Jr., J. Phys. Chem., 63, 1350 (1959).

72. Mills, B., Rev. Sci. Instr., 12, 105 (1941).

73. Zsigmondy, R., Annalen, 301, 361 (1898).

74. Dhar, N. R. and Varadanam, Ch. I., J. Indian Chem. Soc., 13, 602 (1936).

75. Weiser, H. B., Millican, W. O., and Simpson, W. C., J. Phys. Chem., 46, 1051 (1942).

76. Aditya, S., J. Indian Chem. Soc., 29, 296 (1952).

77. Ghosh, B. N. and Ghosh, A. K., J. Indian Chem. Soc., 34, 871 (1957).

78. Brauer, G., Handbook of Preparative Inorganic Chemistry, Vol. I, Academic Press, Inc., New York (1963).

79. Goodman, J. F. and Gregg, S. J., J. Chem. Soc., 1162 (1960).

80. International Critical Tables, Vol. I, McGraw-Hill, New York (1926).

81. CRC Handbook of Chemistry and Physics, 51 ed., Weast, R. C., ed., Chemical Rubber Co., Cleveland (1970).

82. Vernardakis, T. G., Unpublished M.S. Thesis, Oklahoma State University, Stillwater (1968).

83. Ohno, S. and Yasumori, I., Bull. Chem. Soc. Jap., 41, 2227 (1968).

84. Paneja, P. and Henri, A., J. Chim. Phys. Physicochim. Biol., 66, 1575 (1969).

85. Iler, R. K., The Colloid Chemistry of Silica and Silicates, p. 233, Cornell University Press, Ithaca (1955).

86. Kiselev, A. V., Kolloid. Zh., 2, 17 (1936); C. A., 30, 62639 (1936).

87. Kiselev, A. V., Russ. J. Phys. Chem., 38, 1501 (1964); 41, 1338 (1967).

88. Kiselev, A. V. and Lygin, V. I., Kolloid. Zh., 21, 581 (1959); C. A., 55, 69841 (1961).

89. Coulson, C. A., Hydrogen Bonding, Hadzi, D., ed., p. 339, Pergamon Press, London (1957).

90. Young, G. J., J. Colloid Sci., 13, 67 (1958).

91. Benesi, H. A. and Jones, A. C., J. Phys. Chem., 63, 179 (1959).

92. Kiselev, A. V. and Lygin, V. I., Russ. Chem. Rev., 31, 175 (1962).

93. Peri, J. B. and Hannan, R. B., J. Phys. Chem., 64, 1526 (1960).

94. Peri, J. B., J. Phys. Chem., 69, 220 (1965).

95. Eyring, E. M. and Wadsworth, M. E., Mining Engnr., 5, 531 (1956).

96. Roev, L. M. and Terenin, A. N., Proc. Acad. Sci. USSR, Phys. Chem. Sect. (English Transl.), 124, 77 (1959); 125, 293 (1959).

97. Yates, D. J. C., J. Phys. Chem., 65, 746 (1961).

98. Parfitt, G. D., Ramsbotham, J., and Rochester, C. H., Trans. Faraday Soc., 67, 841 (1971).

99. Primet, M., Pichat, P., and Mathieu, M-V., J. Phys. Chem., 75, 1216, 1221 (1971).

100. Blyholder, G. and Richardson, E. A., J. Phys. Chem., 66, 2597 (1962); 68, 3882 (1964).

101. Roginskii, S. Z. and Rufov, Yu. N., Kinetics Catalysis (USSR), 7, 118 (1966).

102. Stuart, W. I. and Whateley, T. L., Trans. Faraday Soc., 61, 2763 (1965).

103. Anderson, P. J., Horlock, R. F., and Oliver, J. F., Trans. Faraday Soc., 61, 2754 (1965).

104. Low, M. J. D. and Matsushita, K., J. Phys. Chem., 73, 908 (1969).

105. Cant, N. W. and Little, L. H., Can. J. Chem., 42, 802 (1964).

106. Herzberg, G., Infrared and Raman Spectra of Polyatomic Molecules, Van Nostrand Co., New York (1945).

107. Little, L. H., Klauser, H. E., and Amberg, C. H., Can. J. Chem., 39, 42 (1961).

108. Little, L. H., J. Chem. Phys., 34, 342 (1961).

109. Parry, E. P., J. Catal., 2, 371 (1963).

110. Eischens, R. P., Francis, S. A., and Pliskin, W. A., J. Phys. Chem., 60, 194 (1956).

111. Chapman, I. D. and Hair, M. L., Trans. Faraday Soc., 61, 1507 (1965).

112. Karagounis, G. and Issa, R. M., Z. Elektrochem., 66, 874 (1962).

113. Karagounis, G. and Issa, R. M., Nature, 195, 1196 (1962).

114. Hendra, P. J. and Loader, E. J., Nature, 216, 789 (1967); 217, 637 (1968).

115. Hendra, P. J., Horder, J. R., and Loader, E. J., Chem. Commun., 563 (1970).

116. Kagel, R. O., J. Phys. Chem., 74, 4518 (1970).

117. Winde, H., Z. Chem., 10, 64 (1970).

118. Hendra, P. J. and Loader, E. J., Trans. Faraday Soc., 67, 828 (1971).

119. Eischens, R. P., Pliskin, W. A., and Low, M. J. D., J. Catal., 1, 180 (1962).

120. Abrams, L. and Sutherland, J. W., J. Phys. Chem., 73, 3160 (1969).

121. Low, M. J. D., Madison, N., and Ramamurthy, P., Surface Sci., 13, 238 (1969).

122. Katiyar, R. S., Dawson, P., Hargreave, M. M., and Wilkinson, G. R., J. Phys. (C): Solid St. Phys., 4, 2421 (1971).

123. Scott, J. F., J. Chem. Phys., 53, 852 (1970).

124. Geist, J. M. and Lashmet, P. K., Advan. Cryog. Eng., 5, 324 (1960); 6, 73 (1961).

125. White, D. and Mann, D. E., Rev. Sci. Instr., 34, 1370 (1963).

126. Barnes, A. J. and Hallam, H. E., Quart. Rev., 23, 392 (1969).

127. Hermann, T. S., Appl. Spectrosc., 23, 473 (1969).

128. King, S. T., J. Phys. Chem., 74, 2133 (1970).

129. Cryo-Tip Instruction and Operating Manual, Air Products and Chemicals, Inc., Allentown, Pennsylvania, January 1965.

APPENDIX A

THE EQUATION FOR SPECIFIC SURFACE AREA EVALUATION

The specific surface area, S, of a solid adsorbent is usually expressed in square meters per gram. In order to calculate S it is necessary to multiply the area, σ_m, which one adsorbed molecule would occupy in a completed monolayer by the number of molecules, N_m, contained in the monolayer volume, V_m. The area σ_m is usually expressed in square angstroms and V_m in cubic centimeters at S.T.P. per gram of adsorbent. Therefore,

$$S = \sigma_m \ (A^2/\text{molecule}) \ N_m \qquad (A-1)$$

In order to obtain S in m^2/g the necessary conversions must be used, as:

$$1 \ A^2 = 10^{-20} \ m^2 \qquad (A-2)$$

Also,

$$N_m = N(V_m/V_M) \qquad (A-3)$$

where N is Avogadro's number (6.023×10^{23} molecules/mole) and V_M is the molar volume at S.T.P. (22414 cm^3/mole).

Therefore, Equation (A-3) becomes:

$$N_m = \frac{(6.023 \times 10^{23})(V_m)}{22414} \qquad \text{(A-4)}$$

$$N_m = (0.269 \times 10^{20}) V_m \quad \text{molecules/g} \qquad \text{(A-5)}$$

Substitution of Equations (A-3) and (A-5) in Equation (A-1) yields:

$$S = (\sigma_m \; A^2/\text{molecule})(10^{-20} \; m^2/A^2) \; X$$

$$X \; (0.269 \times 10^{20} \times V_m \; \text{molecules/g}) \qquad \text{(A-6)}$$

The final form of Equation (A-6) would then be:

$$S = 0.269 \; \sigma_m \; V_m \quad m^2/g \qquad \text{(A-7)}$$

APPENDIX B

VOLUME OF THE STANDARD BULBS AND VOLUME FACTORS

The five bulbs in the burette are given the numbers 1 through 5 starting at the left with the smallest bulb being No. 1. The volume of each bulb is calculated from the mass of mercury necessary to fill the bulb between two etched reference marks and the density of Hg at the appropriate temperature. Calibration was carried out at $26^{\circ}C$ and the density of mercury at this temperature is 13.5314 g/cm^3. Each bulb was filled with mercury twice and weighed each time. In the table below only the average mass of Hg from the two weighings is given.

TABLE VII

VOLUME OF THE STANDARD BULBS

Bulb No.	Temp. ($^{\circ}C$)	Mass of Hg (g)	Volume (cm^3)	Volume Factor, $(f_1)_j$
1	26	94.636	6.994	25.14
2	26	210.245	15.538	55.84
3	26	428.761	31.686	113.88
4	26	905.301	66.904	240.46
5	26	1702.327	125.806	452.16

The volume factors $(f_1)_j$, where j is the number of bulbs, are calculated from: $(f_1)_j = (273.16/76)(V_1)_j$.

The following table lists the 32 possible values of $(f_1)_i$, where i represents the 32 bulb settings. For any bulb setting the digit 1 means that a bulb is filled with gas while the digit 0 means that it is empty

or rather filled with Hg. For example, in a series 10001 the first and fifth bulbs are filled with gas while the second, third, and fourth are filled with mercury. The values of $(V_1)_i$ are also given in the table.

TABLE VIII

VOLUME FACTORS OF THE STANDARD BULBS

Combinations	Bulb Setting	Volume, $(V_1)_i$	Volume Factor, $(f_1)_i$
1	00000	0.000	0.00
2	10000	6.994	25.14
3	01000	15.538	55.84
4	11000	22.532	80.98
5	00100	31.686	113.88
6	10100	38.680	139.02
7	01100	47.224	169.72
8	11100	54.218	194.86
9	00010	66.904	240.46
10	10010	73.898	265.60
11	01010	82.442	296.30
12	11010	89.436	321.44
13	00110	98.590	354.34
14	10110	105.584	379.48
15	01110	114.128	410.18
16	11110	121.122	435.32
17	00001	125.806	452.16
18	10001	132.800	477.30
19	01001	141.344	508.00
20	11001	148.338	533.14
21	00101	157.492	566.04
22	10101	164.486	591.18
23	01101	173.030	621.88
24	11101	180.024	647.02
25	00011	192.710	692.62
26	10011	199.704	717.52
27	01011	208.248	748.46
28	11011	215.242	773.60
29	00111	224.396	806.50
30	10111	231.390	831.64
31	01111	239.934	862.34
32	11111	246.928	887.48

APPENDIX C

TABULAR FORM FOR TAKING AND ANALYZING

THE ADSORPTION DATA

It is usually convenient to take the experimental data in tabular
form and keep the analysis along with the data. The tabulation of both
data and results requires 26 columns. Each column number is listed be-
low along with the corresponding title which shows what the column con-
tains. If a calculation is to be carried out the manner by which it is
to be performed is also shown. Numbers which are underlined refer to
columns whose value is to be used in calculation. For example, in col-
umn 14, Bar pressure = 4 + 5 - 6, means that the uncorrected pressure
from the constant volume manometer is obtained by subtracting the value
given in column 6 from the sum of values in columns 4 and 5.

In the above example column 4 gives the bar pressure to the nearest
tenth of a centimeter just below the mercury level as read from the pre-
cision meter bar; column 5 gives the reading when the cathetometer is
set on the precise position of the mercury level; column 6 gives the
reading when the cathetometer is lowered from the mercury level and set
on the reading of the meter bar of column 4. Columns 5 and 6 are ob-
tained from the scale of the cathetometer to the nearest thousandth of
a centimeter.

The manner by which the experimental data are obtained and the
method of their analysis are shown explicitly in each of the 26 columns
of the tabulation which follows.

Column No.	Column Title
1	Remarks (Sample stopcock opened, closed; He, N_2, H_2)
2	Bulb setting
3	Volume factor, f_1, for bulb setting of column 2; obtained from the tables of Appendix B
4	Bar pressure from precision meter bar (Mark lower than mercury level)
5	Cathetometer reading of exact mercury level
6	Cathetometer reading of bar mark of column 4
7	Upper mercury level of vapor pressure manometer
8	Lower mercury level of vapor pressure manometer
9	Level of liquid refrigerant; nitrogen or hydrogen. (Must be kept within 1/2 inch of a set reference point)
10	Temperature of the sample ($^{\circ}$K)
11	Temperature of the room ($^{\circ}$C)
12	Temperature of burette bulbs in water bath ($^{\circ}$C)
13	Temperature of the main manometer ($^{\circ}$C)
14	Bar pressure = (4 + 5 - 6)
15	Absolute pressure = 14 x correction factor = P
16	Vapor pressure = (7 - 8)
17	Vapor pressure corrected = 16 x correction factor = P_o
18	Absolute pressure correction for V_4. For nitrogen $P_{cor.} = P (1 + 0.05P/76)$, and for hydrogen $P_{cor.} = P (1 + 0.077P/76)$
19	Volume of gas in calibrated burette bulbs $V_1 = (3 \times 15)/(12 + 273.16)$

Column No.	Column Title

20     $V_2 = (f_2 \times \underline{15})/(\underline{11} + 273.16) = (f_2/T_2) \times \underline{15}$

It is best to use (f_2/T_2) obtained from the helium calibration

21     $V_3 = (f_3 \times \underline{15})/(\underline{11} + 273.16) = (f_3/T_3) \times \underline{15}$

22     $V_4 = (f_4 \times \underline{18})/\underline{10}$

23     $V_{total} = \sum_i V_i = \underline{19} + \underline{20} + \underline{21} + \underline{22}$

24     $V_{ads.}$ = Volume of gas in the system $- \underline{23}$

25   Relative pressure $= P/P_o = (\underline{15}/\underline{17})$

26     $\dfrac{(P/P_o)}{V_{ads.} (1 - P/P_o)} = \dfrac{\underline{25}}{\underline{24} \, (1 - \underline{25})}$

APPENDIX D

TABULAR FORM OF PORE-SIZE

DISTRIBUTION CALCULATIONS

The large number of data necessary for the calculation of pore-size distribution curves obtained from the experimental adsorption isotherms require that such calculations be carried out in a tabular form. A table for the analysis of the data and evaluation of results will consist of 16 columns. Shown below are the column numbers together with the corresponding title in which the necessary equations used to obtain the various results are included. When column numbers appear underlined in the title column it means that they are used in the calculation.

Column No.	Column Title
1	P/P_o in equal increments of the relative pressure
2	$V_{ads.}$ in cm^3 at S.T.P. per gram of adsorbent corresponding to the P/P_o values of column 1 and taken from the experimental adsorption isotherms
3	The statistical thickness, t, in A. Equations (54) and (55)
4	The Kelvin radius, r_k, in A. Equations (50) and (51)
5	The pore-wall separation, d, in A. Equation (47) or $d = (\underline{4} + 2 \times \underline{3})$
6	Adsorbed liquid volume. $(V_{liq})_{N_2} = 0.001548\ (\underline{2})_{N_2}$

145

Column No.	Column Title

6   Adsorbed liquid volume. $(V_{liq})_{H_2} = 0.001266\ (\underline{2})_{H_2}$

7     $\Delta X_{x_i} = (V_{liq})_{x_i + \Delta x} - (V_{liq})_{x_i - \Delta x}$

8   R_{x_i}. Equation (42)

9   R'_{x_i}. Equation (43)

10   ΔV_{x_i}. Equations (44) and (75) or

$\Delta V_{x_i} = (\underline{8} \times \underline{7}) - (\underline{9} \times \underline{13} \times 10^{-4})$

11     $\Sigma \Delta V_{x_i} = \Sigma(\underline{10})$

12   ΔS_{x_i}. Equation (76) or $\Delta S_{x_i} = (2 \times \underline{10} \times 10^4)/5$

13     $\Sigma \Delta S_{x_i} = \Sigma(\underline{12})$

14   Δd_{x_i}. Equation (45)

15   Differential pore-volume, $\Delta V/\Delta d = (\underline{10}/\underline{14})$

16   Differential pore-area, $\Delta S/\Delta d = (\underline{12}/\underline{14})$

APPENDIX E

GLOSSARY

A = unit of angstroms equal to 10^{-8} cm

a_i = constant in the derivation of the BET equation

b = constant of the Langmuir equation

b_i = constant in the derivation of the BET equation

c = constant of the BET equation

d = pore-wall separation

E_1 = heat of adsorption in the first layer

E_2, E_3 = heats of adsorption in the second, third, etc., layers

E_L = heat of liquefaction of the bulk liquid adsorbate

$E_1 - E_L$ = net heat of adsorption

f_i = volume factor

g = unit of grams

I = intercept of the linear BET plot

i, j = subscripts

L = subscript used to indicate the liquid phase

M = molecular weight of the adsorbate

m = unit of meters

N = Avogadro's number

N_m = number of molecules contained in the monolayer volume

P = equilibrium pressure of the adsorbed phase

P_o = vapor pressure of the bulk liquid at its normal boiling point

P/P_o = relative pressure

R = ideal gas constant in 8.316×10^7 erg/deg·mole or 1.987 cal/deg·mole

R_{x_i} = first correction factor in the calculation of pore-size distributions

R'_{x_i} = second correction factor in the calculation of pore-size distributions

r_k = Kelvin radius

r_p = radius of circular pores

S = total surface area of the adsorbent

s = slope of the linear BET plot

s_o, s_1 = areas covered by 0,1,.... adsorbed molecular layers

T = absolute temperature

t = statistical thickness of the adsorbed layer

V = total volume of gas adsorbed

V_{ads} = volume of gas adsorbed, same as V

V_{liq} = adsorbed liquid volume

V_M = molar volume of the liquid adsorbate

V_m = volume of gas required to cover the surface S with a monolayer

v_o = volume of gas required to cover a unit area of surface when the monolayer is completely filled

V_{sp} = the specific volume of the adsorbate in the liquid state

X = usually denoted as ΔX_{x_i}, the volume of liquid adsorbate desorbed during equal relative pressure decrements

x = relative pressure, $x = P/P_o$

α = contact angle between the surface of the adsorbed liquid and the wall of the capillary

γ = surface tension of the liquid adsorbate

Δ = used to denote a difference, change, or increment

θ = surface coverage

ρ = density of the adsorbate

Σ = used to denote a summation

σ_m = area which one adsorbed molecule occupies in the complete monolayer

ΔX_{x_i} = volume of liquid adsorbate desorbed during equal relative pressure decrements

ΔV_{x_i} = corrected pore-volume corresponding to ΔX_{x_i}

ΔS_{x_i} = area of the group of pores at x_i

Δd_{x_i} = incremental values of the pore-wall separation at x_i, in going from $d_{(x_i + \Delta x)}$ to $d_{(x - \Delta x)}$

$\Sigma \Delta V_{x_i}$ = cumulative pore-volume

$\Sigma \Delta S_{x_i}$ = cumulative pore-area

$\Delta V/\Delta d$ = differential pore-volume

$\Delta S/\Delta d$ = differential pore-area

VITA

Theodoros Galaction Vernardakis

Candidate for the Degree of

Doctor of Philosophy

Thesis: SURFACE PARAMETERS AND PORE-SIZE DISTRIBUTIONS OF STANNIC OXIDE
GEL FROM NITROGEN AND HYDROGEN ADSORPTION ISOTHERMS

Major Field: Chemistry

Biographical:

Personal Data: Born in Limassol, Cyprus, November 14, 1942, the
son of Galaction G. and Heleni G. Vernardakis.

Education: Graduated from Lanition, Limassol Greek Gymnasium in
Limassol, Cyprus, in 1961; received a Bachelor of Science de-
gree from the College of Emporia, Emporia, Kansas, with majors
in Chemistry and Mathematics and minor in Physics, in May,
1965; received the Master of Science degree from the Oklahoma
State University, with a major in Chemistry, in May, 1968;
completed requirements for the Doctor of Philosophy degree in
May, 1972; received a Graduate Excellence Award (1969-1970),
Dow Chemical Fellowship (Summer 1968, 1969), and Du Pont
Fellowship (Summer, 1968).

Professional Experience: Part-time analyst, Emporia Milling Co.,
Emporia, Kansas, September, 1964 to January, 1965; Graduate
Research Assistant, February, 1965 to August, 1967; Graduate
Teaching Assistant, 1967 to May, 1972.

Membership in Honorary and Professional Societies: Member of Phi
Lambda Upsilon, Honorary Chemical Society; member of the
Society of the Sigma Xi, Scientific Research Society; member
of American Chemical Society.